REDUCTIVE CARBOXYLATION IS A NOVEL PATHWAY OF GLUTAMINE METABOLISM THAT SUPPORTS THE GROWTH OF TUMOR CELLS WITH METABOLIC DEFECTS

APPROVED BY THE SUPERVISORY COMMITTEE

Ralph DeBerardinis, MD, PhD.

John Abrams, PhD.

Shawn Burgess, PhD.

Gray Pearson, PhD.

For my teachers

REDUCTIVE CARBOXYLATION IS A NOVEL PATHWAY OF GLUTAMINE METABOLISM THAT SUPPORTS THE GROWTH OF TUMOR CELLS WITH METABOLIC DEFECTS

By

Andrew Robbins Mullen

DISSERTATION

Presented to the Faculty of the Graduate School of Biomedical Sciences

The University of Texas Southwestern Medical Center at Dallas

In Partial Fulfillment of the Requirements

For the Degree of

DOCTOR OF PHILOSOPHY

The University of Texas Southwestern Medical Center at Dallas

Dallas, Texas

December, 2013

ACKNOWLEDGEMENTS

I owe a great deal of my success over the last five years to the excellent mentorship I received from my advisor, Ralph DeBerardinis. I am grateful for his support and encouragement. Second, I would like to acknowledge the entire DeBerardinis lab, particularly Tzuling Cheng, Chendong Yang, and Jessica Sudderth, who have been extremely influential in my training over the last five years. I am also grateful for the assistance of Pei-Hsuan Chen, Zeping Hu, and Xiaolei Shi, who provided experimental support for aspects of this work. Additionally, I would like to acknowledge my collaborators, including Navdeep Chandel, Lucas Sullivan, William Wheaton and Elena Anso. I would also like to thank my thesis committee members John Abrams, Shawn Burgess and Gray Pearson. In particular, I am grateful to John Abrams, who has been a constant personal advocate at every stage of my scientific training. Finally, this work would not have been possible without the encouragement and support of my parents and family.

Reductive carboxylation is a novel pathway of glutamine metabolism that supports the growth of tumor cells with metabolic defects

Andrew Robbins Mullen

The University of Texas Southwestern Medical Center at Dallas, 2013

Advisor: Ralph DeBerardinis, MD, PhD.

In growing cancer cells, oxidative metabolism of glucose and glutamine in the mitochondria provide precursors needed for *de novo* synthesis of proteins, nucleic acids and lipids. Yet, a subset tumors harbor genetic mutations in the electron transport chain or tricarboxylic acid cycle that disable normal oxidative mitochondrial function. Importantly, it has been unknown how these cells generate the biosynthetic precursors required for growth. To address this, I used models of mitochondrial dysfunction in isogenic cancer cell lines and studied their metabolism using a combination of Gas Chromatography-Mass Spectrometry and Nuclear Magnetic Resonance spectroscopy. In all cases, mitochondrial dysfunction stimulated a novel pathway of glutamine metabolism, characterized by reversal of the canonical tricarboxylic acid cycle, termed reductive carboxylation; providing a plausible mechanism for how cancer cells with mitochondrial defects generate biosynthetic precursors required for growth. To gain mechanistic insight into how this unusual pathway was regulated I carried out a targeted metabolomics analysis in our isogenic tumor cell models. This led to the striking discovery that cells engaged in the reductive carboxylation pathway also operate an additional metabolic pathway that, at first glance, would appear to be superfluous and inefficient. Functional characterization of this second pathway revealed, however, that its activity was necessary for the optimal function of the reductive carboxylation pathway. In summary, this work has given us insights into how cancer cells are able to grow in the context of defective mitochondria. Additionally, this has exposed a potential Achilles ' heel that might be used to selectively kill tumors which rely on this pathway for growth.

PUBLICATIONS

1. Providence KM, Higgins SP, **Mullen AR**, Battista A, Samarakoon R, Higgins C, Wilkins-Port CE, Higgins PJ (2008). SERPINE1 (PAI-1) is deposited into keratinocyte migration "trails" and is required for optimal monolayer wound repair. *Archives of Dermatological Research*. 300 (6): 303-10.

2. Cheng T, Sudderth J, Yang C, **Mullen AR**, Jin ES, Matés JM, DeBerardinis RJ (2011). Pyruvate carboxylase is required for glutamine-independent growth of tumor cells. *Proceedings of the National Academy of Science*. 108(21):8674-9.

3. Shanware NP*, **Mullen AR***, DeBerardinis RJ, Abraham RT (2011). Glutamine: pleiotropic roles in tumor growth and stress resistance. *Journal of Molecular Medicine*. 89(3):229-36. (* denotes equal authorship).

4. **Mullen AR**, Wheaton WW, Jin ES, Chen PH, Sullivan LB, Cheng T, Yang Y, Linehan WM, Chandel NS, DeBerardinis RJ (2012). Reductive carboxylation supports growth in tumour cells with defective mitochondria. *Nature.* 481, 385-8.

5. **Mullen AR** and DeBerardinis RJ (2012). Genetically-defined metabolic reprogramming in cancer. *Trends in Endocrinology and Metabolism*. 23(11):552-9

6. Anso E, **Mullen AR**, Felsher D, DeBerardinis RJ, Chandel NS (2013). Metabolic changes in cancer cells upon inactivation of MYC. *Cancer & Metabolism*. 1:7.

7. Hamanaka RB, Glasauer A, Hoover P, Yang S, Blatt H, **Mullen AR**, Getsios S, Gottardi CJ, DeBerardinis RJ, Lavker RM, Chandel NS (2013). Mitochondrial ROS regulate epidermal differentiation and hair follicle development. *Science Signaling.* 6 (261), 8.

8. Sullivan LB, Martinez E, **Mullen AR**, Nguyen H, Dufour E, Sudarshan S, Yang Y, Linehan WM, Licht JD, DeBerardinis RJ, Chandel NS. The proto-oncometabolite fumarate binds glutathione to amplify ROS dependent signaling. (In Press, *Molecular Cell).*

TABLE OF CONTENTS

LIST OF FIGURES

LIST OF TABLES

LIST OF ABBREVIATIONS

ATP	Adenosine Triphosphate
CHX	Cycloheximide
DOX	Doxycycline
ETC	Electron Transport Chain
DNA	Deoxyribonucleic acid
FA	Fatty Acid
GAPDH	Glyceraldehyde 3-phosphate dehydrogenase
GCMS	Gas Chromatography Mass Spectrometry
GTP	Guanosine-5'-triphosphate
LC/MS	Liquid Chromotography Mass Spectrometry
NADH	Nicotinamide adenine dinucleotide
NADPH	Nicotinamide adenine dinucleotide phosphate
NMR	Nuclear Magnetic Resonance Imaging
RNA	Ribonucleic acid
RNAi	RNA interference
ROS	Reactive oxygen species
shRNA	Short hairpin RNA
siRNA	Small interfering RNA

Chapter One

Metabolic Pathways support cell growth and proliferation

Cell proliferation requires the uptake of nutrients for energy production and biosynthetic activities to support protein, lipid, nucleic acids and amino acid synthesis. Glucose and glutamine are the most abundant nutrients in the body and support cell growth in myriad ways. Importantly, tumor cells exhibit altered metabolism of glucose and glutamine in ways which distinguish them from non-transformed cells. The oldest and well studied of these dates back to the work of the German biochemist Otto Warburg, who made the observation that tumor cells had enhanced glucose uptake and lactate secretion even under conditions of adequate oxygen (Warburg et al., 1927). Today, enhanced aerobic glycolysis, known as The Warburg Effect in homage to Warburg, is a metabolic phenotype observed across the majority of tumor types and is an important diagnostic tool in detecting and treating cancer (Vander Heiden et al., 2009). Similarly, tumor cells also exhibit enhanced metabolism of glutamine (DeBerardinis and Cheng, 2010). Here, I will review how glucose and glutamine metabolism support the demands of cell growth.

Glucose metabolism contributes to ATP production

Glycolysis consists of sequential enzymatic reactions which convert glucose into two molecules of pyruvate. This pathway generates two ATP molecules per glucose. Oxidation of glucose carbon through the activity of the tricarboxylic acid cycle (TCA) and electron transport chain (ETC) in the mitochondria can generate up to 36 molecules of ATP (Salway, 2004). Rapidly proliferating cells, including tumor and non-transformed cells, preferentially secrete the majority of glucose-derived pyruvate as lactate (DeBerardinis et al., 2007; Hedeskov, 1968; Hume et al., 1978; Warburg et al., 1927). Although inefficient, this is capable of generating ATP at a rate faster than through oxidative phosphorylation (Pfeiffer et al., 2001), and in some cancer cells can account for as much as 50% of the total cellular ATP pool (Zu and Guppy, 2004). Importantly, this phenotype occurs despite any

measurable defect to oxidative phosphorylation (Moreno-Sanchez et al., 2007). Thus, enhanced glucose uptake supports ATP production in growing cells.

Glucose contributes to non-essential amino acid biosynthesis

Glycolysis supports the biosynthesis of three important non-essential amino acids: serine, glycine and alanine. Serine and glycine can be formed from the glycolytic intermediate 3-phosphoglycerate (3PG) (de Koning et al., 2003; Snell et al., 1988). This biosynthetic pathway begins with the oxidation of 3PG by the enzyme phosphoglycerate dehydrogenase (PHGDH) to generate 3-phosphohydroxypuruvate (3POHpyr) which is followed by transamination by phosphoserine aminotransferse-1 (PSAT1) to generate phosphserine and subsequently serine. An additional enzymatic step catalyzed by serine hydroxymethyltransferase (SHMT) generates glycine and 5,10-methylenetetrahydrofolate, the primary source of cellular one-carbon units (de Koning et al., 2003).Together these amino acids are important precursors for diverse cellular processes which will be discussed in more detail later in this chapter. Importantly, the role of this metabolic pathway in cancer cell growth is underscored by the observation that multiple enzymes in the biosynthetic pathway are found to be overexpressed in various cancers (Fu et al., 2001; Locasale et al., 2011; Nikiforov et al., 2002; Pollari et al., 2011; Possemato et al., 2011; Snell et al., 1988). (Figure 1-1).

Glucose contributes to alanine production, an amino acid required for proteins synthesis. In this pathway, alanine is formed through the reductive amination of glucose-derived pyruvate by alanine aminotransferase (ALT), with glutamate serving as a nitrogen donor (Salway, 2004). In some cancer cell lines this is the most active transamination reaction, where upwards of 10% of glucose carbon taken into the cells is secreted as alanine (DeBerardinis et al., 2007). Thus, glucose metabolism supports cancer cell growth through biosynthesis of amino acids (Figure 1-1).

Glucose contributes to de novo nucleotide biosynthesis

Purine and pyrimidines are precursors for important cellular components including DNA/RNA, ATP, GTP, and NADH, and cell growth is dependent on the abundance of these important building blocks. Glycolysis supports nucleotide metabolism in several ways. First, glucose contributes five carbons to purine and pyrimidine biosynthesis in the form of ribose-5-phosphate (R5P) which is formed in the glucose-dependent pentose phosphate pathway (PPP) (Figure 1-1). Formation of R5P can occur through two distinct branches of the PPP: the oxidative, which generates NADPH, and the non-oxidative pathway. In most cancer cells the non-oxidative arm of the PPP is the primary route of R5P synthesis (Tong et al., 2009). This pathway uses the glycolytic intermediates fructose-6-phosphate and glyceraldehydes 3 phosphate. Importantly, entry of carbon into this arm of the pathway is dependent on substrate concentration (Schenk et al., 1998). Thus, enhanced glycolysis is necessary to allow these cells to maintain high levels of glycolytic-intermediates to sustain flux into this pathway.

Up to four of the other carbons in purines can be derived from glucose, specifically through activity of the serine-glycine biosynthetic pathway (Figure 1-1). Two of these carbon units are from glycine, which as discussed earlier is synthesized from the glycolytic intermediate 3PG. Finally, two carbons in purines are derived from the one carbon folate pool in the form of N^{10} formyl-tetrahydrofolate. This one carbon molecule is generated from 5,10-methylenetetrahydrofolate, formed by the conversion of serine to glycine by SHMT (Cook, 2000; Lunt and Vander Heiden, 2011).

Glucose contributes to de novo lipid biosynthesis

It is well recognized that most tumors generate the majority of their cellular lipids and fatty acids through *de novo* metabolic pathways (Kuhajda, 2000). Glucose metabolism contributes to fatty acid biosynthesis through several distinct mechanisms (Figure 1-2). Acetyl-coA is the primary precursor for the synthesis of fatty acids, cholesterol and related lipids. Glucose metabolism generates pyruvate

which is transported into the mitochondria and is decarboxylated by pyruvate dehydrogenase (PDH) to generate acetyl-coA(Kuhajda, 2000). However, to participate in lipid synthesis reactions acetyl-coA must first be transported out of the mitochondria. Because mammalian cells do not transport acetyl-coA across membranes, mitochondrial acetyl-CoA is condensed with the glutamine-derived TCA cycle intermediate oxaloacetate (OAA) to generate citric acid. Citrate can be exported out of the mitochondria where, where it is cleaved by ATP citrate lyase (ACL) to regenerate OAA and acetyl-coA. Here, acetyl-coA can support lipid synthesis and other biosynthetic reactions. This pathway has been demonstrated to be required for the growth of tumors both *in vitro* and *in vivo* (Bauer et al., 2005; Hatzivassiliou et al., 2005). Additionally, this pathway is also necessary to generate acetyl-coA for use in acetylation reactions of proteins and histones (Wellen et al., 2009). Interestingly, some tumor cell lines generate both acetyl-coA and OAA directly from glucose carbon through the pyruvate carboxylase (PC) pathway (Cheng et al., 2011) (Figure 1-2). In this pathway, glucose-derived pyruvate is carboxylated to form OAA which can combine with glucose-derived acetyl-coA to form citrate, thereby supporting lipid synthesis in the absence of glutamine.

Glucose metabolism is able to contribute to lipid synthesis through additional metabolic pathways. For example, the glycolytic intermediate dihydroxyacetone phosphate contributes to phospholipid and triacylglycerol synthesis, both abundant components of cell membranes. Dihydroxyacetone phosphate is formed along with glyceraldehyde-3-phosphate (G3P) from the breakdown of fructose 1,6-bisosphate and is metabolized to glycerol-3-phosphate, which can then be incorporated into phospholipids and triacylglycerols (Figure 1-2). Similarly, the glycolytic intermediate3PG can be metabolized to ceramide to support *de novo* shingolipid synthesis. Here serine produced from 3PG via the serine biosynthetic pathway condenses with palmityl-coA to generate ceramide and subsequent metabolic steps generate other shingolipid species (Lunt and Vander Heiden,

2011). Additionally, glucose-dependent flux through the oxidative PPP generates NADPH required for lipid synthesis (Cairns et al., 2011).

Glutamine contributes to non essential amino acid biosynthesis

Glutamine donates nitrogen through transamination reactions to form either alanine or aspartate, and many other nonessential amino acids (Figure 1-3). Alanine is formed through reductive amination of pyruvate by alanine aminotransferase (ALT). As discussed earlier, this reaction is highly active in some cancers and is a way to secrete excess glucose carbon out of the cell. In a similar reaction, the amino acid aspartate is formed through the reductive amination of OAA by aspartate aminotransferase (AST). Aspartate can then participate in the malate-aspartate shuttle to transfer reducing equivalents generated from glycolysis into the mitochondria to support maximal ATP production. In this shuttle, aspartate is exported to the cytoplasm and converted to OAA which can then be reduced to malate. Malate can then enter the mitochondria and be oxidized back to OAA and the reducing equivelents donated to the electron transport chain. This shuttle is known to be highly active in many tumor cell lines (Greenhouse and Lehninger, 1976).

Aspartate is also an important nitrogen donor for nucleotide biosynthesis and is a precursor for the amino acid asparagine (Figure 1-3). In this reaction aspartate is converted to asparagine by asparagine synthetase (AS). Importantly, certain ALL lymphoblastic lymphomas lack the expression of AS and are dependent on uptake of asparagine from the serum (Avramis and Tiwari, 2006). This auxotrophy is exploited in the treatment of patients with ALL through administration of L-asparaginase, which converts free asparagine in the serum to aspartate, thereby depleting asparagine from the circulation. L-asparaginase has been a component of the standard of care for decades and has greatly improved clinical outcomes (Avramis and Tiwari, 2006).

Glutamine contributes carbon for the synthesis of proline, the only proteinogenic secondary amino acid (Phang et al., 2010). The proline biosynthetic pathway begins with the conversion of glutamine to Δ1-pyrroline-5-carboxylate (P5C) by P5C synthatase and subsequent reduction by P5C reductase to form proline. Interestingly P5C has recently been shown to be required for growth in a model of Burkitt lymphoma (Liu et al., 2012).

Glutamine contributes to nucleotide biosynthesis

Glutamine directly contributes nitrogen to *de novo* purine biosynthesis at three distinct steps (Figure 1-3). Glutamine donates one nitrogen molecule to the rate limiting step in purine synthesis, catalyzed by glutamine phosphoribosylpyrophosphate amidotransferse; this generates glutamate and phosphoribosylamine. Several enzymatic steps later glutamine donates a second nitrogen in a reaction catalyzed by phosphoribosylformylgycinamidine synthase. Glutamine donates a third nitrogen to convert xanthine monophosphate to guanosine monophospate (GMP) (Cory and Cory, 2006).

Glutamine contributes two nitrogens to pyrimide biosynthesis. One nitrogen is donated at the rate limiting step in pyrimidine biosynthesis by carbamoyl phosphate synthetase. A second nitrogen is donated at the last committed step in the pathway to generate cytidine triphosphate (CTP) through CTP synthetase (Cory and Cory, 2006). Incorporation of other nitrogen molecules to purine an pyrimidine synthesis are donated by aspartate and glycine which, as described earlier, often initially receive these nitrogen molecules from glutamine. It has recently been shown that some transformed cells show delayed progression through the S-phase of the cell cycle under conditions of glutamine deprivation (Gaglio et al., 2009).

Glutamine contributes to both glucose-dependent and –independent lipid synthesis

Glutamine oxidation in the TCA cycle supports glucose-dependent lipid synthesis. To reiterate, acetyl-coA is the major precursor for *de novo* lipid synthesis and is generated from oxidation of glucose-derived pyruvate in the mitochondria. Acetyl-coA is condensed with the TCA cycle intermediate OAA to form citrate; citrate export out of the mitochondria and cleavage by ACL generates acetyl-coA which can be used for lipid synthesis reactions. To sustain this cataplerotic flux of citrate out of the TCA cycle, cells must replenish lost intermediates from other sources; this process is known as anaplerosis (from the Greek word 'to fill up'). Glutamine is the major anaplerotic substrate for many growing cancer cells (DeBerardinis and Cheng, 2010). In this pathway, glutamine-derived glutamate is converted to the TCA cycle intermediate αKG (Figure 1-4). This can occur through tranamination reactions or activity of glutamate dehydrogenase (GDH); under most conditions GDH activity is inhibited and transamination accounts for the majority of glutamate-dependent αKG production (DeBerardinis et al., 2007). It is through this pathway that glutamine contributes the majority of the four-carbon units to the TCA cycle, supporting glucose-dependent lipid synthesis and other processes.

Glutamine can contribute to acetyl-coA production in the absence of glucose. In glucose-depleted conditions, the dominant pathway of αKG formation (ALT-dependent transamination) cannot be engaged, as the ALT reaction requires pyruvate as a substrate. To maintain glutamine carbon flux into the TCA cycle under these conditions, cells engage an alternative pathway of αKG production through enhanced activity of GDH (Yang et al., 2009). In this reaction, GDH deaminates glutamate to generate αKG and ammonia, supporting continued anaplerotic flux of glutamine into the TCA cycle (Figure 1-4). Additionally, flux of malate out of the TCA cycle was shown to allow these cells to generate pyruvate and subsequently acetyl-coA in the absence of glucose. Under normal conditions the malic enzyme pathway usually contributes only a small portion of total lipogenic-acetyl-coA.

Glutamine can contribute carbon to lipid synthesis through an additional pathway that is independent of malic enzyme. For example, brown adipocytes have been shown to generate approximately 30% of their lipogenic acetyl-coA through reductive metabolism of glutamine (Yoo et al., 2008). In this pathway, glutamine-derived αKG is carboxylated through reverse activity of isocitrate dehydrogenase (IDH) to generate isocitrate and subsequently citrate (Figure 1-5). IDH exists in three isoforms that differ from one another based on either their subcellular localization or cofactor preference (NAD+/NADH or NADP+/NADPH). In these cells it was speculated that this reaction was dependent on the NADP+/NADPH-dependent isoforms. This pathway has also been reported to contribute to a minor fraction of citrate formation in SF188 glioblastoma cancer cells (Ward et al., 2010).

Glutamine metabolism protects from oxidative stress

Glutamine metabolism protects growing cells from oxidative stress. Reactive oxygen species (ROS) are byproducts of electron transport chain activity. At physiologic levels ROS mediate important signaling events and are required for cell growth (Hamanaka and Chandel, 2009). At high levels, however, ROS damage cellular components and can lead to cell death (Wellen and Thompson, 2010). Thus, cells need to protect themselves from the deleterious effects of ROS in order to grow. Glutamine is a precursor for the *de novo* synthesis of the most abundant cellular antioxidant glutathione (GSH), a tripeptide of glutamate, glycine and cysteine. In vitro, it has been shown that inhibition of glutamine metabolism through removal of glutamine from the cell culture media or siRNA knockdown of GLS results in a decrease in total GSH levels (Lora et al., 2004; Yuneva et al., 2007). Additionally, glutamine metabolism generates NADPH needed to keep GSH in the reduced state, through production of malate for flux through ME, which generates NADPH.

II. Glucose and glutamine metabolism are regulated by oncogenes and tumor suppressors

Proto-oncogenes and tumor suppressors have normal roles regulating cell growth and homeostatsis. Genomic alterations, including gain of function and loss of function mutations, amplifications and deletions, dysregulate the normal function of these proto-oncogenes and tumor suppressors leading to aberrant cell growth and the other "hallmarks" of cancer (Hanahan and Weinberg, 2000). It is now appreciated that most, if not all, oncogenes and tumor suppressors also regulate metabolic pathways. Here, I will review the regulation of key metabolic pathways by oncogenes and tumor suppressors commonly dysregulated in cancer.

Hypoxia-inducible factors

Hypoxia-inducible factors (HIFs) are transcriptional regulators of the cellular response to decreased oxygen availability. HIF is a heterodimer composed of one stable β subunit and one of three unstable α subunits (HIF1α, HIF2α, HIF3α). Both α and β subunits are constitutively expressed yet under normal oxygen tension the α subunit is hydroxylated by a family of prolyl hydroxylases (PHDs), leading to its degredation by the proteasome (Majmundar et al., 2010). Importantly, these PHDs use the TCA cycle intermediate αKG as a cofactor (Kaelin and Ratcliffe, 2008), which has important implications for HIF regulation, discussed later. Under conditions of decreased oxygen, the HIF α subunit is stabilized and can dimerize with HIF β to induce transcription of genes involved in tumorgenesis, inflammation, vascular remodeling and metabolism. Aberrant regulation of HIFs even in the absence of hypoxia frequently occurs as a result of activation of oncogenes or inactivation of tumor suppressors (Kim et al., 2006; Majmundar et al., 2010; Ratcliffe et al., 1998). Alternatively, mitochondrial-derived ROS have been shown to negatively regulate PHD activity, leading to enhanced HIF1 expression (Hamanaka and Chandel, 2009).

HIF activation enhances glucose metabolism through several mechanisms (Figure 1-6). HIF induces the transcription of glucose transporters, several glycolytic enzymes and lactate dehydrogenase-

A (LDHA) (to sustain maximal glycolysis) (Majmundar et al., 2010; Semenza et al., 1994). Additionally, HIF suppresses oxidative metabolism of pyruvate by inducing transcription of pyruvate dehydrogenase kinases (PDKs), negative regulators of PDH activity (Kim et al., 2006; Papandreou et al., 2006). Inhibition of mitochondrial metabolism is believed to be cell protective, as hypoxia increases mitochondrial-derived ROS (Kirito et al., 2009). In summary, the metabolic outcome of HIF activation is increased glucose consumption and lactate secretion and decreased oxidative metabolism.

C-Myc

C-Myc (Myc) is a basic helix–loop–helix zipper (bHLHZ) protein which can exert activating and repressing transcriptional events related to cell growth, mitochondrial biogenesis and metabolism (Adhikary and Eilers, 2005). Myc function is dysregulated in up to 50% of tumors through chromosomal translocations or amplifications of the *MYC* gene (Dang et al., 2009a). Myc is capable of enhancing glucose and glutamine metabolism in several ways (Figure 1-6). Like HIF1α, Myc can transcriptionally up-regulate the expression of glucose transporters, glycolytic enzymes and LDHA to maximize glycolysis. Myc can also induce expression of PDK1 to negatively regulate pyruvate oxidation in the mitochondria. Similarly, Myc stimulates metabolism of glutamine through up-regulation of glutamine transporters (Wise 2008; Dang 2009). Myc also enhances glutaminolysis by enhancing GLS expression; rather than direct up-regulation, Myc suppress transcription of two microRNAs (miRNA23a/b) which negatively regulate GLS mRNA stability (Gao et al., 2009).

Myc is also capable of enhancing expression of enzymes in nearly every biosynthetic pathway important for growth. Myc up-regulates genes in *de novo* nucleotide, lipid and amino acid biosynthetic pathways (Liu et al., 2008; Mannava et al., 2008; Nikiforov et al., 2002; O'Connell et al., 2003). Additionally, to defend against oxidative stress, Myc regulates GSH biosynthesis through up-regulation of the rate-limiting step in GSH biosynthesis. In summary, Myc activation leads to enhanced expression

of transporters and enzymes in biosynthetic pathways resulting in enhanced glucose and glutamine metabolism and the diversion of their downstream intermediates into pathways required for cell growth. The importance of glutamine metabolism, in particular, to Myc-dependent cell growth is underscored by the observation that Myc-amplified cells have been shown to die in the absence of glutamine (Wise et al., 2008; Yuneva et al., 2007).

PI3K/AKT/mTOR pathway

The serine/threonine protein kinase AKT (also known as protein kinase B) mediates a diverse array of pathways related to growth, survival and metabolism. Consequently, this pathway is found to be dysregulated in many cancer types (Manning and Cantley, 2007). In response to growth factor signaling, phosphoinositide 3-kinase (PI3K) activates AKT, leading to its association with the plasma membrane and the activation of downstream effectors (Gonzalez and McGraw, 2009). Notably, AKT activates the major transducer or cell growth signals, the mechanistic target of rapamycin complex 1 (mTORC1), through down regulation of tuberous sclerosis-2 (TSC2). TSC2 is part of the TSC1-TSC2 complex which negatively regulates mTORC1 activity. Once activated, mTORC1 up-regulates downstream targets, including HIF1α and c-Myc, to initiate a suite metabolic rearrangements required for cell growth (Laplante and Sabatini, 2012). Additionally, mTORC1 also enhances lipid synthesis through activation of the sterol regulatory element binding protein 1 (SREBP-1). This is a member of the SREBP family of transcription factors which control the expression of genes involved in fatty acid synthesis (Cantor and Sabatini, 2012).

AKT is also capable of directly enhancing glucose metabolism (Figure 1-6). First, AKT increases glucose uptake through stimulating the translocation of glucose transporters to the plasma membrane (Kohn 1996). Separately, AKT can directly or indirectly activate several glycolytic enzymes, including hexokinase and phosphofructokinase, the first step and the rate limiting step in glycolysis, respectively

(Deprez et al., 1997; Gottlob et al., 2001). Consequently, AKT is sufficient to induce non-transformed cells to exhibit a robust Warburg Effect (Elstrom et al., 2004). AKT also enhances acetyl-coA production for acetylation reactions through activation of ATP citrate lyase (ACL), which cleaves citrate to generate acetyl-coA in the cytoplasm (Berwick et al., 2002). This supports acetylation reactions, lipid synthesis and maximizes glycolysis through reducing the cytoplasmic concentration of citrate, which can allosterically inhibit steps in glycolysis(Ward and Thompson, 2012). In summary, AKT is capable of both directly and indirectly enhancing metabolic activities, particularly those related to glucose metabolism.

p53

p53 is a tetrameric transcription factor which can respond to a diverse array of stress stimuli, including DNA damage, hypoxia, and oncogene activation. In response, it can mediate transcriptional events to stimulate important biological outcomes, including apoptosis, cell cycle arrest or DNA damage repair and metabolism. p53 is dysregulated in approximately 50% of all human cancers (Menendez et al., 2009; Riley et al., 2008). p53 can regulate glucose metabolism through several mechanisms, with conflicting outcomes. First, p53 can decrease glucose uptake by suppressing the expression of the glucose transporters, GLU1 and GLUT4 (Vousden and Ryan, 2009) (Figure 1-6). p53 is also capable of suppressing glycolysis by decreasing the expression of the glycolytic enzyme phosphoglycerate mutase (PGM). Additionally, p53 can also induce expression of TIGAR (TP53-induced glycolysis and apoptosis regulator), which impedes glycolytic flux (Bensaad et al., 2006). Contradictory to this suppressive role, p53 can also enhance glucose metabolism by inducing the expression of hexokinase II, the first enzymatic step in glycolysis (Mathupala et al., 1997).

p53 enhances mitochondrial metabolism through several mechanisms. First, p53 can transcriptionally upregulate cytochrome c oxidase 2 (SCO2) to promote oxidative phosphorylation (Matoba et al., 2006). Second, p53 also supports oxidative phosphorylation through enhanced

transcription of subunit I of cytochrome c oxidase (COI) (Vousden and Ryan, 2009). Third, p53 induces expression of glutaminase 2 (GLS2), which converts glutamine to glutamate in the mitochondria (Hu et al., 2010; Suzuki et al., 2010). This isoform was found to be particularly important for redox defense. In summary, p53 regulation of metabolism is complex but appears to suppress biosynthetic metabolic pathways.

III. Tumors with metabolic defects

Warburg's theory that all human tumors are the result of defects to the mitochondria is untrue. In fact, most tumors have enhanced mitochondrial metabolism in order to support the demands of cell growth (Vander Heiden et al., 2009). However, in rare cases, mutations in metabolic enzymes, including mitochondrial enzymes, promotes cancer. Intense study of these situations has provided insight into the role of metabolism in malignant transformation. Here, I will review the mechanisms underlying how metabolic enzymes can behave as oncogenes and tumor suppressors to independently drive cells towards malignancy.

The role of mtDNA mutations in cancer

Mitochondria contain their own genome (mtDNA) which codes for 13 polypeptides, 2 ribosomyl RNAs, and 22 tRNAs (Vafai and Mootha, 2012). The mtDNA is inherited maternally and alterations to mtDNA are frequently observed in human disease, including cancer. To date there are no examples of mtDNA mutations predisposing to cancer formation; however, tumors are commonly found to contain mtDNA mutations and changes in mtDNA content or expression of mtDNA-derived proteins (Chatterjee et al., 2006). Literature on the role of mtDNA mutations in tumor growth has been mixed. For example, one report has shown that various cancer cell lines depleted of mtDNA have increased *in vivo* proliferative capacity in mouse xenograft experiments compared to isogenic controls; in this case, however, the proliferative advantage varied based on the anatomical site of cell implantation (Morais et

al., 1994). Conversely, a separate report has shown that mtDNA depletion resulted in decreased tumor formation as indicated through reduced anchorage-independent growth (Cavalli et al., 1997). Thus, there has been little consensus on the functional role of the mtDNA genome in tumor formation.

Interestingly, it has recently been reported that mtDNA mutations are sufficient to regulate metastasis. In one report, the authors identified mouse tumor cell lines derived from a Lewis lung carcinoma with either low or high metastatic potential (Ishikawa et al., 2012). These highly metastatic cells were found to contain a loss of function mutation in a mtDNA gene, *ND6*, important for Complex I function. To test if this mtDNA mutation was necessary and sufficient to induce a cell with a low metastatic potential to become a high-metastatic cell, and vice versa, they depleted both cells of their mtDNA and repopulated each with the mtDNA of the other. Remarkably, this was sufficient to render the low-metastatic cell capable of metastasizing, as well as ablating the high-metastatic ability of the other cell. In other words, the metastatic ability of these cells was independent of their nuclear genome, and entirely dependent on their mtDNA makeup. The authors identified that this effect was mediated by ROS produced as a result of Complex I dysfunction, where ROS resulted in an up-regulation of genes involved in tumorgenesis, including HIF1α and vascular endothelial growth factor (VEGF). Similarly, complex I dysfunction due to loss-of-function of another mtDNA gene, *ND5*, has also been shown to promote tumorgenesis through ROS-induced Akt activation (Sharma et al., 2011). Taken together, these studies suggest mtDNA mutations may potentiate, rather than independently initiate and/or drive tumorgenesis.

Isocitrate dehydrogenase-1 and -2 are metabolic proto-oncogenes

Isocitrate dehydrogenase isoforms catalyze the oxidative decarboxylation of isocitrate to αKG. There are three mammalian isoforms, which differ from one another based on their sub-cellular localization and cofactor preference. IDH3 is the canonical TCA cycle enzyme and functions as a multi-

subunit complex which uses NAD/NADH as a cofactor in an irreversible reaction confined to the mitochondria. IDH1 and IDH2 share no sequence similarity to IDH3 and use NADP/NAPDH in reversible reactions which occur in either the cytoplasm or mitochondria, respectively. Additionally, IDH1 has been shown in certain contexts to localize to the peroxisome, where it is believed to be the major source of NADPH for peroxisomal NADPH-dependent enzymes (Geisbrecht and Gould, 1999; Shechter et al., 2003).

Recently, tumor genome sequencing efforts identified somatic, heterozygous mutations in IDH1 and IDH2 in up to 75% of low grade gliomas and secondary glioblastoma multiforme (GBM), approximately 20% of acute myeloid leukemia (AML), as well as chondrosarcomas (Amary et al., 2011; Green and Beer, 2010; Parsons et al., 2008; Yan et al., 2009). These tumors were all shown to have the same amino acid substitution in the enzyme active site, R132H in IDH1 and R170K in IDH2, which were shown to ablate the oxidative enzyme activity. More recently, other mutations in the IDH1/2 active site have also been described yet no mutations resulting in frame shift or stop codons have ever been observed (Ward et al., 2011).

In 2009 it was discovered that mutations in IDH1 or IDH2 result in a neomorphic activity to convert αKG to the structurally similar metabolite R-2-hydroxyglutarate (R-2HG) (Dang et al., 2009b) (Figure 1-7). In normal cells this metabolite is present at scarce levels, however in primary tumors with mutations in either IDH1 or IDH2 or in cells engineered to over-express either of these mutant alleles, levels of R-2HG are massively elevated (Dang et al., 2009b; Ward et al., 2010). Interestingly, R-2HG or its enantiomer S-2HG (also known through different nomenclature as D-2HG and L-2HG) have been shown to accumulate in two rare metabolic disorders: D-2HG aciduria and L-2HG aciduria. These disorders are the result of germline, recessive loss of function mutations in either of the dehydrogenaes which convert D-2HG or L-2HG to αKG (D-2HG dehydrogenae or L-2HG dehydrogenase, respectively). These

patients accumulate D-2HG or L-2HG and develop severe neurological defects (Kranendijk et al., 2012). Germline, dominant mutations in IDH2 have also been shown to be sufficient to induce D-2HG aciduria in the absence of mutations in either D- or L-2HG-dehydrogenase (Kranendijk et al., 2010)). Interestingly, patients with L-2HGDH deficiency, but not D-2HGDH deficiency, have been shown to develop brain tumors (Kranendijk et al., 2012). This strongly suggests 2-HG contribute to oncogenesis.

Due to its close structural similarity to αKG, R-2HG can inhibit a broad class of αKG-dependent enzymes (Figure 1-7). This has been shown to alter epigenetic gene expression in ways that contribute to tumorgenesis. For example, R-2HG directly inhibits the jumonji-C domain-containing protein 2A (JMJD2A) histone demethylase, leading to an R-2HG-dependent increase in histone methylation (Chowdhury et al., 2011). Additionally, R-2HG inhibits the ten-eleven translocation (TET) family of αKG-dependent enzymes, leading to a genome wide increase in DNA methylation in IDH1/2 mutated cells. (Delhommeau et al., 2009; Xu et al., 2011). Moreover, this recapitulates the CpG island methylator phenotype (Turcan et al., 2012), which is observed in other tumor types independent of IDH1/2 mutations and has important clinical implications for the treatment of patients (Issa, 2004). IDH1/2-depdendent epigenetic alterations have been shown to significantly alter differentiation of several cell types (Figueroa et al., 2010; Lu et al., 2012). Alternatively, 2HG has also been reported to stimulate the αKG-dependent prolyl hydroxylation of HIF1α by serving as a co-substrate for the PHDs, leading to enhanced HIF1α degradation (Koivunen et al., 2012). The implications of this work suggest a tumor suppressor role of HIF1α, which will be discussed later in this chapter. Small-molecule inhibitors of mutant IDH1 and IDH2 have been recently been described (Rohle et al., 2013; Wang et al., 2013). Studies with these inhibitors in IDH1 or IDH2 mutant cells has indicated that blocking R-2HG production is sufficient to slow the growth of cells and reverse the differentiation phenotype. Interestingly, while inhibition of mutant IDH1 was shown to promote differentiation of gliomas cells, it did so without

altering the R-2HG-induced DNA hypermethylation, suggesting yet unknown functions of R-2HG cells (Rohle et al., 2013).

Succinate dehydrogenase is a metabolic tumor suppressor

Succinate dehydrogenase (SDH), also known as Complex II of the electron transport chain, is a TCA cycle enzyme which oxidizes succinate to form fumarate and $FADH_2$, and donates electrons to the ETC (Figure 1-8). SDH is composed of four subunits encoded by the nuclear genome: SDHA, SDHB, SDHC, SDHD. Loss of function mutations in any of these subunits have been found to predispose individuals to develop the neuroendocrine tumors pheochromoacytoma and paragangliomas, as well as gastrointestinal stromal tumors (Astuti et al., 2001; Baysal et al., 2000; Killian et al., 2013; Niemann and Muller, 2000). Additionally, mutations in SDH5, an enzyme which attaches a necessary flavin group to SDHA, have also been reported to lead to paragangliomas (Hao et al., 2009). Mutations in these subunits predispose to tumors through an autosomal dominant inheritance pattern, where individuals inherit one loss of function mutation and tumors develop after loss of heterozygosity of the wild type allele. Interestingly, tumors arising from mutations in SDHD are dependent on the parent of origin (Hensen et al., 2004). In these cases, tumors form only if the mutant allele is inherited paternally, suggesting the maternally-derived mutant allele is imprinted and is not expressed in offspring. While the SDHD locus shows no evidence of imprinting, it has recently been reported that an alternative promoter of a lincRNA (UPGL) nearby the SDHD locus is heavily methylated on the maternally inherited allele; this also occurs in a tissue specific manner (Baysal et al., 2011).

Loss of SDH activity leads to a massive intracellular increase in succinate which has been shown to lead to an aberrant pattern of gene expression that promotes tumorgenesis (Figure1-8a). High intracellular succinate leads to the normoxic stabilization of HIF1α. Succinate exerts this effect through direct inhibition of prolyl hydroxylases (PHDs) which negatively regulate HIF1α expression under normal

oxygen tension (Figure 1-8b) (Kaelin and Ratcliffe, 2008; Koivunen et al., 2007; Selak et al., 2005). This results in the transcriptional up-regulation of a broad class of genes related to metabolism, vascular remodeling, inflammation and tumorigenesis, one potential mechanisms underlying the highly vascular nature of pheochromocytomas and paragangliomas. Additionally, carotid body paragangliomas have an increased incidence in individuals living at high-altitude, suggesting that HIF stabilization through SDH dysfunction recapitulates tumor formation through environmental hypoxia (Raimundo et al., 2011).

Elevated succinate leads to aberrant epigenetic modifications through inhibition of other αKG-dependent enzymes (Figure 1-8b). For example, succinate has been reported to directly inhibit the jumonji-domain histon demethylaes (JmJD), leading to hypermethylation of histones (Cervera et al., 2009). Additionally, succinate is able to inhibit DNA demethylation to produce the Hypermethylator phenotype in paragangliomas and gasto stromal tumors (Killian et al., 2013; Letouze et al., 2013). DNA hypermethylation, discussed in relation to IDH1/2 mutations, is commonly observed in other tumor types and is a clinically-important diagnostic and prognostic phenotype (Issa, 2004). Elevated succinate has also been linked to resistance to apoptosis in pheochromacytoma through succinate-dependent inhibition of the pro-apoptotic prolylhydroxylase Egln3 (Lee et al., 2005).

Fumarate Hydratase is a metabolic tumor suppressor

Fumarate Hydratase (FH) is a TCA cycle enzyme which catalyzes the reversible hydration of fumarate to malate (Figure 1-8a). Loss of function mutations in FH predispose individuals to a disorder known as hereditary leiomyomomatosis and renal cell carcinoma (HLRCC). This is a triad of disorders which include benign cutaneous and uterine leiomyomas as well as highly aggressive renal tumors, including collecting duct and Type-2 papillary (Tomlinson et al., 2002). Like mutations in SDH, the disease mechanisms for HLRCC involves inheritance of one loss-of-function FH allele and subsequent loss of heterozygosity, resulting in renal tumors which lack FH activity. These mutations are most

commonly missense, nonsense or frame shift events and can occur throughout the *FH* locus (Bayley et al., 2008). The use of both patient-derived cell lines and mouse models of FH dysfunction have shed light on how loss of FH leads to tumor formation.

Loss of FH enzyme activity leads to a massive intracellular increase in fumarate. Like R-2HG and succinate, fumarate is able to inhibit a wide variety of αKG-dependent enzymes (Figure 1-8b). These include epigenetic factors including the TET family of 5mC hydroxylases and JMJD family of histone demethylases (Xiao et al., 2012). Similarly, fumarate inhibits prolyl hydroxylation of HIF1α, leading to HIF-mediated transcription (Issa, 2004; Koivunen et al., 2007). However, several recent reports have questioned the role of HIF1α in the pathophysiology of FH-deficient tumors. First, it has been shown that renal cyst formation in FH deficient mice is not dependent on HIF1α stabilization (Adam et al., 2011). In fact, this study found that the combinatorial knockout of FH and HIF1α or FH and various PHDs exacerbated renal cyst formation; suggesting HIF1α may be negatively regulating growth in this model. Additionally, siRNA knockdown of FH in human fibroblasts or renal epithehelial cells has been shown sufficient to render these cells resistant to apoptosis even in the absence of HIF1a expression (Bardella et al., 2012). These findings corroborate other reports which suggest HIF1α functions as a tumor suppressor in some contexts (Shen et al., 2011). Together, these indicate that tumor formation in FH deficient cells is likely a consequence of more than just HIF1α activity.

To this end, fumarate has been shown to inhibit the function of proteins through a direct post-translational modification known as succination (Figure 1-8c). In this reaction, fumarate covalently reacts with cysteine residues in proteins through a Michael addition to form S-(2-succinyl) cysteine (2SC) (Alderson et al., 2006). FH-dependent succination of the protein Kelch like-ECH-associated protein 1 (Keap1) has been shown to lead to an up-regulated antioxidant response in FH deficient renal cysts. Keap1 is an electrophilic sensor which negatively regulates the expression of the nuclear factor

(erythroid-derived 2)-like 2 (Nrf2), a key transcriptional mediator of the cellular antioxidant response. In the absence of oxidants, Keap1 negatively regulates Nrf2 expression by serving as the adaptor for the Cul-E3 ubiquitin ligase system, resulting in the proteolytic degradation of Nrf2. Under conditions of oxidative stress, oxidants react with cysteine residues on Keap1, disrupting its interaction with Nrf2 and leading to stabilization and induction of Nrf2-dependent antioxidant-defense genes (Wakabayashi et al., 2004; Zhang, 2010). Intriguingly, FH deficiency induces fumarate-dependent succination of these very cysteine residues on Keap1, resulting in constitutive Nrf2-dependent gene transcription in these cells (Adam et al., 2011). Nrf2 has been known to promote the growth of other tumors and is thus likely contributing to the growth and survival of FH deficient cells, including their adaptation to high fumarate (DeNicola et al., 2011).

A separate report has proposed that FH-deficiency also induces oxidative stress in patient-derived renal carcinoma cells (Figure 1-8c). In this study, it was found that fumarate-dependent succination of the cellular antioxidant glutathione (GSH) creates a novel metabolite: succinated glutathione (GSF). This metabolite was found to deplete total NADPH, resulting in decreased antioxidant capacity and amplified ROS dependent signaling of HIF1α; supporting a PHD-independent mechanism by which fumarate induces HIF1α expression (Sullivan et al., 2013). This study presents an alternative, but not mutually exclusive, mechanism by which FH loss leads to HIF induction. Additionally, it indicates that FH dysfunction contributes to oxidative stress while at the same time independently enhancing antioxidant defense.

In summary, metabolic dysfunction through mutations in IDH1/2, SDH or FH, initiate tumorgenesis through shared mechanisms. Interestingly, however, there appears to be very little phenotypic overlap in terms of the anatomical location where tumors develop or their aggressiveness. Even the primary metabolic disturbance appears to be highly context specific. In the case of HLRCC,

though presumably every tissue has the ability to lose heterozygosity (and likely does), it is unknown why only leiomyomas of the skin and uterus and tumors of the kidney form. Furthermore, it is unknown why the leiomyomas, which also show biallelic loss of FH, are almost always benign and do not show the aggressive behavior of the renal tumors. Similarly, it is unknown why tumors have been observed following the constitutive accumulation of S-2HG in patients with L-2-hydroxyglutaric aciduria, but not R-2HG, which is the metabolite that drives tumor formation due to mutations in IDH1/2. Separately, very little is known about how tumors without SDH or FH activity overcome these severe metabolic disturbances and generate biosynthetic precursors required for growth. My hypothesis is that tumors with metabolic defects generate biosynthetic precursors through novel and/or unusual metabolic pathways. Indentifying these has the potential to uncover metabolic-vulnerabilities which could be therapeutically targeted.

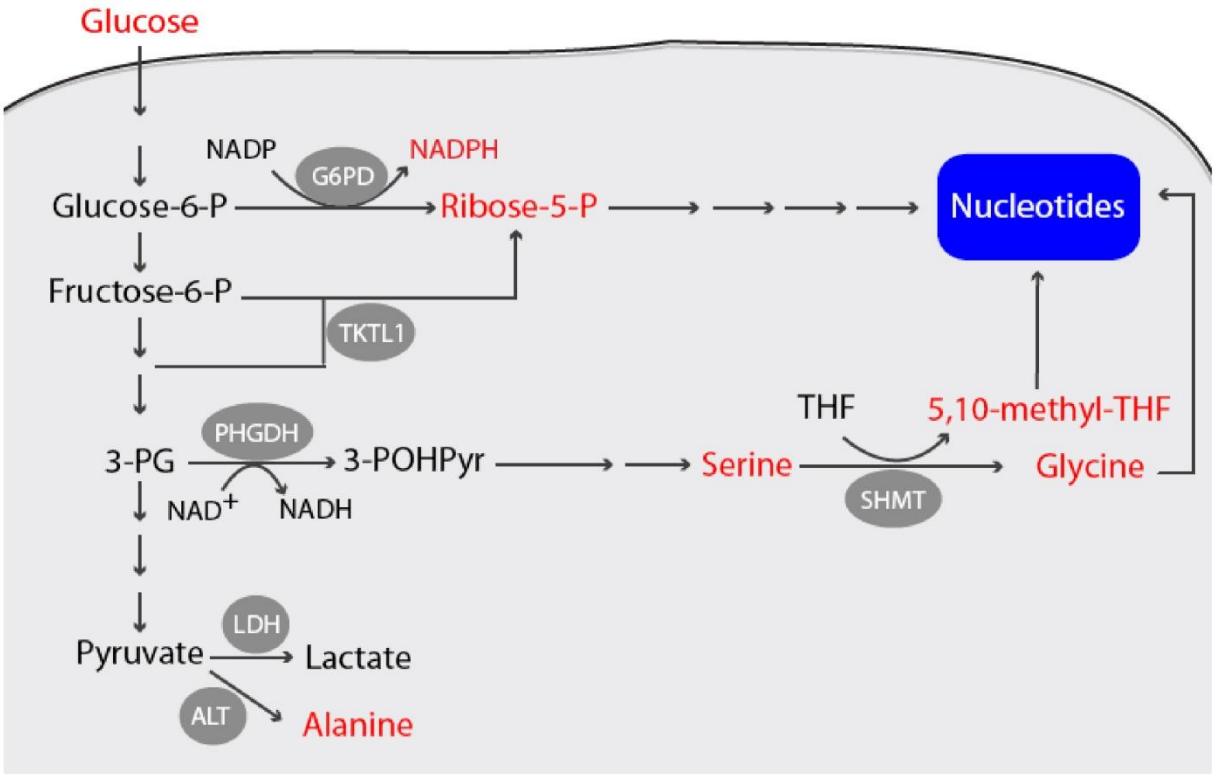

Figure 1.1: Glucose metabolism contributes to non-essential amino acid and nucleotide biosynthesis. Glycolytic intermediates, including glucose-6-phosphate (glucose-6-P), fructose-6-phosphate (fructose-6-P) are diverted out of glycolysis to generate ribose-5-phosphate (ribose-5-P). This is metabolized in a series of reactions leading to nucleotide biosynthesis. The glycolytic intermediate 3-phosphoglycerate (3-PG) is diverted out of the glycolysis pathway to generate serine. Conversion of serine to glycine by serine hydroxylmethyltransferase (SHMT) generates 5,10-methyl-Tetrahydrofolate (5,10-methyl-THF). Glycine and 5,10-methy-THF are used for synthesis of nucleotides. Transamination of pyruvate by alanine aminotransferases (ALT) generates alanine. Abbreviations: G6PD, glucose-6-phosphate dehydrogenase; TKTL1, transketolase-like protein-1; 3-PG, 3-phosphoglycerate; PHGDH, phosphoglycerate dehydrogenase; 3-POHpyr, 3-phosphonoxypyruvate; THF, tetrahydrofolate; SHMT, serine hydroxymethyl transferase; LDH lactate dehydrogenase; ALT, alanine aminotransferases

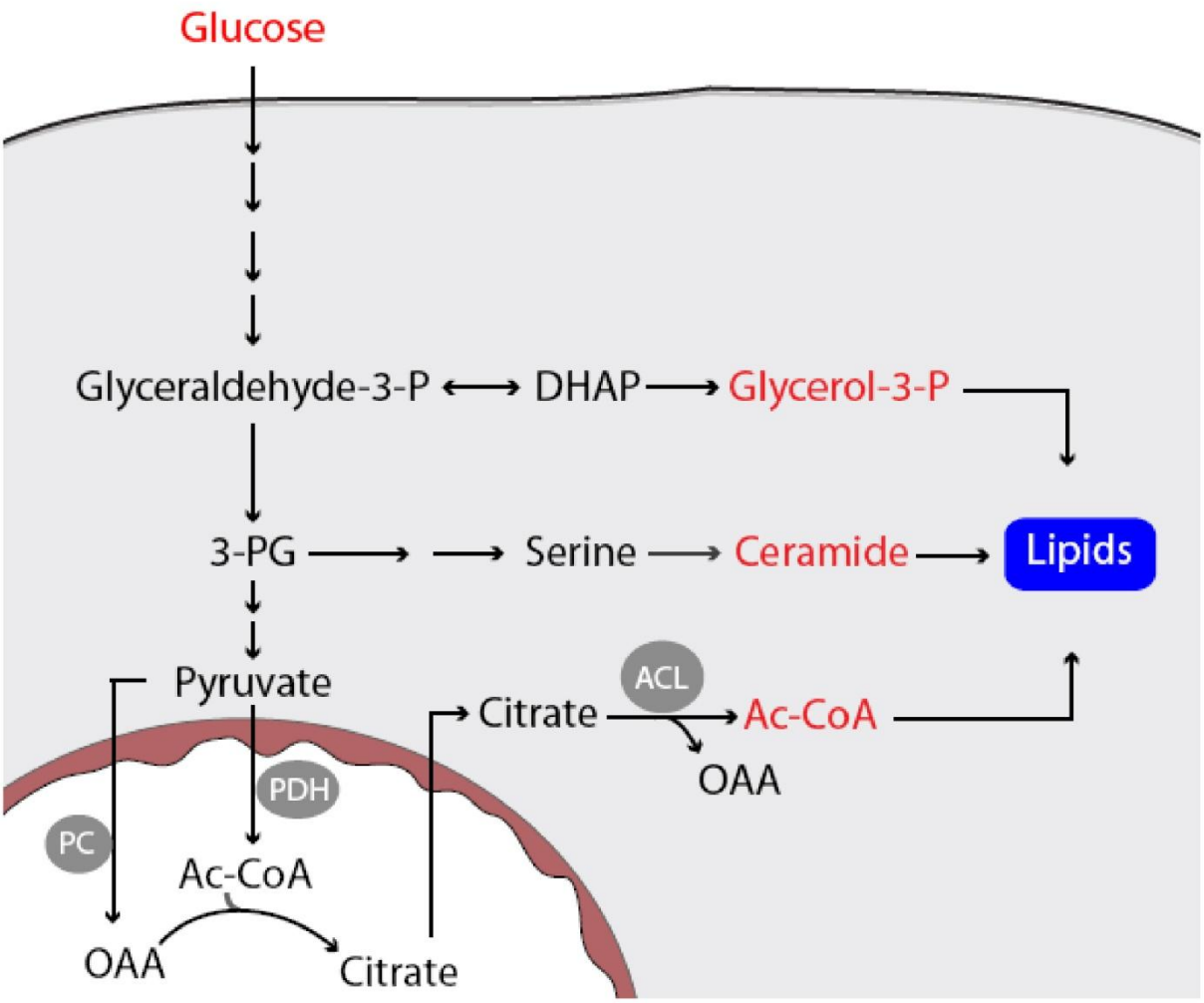

Figure 1.2: Glucose metabolism supports *de novo* lipid synthesis
The glycolytic intermediate glyceraldehyde-3-phosphate (glyceraldehydes-3-P) is diverted out of glycolysis to generate glycerol-3-phosphate (glycerol-3-P) which is a precursor for lipids. The serine biosynthetic pathway supports ceramide production which is an additional precursor for lipid synthesis. Oxidation of glucose-derived pyruvate by pyruvate dehydrogenase (PDH) in the mitochondria generates acetyl-coA. This is combined with the intermediate oxaloacetate (OAA) to form citrate. Export of citrate out of the mitochondria and cleavage by ATP citrate lyase (ACL) regenerates acetyl-coA and OAA. OAA can be formed from directly from glucose through the activity of pyruvate carboxylase (PC). Abbreviations: DHAP, dihydoxyacetone phosphate; 3-PG, 3-phosphoglycerate; PC, pyruvate carboxylase; PDH, pyruvate dehydrogenase; OAA, oxaloacetate; ACL, ATP citrate lyase.

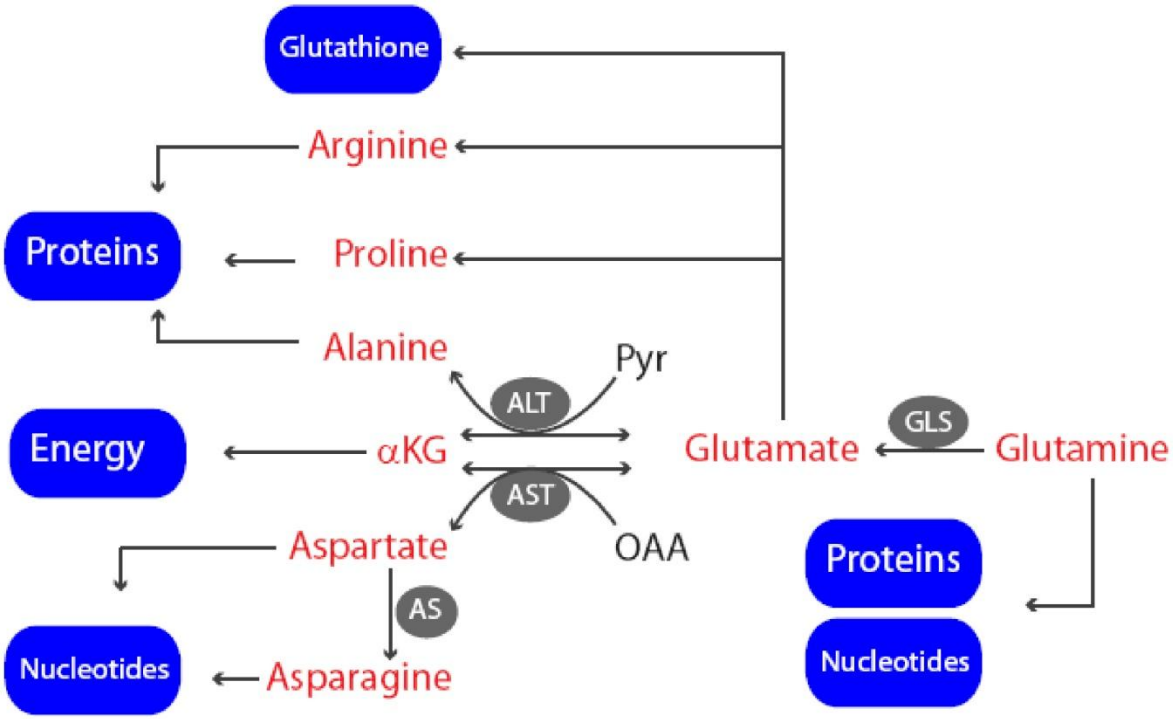

Figure 1.3: Metabolism of glutamine generates non-essential amino acids
Glutamine is an abundant nutrient which is directly incorporated into proteins and is an obligate nitrogen donor for nucleotide biosynthesis. Metabolism of glutamine by glutaminase (GLS) generates glutamate. Glutamate is metabolized in several distinct pathways to support biosynthesis of arginine, proline, and glutathione. Glutamate donates nitrogen through transamination reactions, most commonly ALT or AST, which generate alanine and aspartate, respectively. Alpha-ketoglutarate (αKG) is oxidized in the TCA cycle to support energy production. Aspartate is a precursor for asparagines which is incorporated into nucleotides. Abbreviations: GLS, glutaminase, ALT, alanine aminotransferases; AST, aspartate aminotransferases; OAA, oxaloacetate; AS, asparagines synthetase; αKG, alpha-ketoglutarate.

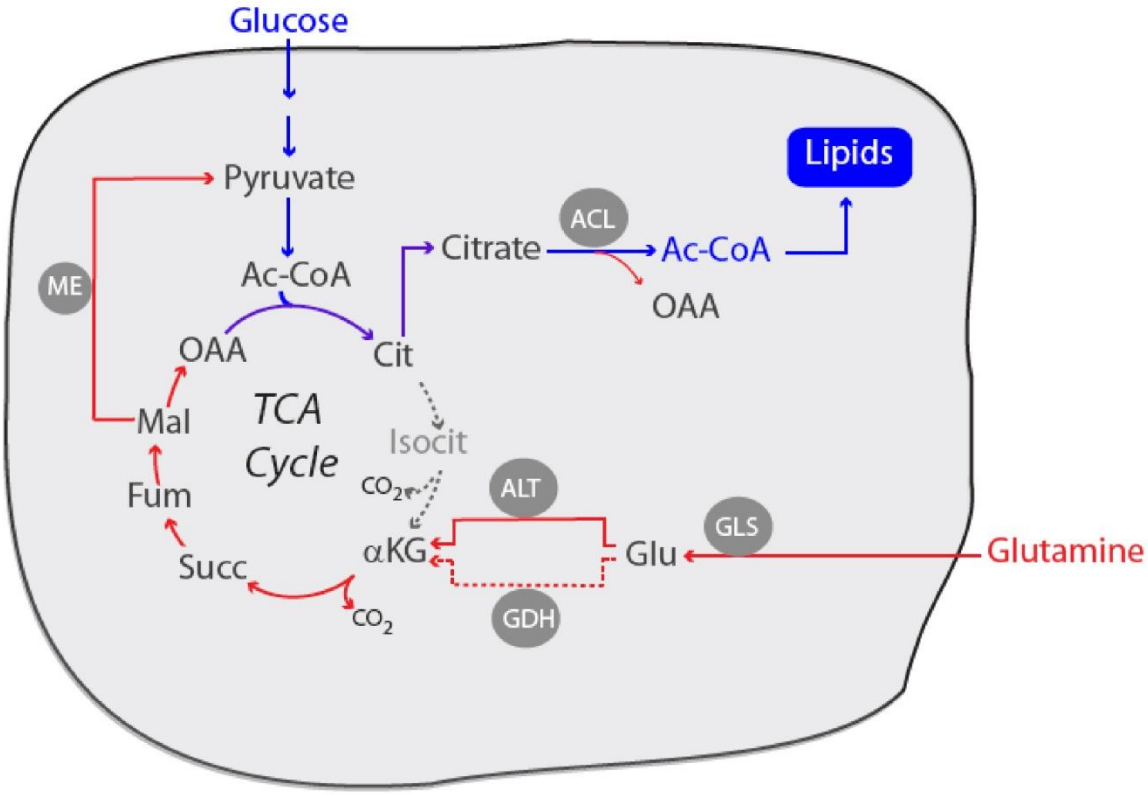

Figure 1.4: Glutamine supports glucose-dependent lipid synthesis.
Glucose is metabolized via glycolysis (blue arrows) to pyruvate. Pyruvate is converted to Acetyl-coA. Condensation of this acetyl-coA oxaloacetate (OAA) generates citrate. The glutamine anaplerotic pathway (red arrows) begins with the conversion of glutamate to αKG and generates the four carbon TCA cycle intermediates, including OAA. Cleavage of citrate by ATP citrate lyase (ACL) generate acetyl-coA which is used for *de novo* lipid synthesis reactions. In the absence of glucose, glutamate dehydrogenase (GDH) activity increases to support αKG production in the TCA cycle. Malate can be exported out of the cycle and converted to pyruvate by malic enzyme (ME) to support acetyl-coA production. Abbreviations: ACL, ATP citrate lyase; OAA, oxaloacetate; GLS, glutaminase; GLU, glutamate; ALT, alanine aminotransferases; GDH, glutamate dehydrogenase; αKG, alpha-ketoglutarate; Succ, succinate; Fum, fumarate; Mal, malate; ME, malic enzyme Cit, citrate.

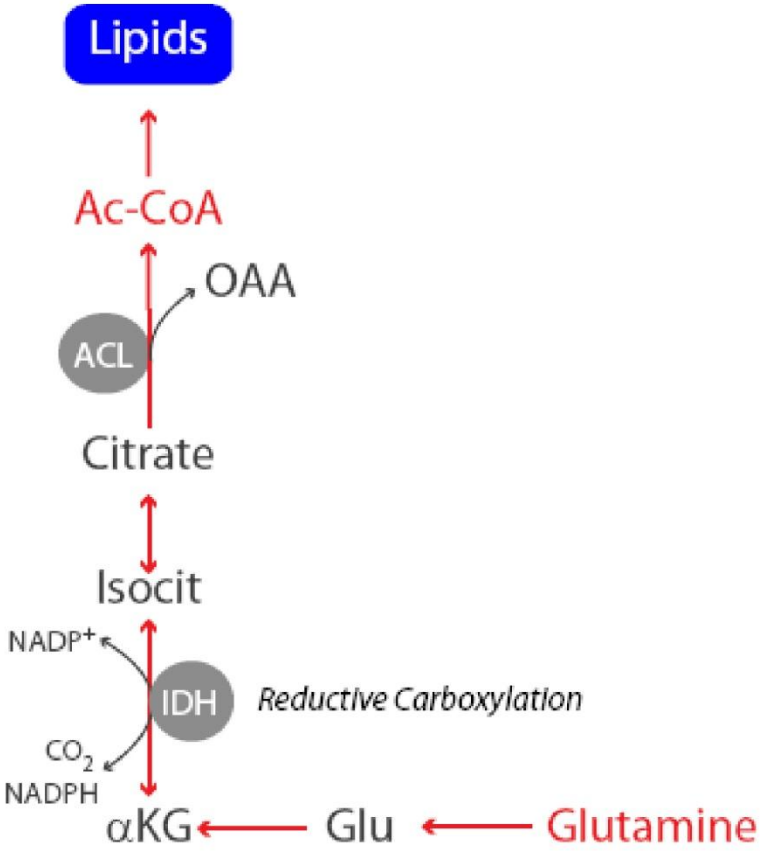

Figure 1.5: Glutamine-dependent lipid synthesis
In some cells glutamine-derived αKG is metabolized through reductive activity of IDH. This reaction requires NADPH and generates isocitrate and subsequently citrate. Cleavage of citrate supports acetyl-coA production. Abbreviations: Glu, glutamate, αKG, alpha-ketoglutarate; IDH, isocitrate dehydrogenase; Isocit, isocitrate; ACL, ATP citrate lyase; OAA, oxaloacetate.

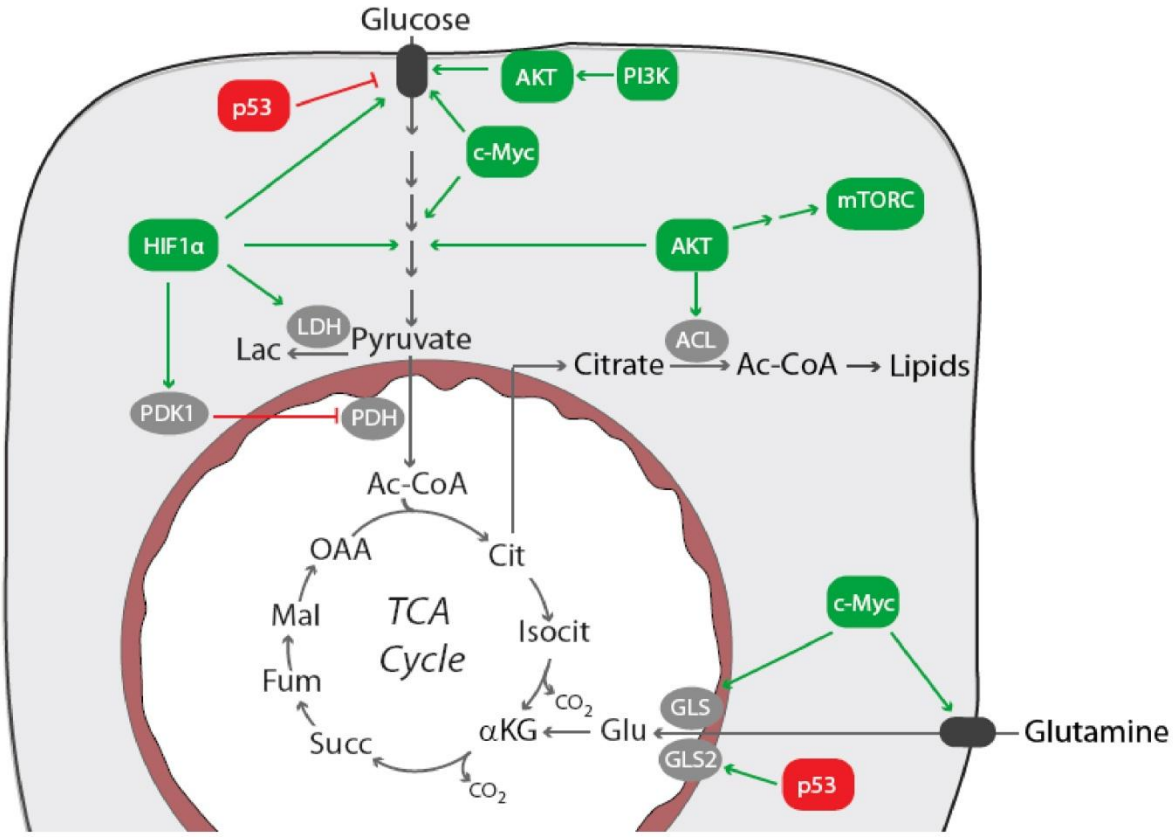

Figure 1.6: Oncogenes and tumor suppressors regulate glucose and glutamine metabolism
Glucose uptake is enhanced by the oncogenes HIF1α, AKT and c-Myc. These oncogenes are also capable of directly or indirectly enhancing the activity of glycolytic enzymes as well as LDH to sustain maximal glycolysis. HIF1α upregulates pyruvate dehydrogenase kinase-1 (PDK1), which negatively regulates pyruvate dehydrogenase (PDH) activity. This results in decreased pyruvate oxidation in the mitochondria. AKT activates ATP citrate lyase (ACL) to enhance acetyl-coA production for lipid synthesis. The tumor suppressor p53 is capable of suppressing glucose uptake. c-Myc enhances glutamine uptake and metabolism. Abbreviations, LDH, lactate dehydrogenase; PDK1, pyruvate dehydrogenase kinase-1; PDH, pyruvate dehydrogenase; ACL, ATP citrate lyase; GLS, glutaminase; OAA, oxaloacetate; GLU, glutamate; αKG, alpha-ketoglutarate; Succ, succinate; Fum, fumarate; Mal, malate; Cit, citrate.

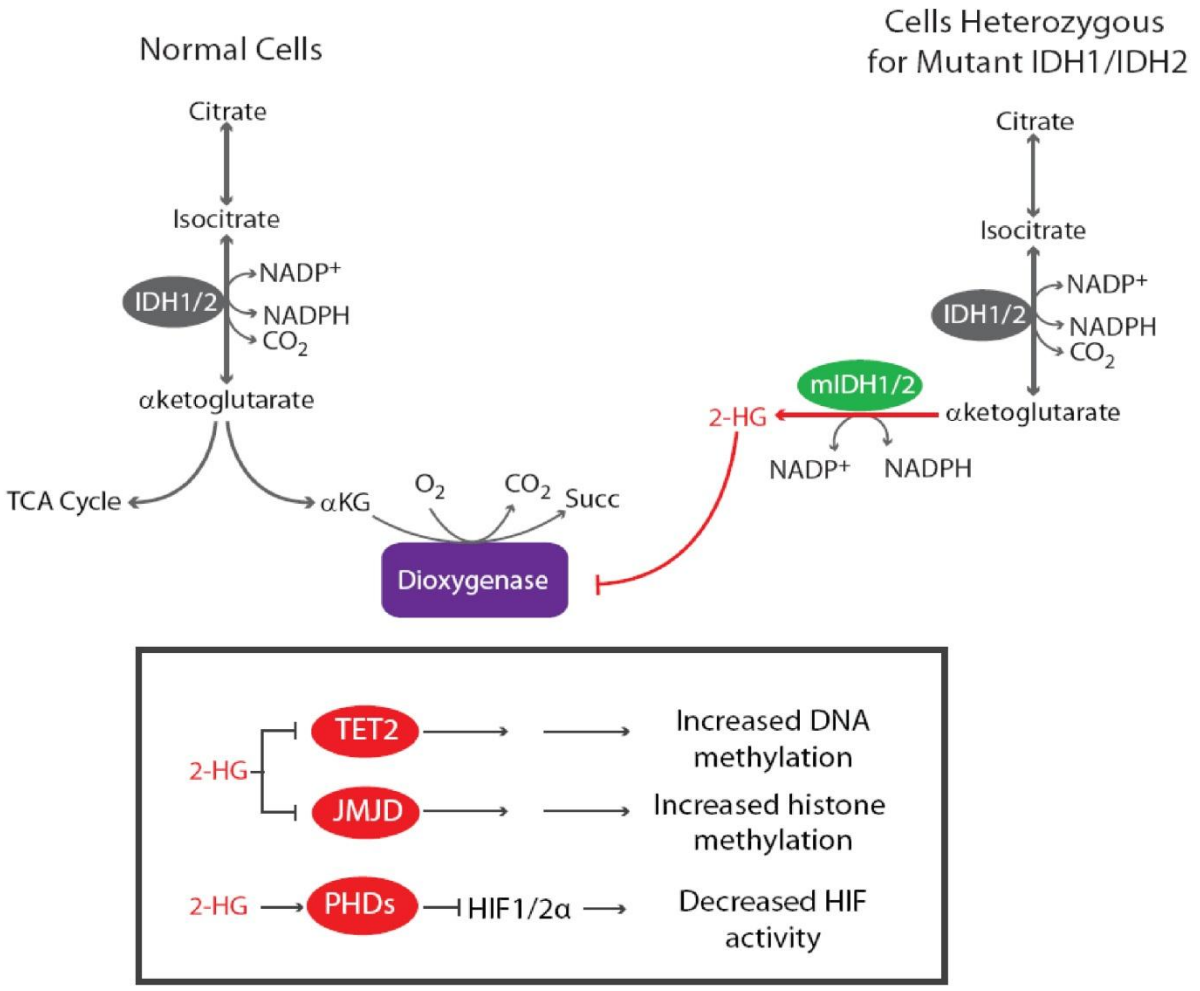

Figure 1.7: Mutant IDH1/2 enzymes produce an oncometabolite with pleiotropic effects on cell signaling and epigenetics.

Normal cells contain wild-type isocitrate dehydrogenases IDH1 and IDH2 (gray). These enzymes catalyze the reversible conversion of isocitrate to α-ketoglutarate (αKG), generating NADPH and CO_2. αKG can be oxidized in the TCA cycle or used as a cofactor by αKG -dependent dioxygenase enzymes. Tumor cells with somatically-acquired, heterozygous active site mutations in IDH1 or IDH2 (mIDH1/2, green) display a neomorphic enzyme activity that reduces αKG to R-2-hydroxyglutarate (R-2HG) using NADPH as a cofactor. Owing to its structural similarity to αKG, R-2HG modulates the function of αKG -dependent dioxygenases, stimulating prolyl hydroxylase activity, and inhibiting several enzymes that regulate histone and DNA modifications. Abbreviations: TET2, ten-eleven translocation-2; JMJD, jumonji-C-domain containing protein; PHD, prolyl hydroxylase; HIF, hypoxia inducible factor.

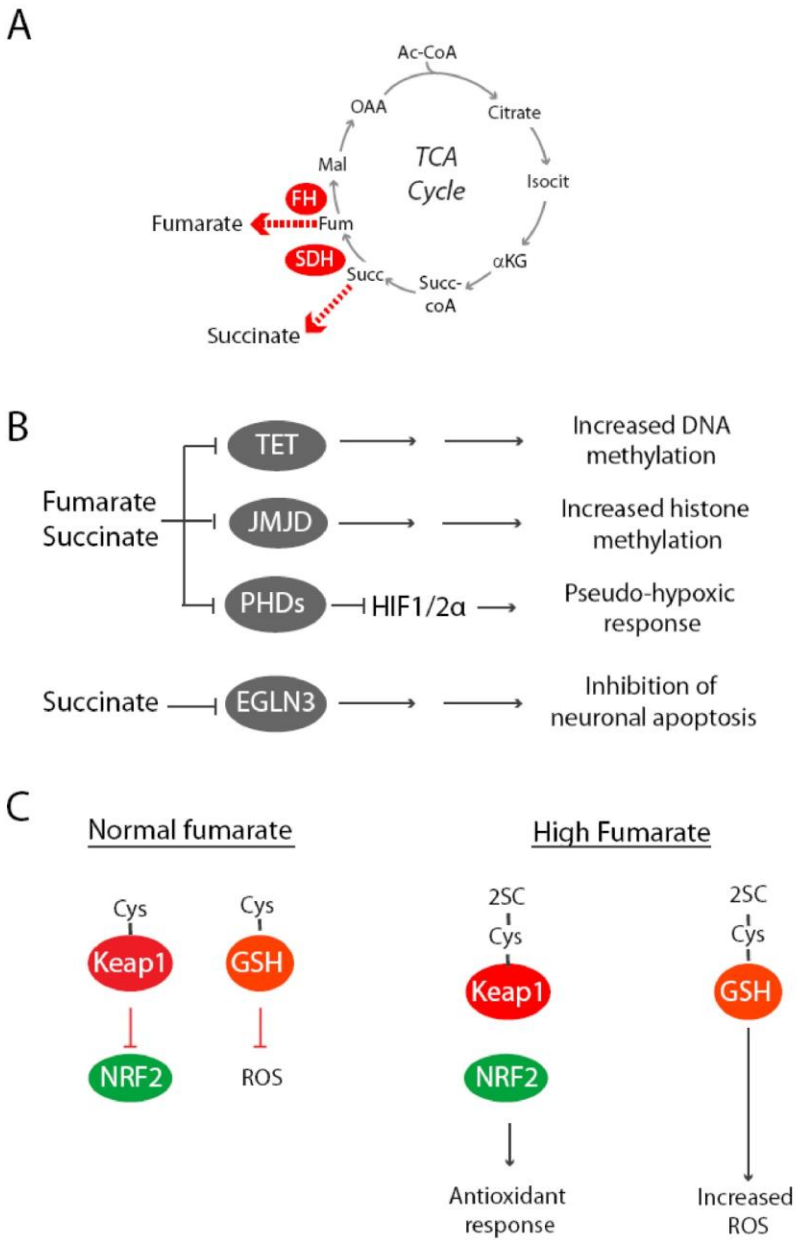

Figure 1.8: Loss of SDH and FH activity promote malignancy: **(a)** Succinate dehydrogenase (SDH) is a TCA cycle enzyme which converts succinate to fumarate. Fumarate hydratase (FH) catalyzes the hydrationof fumarate to malate. Loss of function mutations in SDH or FH cause accumulation of succinate and fumarate, respectively. **(b)** Accumulation of succinate and fumarate directly inhibit the activity of dioxygenase enzymes. This includes the JMJD histone demethylase; inhibition results in an increase in histone methylation marks. Inhibition of PHDs leads to constitutive HIF1α transcription and a pseudohypoxic gene signature. Succinate-dependent inhibition of EGLN3 renders the neurnonal precursor cells resistant to apoptosis. **(c)** Keap1 is an electrophile sensor. In the absence of fumarate and other electrophiles, Keap1 negatively regulates the transcription factor Nrf2, targeting it for degradation. Glutathione (GSH) is a cellular antioxidant. In FH-deficient cells, cysteine residues on Keap1 and GSH are modified by fumarate-dependent succination, in which cysteine is converted to S-(2-

succinyl)-cysteine (2SC). The consequence of this is enhanced Nrf2-dependnet transcription of genes involved in antioxidant response. Succunated-GSH decreases the antioxidant capacity of the cells. Abbreviations: Isocit, isocitrate; aKG, alpha-ketoglutarate; Succ-coA, succinyl-coA; Succ, succinate; Fum, fumarate; Mal, malate; OAA, oxaloacetate; TET, ten-eleven translocation-2; JMDJ, jumonji-C-domain containing protein; PHD, prolyl hydroxylase; HIF, hypoxia inducible factor; EGLN3, egl nine-homolog 3; Keap1, kelch-like ECH-associated protein1; NRF2, nuclear factor (erythroid-derived 2)-like 2; GSH, glutathione; 2SC, S-(2-succinyl)-cysteine

Chapter Two

Reductive Carboxylation supports the growth of tumor cells with metabolic defects

Introduction

Glucose and glutamine are the most abundant nutrients in the body and tumors exhibit robust metabolism of these nutrients. Proliferating cells divert glucose and glutamine into pathways of nucleotide, amino acid and lipid biosynthesis which are required for growth. (Vander Heiden et al., 2009). The importance of these metabolic pathways is highlighted by the observation that many oncogenes and tumor suppressors regulate the uptake and subsequent metabolism of these two nutrients (Cantor and Sabatini, 2012).

Some tumors have metabolic defects in TCA cycle enzymes which independently drive tumorigenesis. These include loss of function mutations in genes encoding components of Succinate dehydrogenase (SDH) that are associated with familial neuroendocrine tumors, or loss of function mutations in fumarate Hydratase (FH) which are associated with familial forms of renal cancer. Loss of function mutations in either SDH or FH lead to accumulation of succinate or fumarate, respectively, which drives the malignant growth of these cells. Importantly, it has been unknown how these cells generate biosynthetic precursors in the context of severe metabolic dysfunction. We hypothesized that these cells grew through novel and/or unusual metabolic pathways.

Results

Cells deficient in oxidative phosphorylation have enhanced aerobic glycolysis

We first studied the metabolism of isogenic 143B human osteosarcoma cells that contained or lacked a loss-of-function mutation in ETC complex III (cytochrome b–c1 complex). These cell lines were generated by depleting 143B mitochondrial DNA (mtDNA) and repopulating with either wild-type mtDNA or mtDNA containing a frame shift mutation in the gene encoding cytochrome b (CYTB: also known as MT-CYB), an essential complex III component (Rana et al., 2000). Despite lack of respiration and complex III function in the mutants (Figure 1a), both wild-type (143Bwt) and CYTB mutant (143Bcytb) cells form colonies in soft agar (Weinberg et al., 2010) and proliferate at comparable rates (Figure 1 b), making these cells a good model in which to study growth during mitochondrial dysfunction. As expected for cells with defective oxidative phosphorylation, 143Bcytb cells had higher glucose consumption and lactate production than 143Bwt, indicating a metabolic shift towards aerobic glycolysis (Figure 1c,d). Additionally, both cell lines consumed glutamine at equivalent rates (Figure 1e).

Reductive carboxylation supports TCA cycle intermediate production in 143Bcytb

To study activity of the TCA cycle in both these cells we quantified the levels of several important TCA cycle intermediates. Both cell lines had detectable TCA cycle intermediates, although citrate was less abundant and succinate was significantly more abundant in the 143Bcytb cells (Figure 2a). To determine the effects of CYTB mutation on the metabolic fates of glucose, we cultured both cell lines in medium containing U-^{13}C-glucose (here U indicates uniformly ^{13}C-labelled) and measured ^{13}C enrichment of intracellular metabolites by mass spectrometry. In 143Bwt cells, most of the citrate molecules contained glucose-derived ^{13}C (Figure 2b). Citrate m+2 (citrate containing two additional mass units from ^{13}C) results from oxidative decarboxylation of glucose-derived pyruvate by pyruvate dehydrogenase (PDH) to form 1,2-^{13}C-acetyl-coenzyme A (acetyl-coA), followed by condensation with an

unlabelled oxaloacetate (OAA). Processing of this citrate m+2 around one turn of the TCA cycle produces citrate m+4 (Figure 2e). In 143Bcytb cells, most citrate contained no glucose-derived ^{13}-carbon (m+0), indicating suppressed PDH contribution to acetyl-CoA (Figure 2b). Fumarate and malate m+2 were also decreased (Figure 2 c,d). In 143Bcytb these metabolites also contained a modest increase m+3. Entry of three ^{13}C masses occurs when glucose-derived pyruvate is carboxylated to form OAA, malate and fumarate (Figure 2 c,d) (Cheng et al., 2011). These results indicate that oxidative metabolism of glucose-derived pyruvate contributes a substantial fraction of the two-carbon units in citrate in 143Bwt cells and very little in 143Bcytb cells.

Glutamine is a major respiratory substrate in cancer cells, providing energy and carbon for growth (DeBerardinis et al., 2007). Such cells use glutamine to supply anaplerosis, the replenishment of TCA cycle intermediates withdrawn from the cycle to feed biosynthetic pathways. Both 143Bwt and 143Bcytb cells have previously been shown to require glutamine for colony formation, implying a respiration independent function for glutamine in cell growth (Weinberg et al., 2010), and both cell types consumed glutamine at similar rates (Figure 1d). We cultured both cell lines with U-^{13}C-glutamine to define the metabolic fates of glutamine. Like other glutamine-dependent cancer cells (Cheng et al., 2011), 143Bwt cells used glutamine as the major anaplerotic precursor, resulting in a large amount of fumarate, malate and citrate m+4 (Figure 3 a, b, c,). In contrast, 143Bcytb cells produced only trace quantities of citrate m+4. Instead, they appeared to produce citrate m+5 through reductive carboxylation of glutamine-derived α-ketoglutarate (Figure 3 a, b, c). This reaction involves addition of an unlabelled carbon by isocitrate dehydrogenase (IDH) acting in reverse relative to the canonical oxidative TCA cycle (Figure 3e) (Des Rosiers 1994). Cleavage of citrate m+5 by ATP-citrate lyase then produces acetyl-CoA m+2 and OAA m+3, with the unlabelled carbon retained on OAA (Figure 3e). Examination of other TCA cycle intermediates in 143Bcytb cells, including fumarate and malate, suggested that they were formed downstream of citrate m+5 and OAA m+3, as these cells contained

abundant malate and fumarate m+3, which was essentially absent from 143Bwt cells (Figure 3 b, c). Together, these data suggest that these metabolites are generated from reductive, rather than oxidative, glutamine metabolism. Interestingly, the succinate pool in 143Bcytb contained large amounts of m+3 and m+4 succinate, indicating succinate is formed through both reductive and oxidative glutamine metabolism in 143Bcytb cells (Figure 3d).

There are additional metabolic pathways independent of reductive carboxylation, which might account for citrate m+5 in cells cultured with U-^{13}C-gutamine. Specifically, this would require export glutamine-derived malate out of the TCA cycle and concurrent re-entry through the pyruvate carboxylase (PC) and pyruvate dehydrogenase (PDH) pathways, generating citrate with five ^{13}C atoms. To rule out this alternative explanation of our data, we cultured 143Bwt and 143Bcytb with additional metabolic tracers to specifically examine the reductive carboxylation pathway. Reductive carboxylation activity can be directly quantified with 1-^{13}C-labeled glutamine. Here, 1-^{13}C-glutamine generates αKG labeled on the first carbon, 1-^{13}C-αKG (Figure 4e) (Comte et al., 1997). During oxidative metabolism of αKG by alpha-ketoglutarate dehydrogenase (αKGDH) this carbon will be lost during conversion to succinyl-coA, generating unlabeled succinyl-coA (m+0); subsequent oxidative metabolism of will generate unlabeled fumarate, malate, OAA and citrate (Figure 4e). Thus, this ^{13}C-label will not be retained on any intermediates during oxidative TCA cycle activity. Alternatively, reductive carboxylation of 1-^{13}C-αKG through IDH will generate 1-^{13}C-citrate (citrate m+1). This ^{13}C will be retained during subsequent cleavage of citrate, generating OAA, malate and fumarate m+1 (where all are labeled at the 4-position carbon). In other words, detection of this ^{13}C-label will only occur if these metabolites are formed through the reductive carboxylation pathway. We cultured both 143Bwt and 143Bcytb cells with 1-^{13}C-glutamine and measured incorporation of ^{13}C into the TCA cycle intermediates (Figure 4a-d). We detected essentially no labeling in citrate or fumarate in 143Bwt cells, consistent with these metabolites being formed through oxidative TCA cycle activity. On the contrary, 143Bcytb showed robust citrate and

fumarate m+1 labeling. This pattern is consistent with these metabolites being formed through the reductive carboxylation pathway.

To validate that the four-carbon TCA cycle intermediates (malate, fumarate, succinate) were formed downstream of citrate cleavage, we cultured both 143Bwt and 143Bcytb in media containing 5-^{13}C-glutamine. Here, metabolism of 5-^{13}C-glutamine generates 5-^{13}C-αKG. During oxidative metabolism this carbon is retained in the TCA cycle on all of the four-carbon intermediates, generating OAA, fumarate, and malate m+1 (either or 1- or 4-position) (Figure 4e). Condensation of OAA with an unlabeled acetyl-coA generates citrate m+1. If the reductive carboxylation pathway is active, 5-^{13}C-αKG will be carboxylated to generate 5-^{13}C-citrate (also m+1). Importantly, during cleavage of citrate by ACL this ^{13}C will be retained on acetyl-coA and will not be incorporated into any of the four carbon intermediates formed downstream of citrate; generating malate and fumarate m+0. We cultured both 143Bwt and 143Bcytb cells with 5-^{13}C-glutamine and measured incorporation of ^{13}C into the TCA cycle intermediates (Figure 4 c, d). As expected, 143Bwt showed robust citrate and fumarate m+1. 143Bcytb also showed robust citrate m+1 and minimal labeling in fumarate. The presence of labeled citrate and lack of labeling in fumarate is consistent with formation of the four-carbon intermediates reductively, post-citrate cleavage. This experiment, together with the U-^{13}C- and 1-^{13}C-glutamine labeling data, excludes alternative metabolic pathways and confirms that reductive carboxylation of glutamine-derived αKG generates citrate, fumarate, malate and succinate in 143Bcytb.

We next assessed the effect of other amino acids not found in the 143B growth media (Dulbecco's Modified Eagles Medium, DMEM) on reductive carboxylation activity in 143Bcytb. To do this, we cultured 143Bwt and 143Bcytb in Roswell Park Memorial Institute (RPMI) medium, which contains the full complement of amino acids not found in DMEM media and studied the metabolism of U-^{13}C-glucose or U-^{13}C-glutamine in both cells. As in DMEM, 143Bcytb cells displayed minimal oxidation of glucose carbon in the mitochondria indicated by a reduced citrate m+2 (Figure 5a). Metabolism of U-

^{13}C-glutamine in 143Bcytb indicated fumarate/malate m+3 as well as citrate m+5, indicating robust reductive carboxylation activity (Figure 5 b-d). These data indicate that glutamine-dependent reductive carboxylation is active even in the presence of other oxidizable amino acids.

Reductive carboxylation requires the NADP/NADPH isoforms of Isocitrate dehydrogenase

There are three mammalian isoforms of isocitrate dehydrogenase (IDH), which differ based on their sub-cellular localization and co-factor preference (Figure 6a). To determine which of the three IDH isoforms contributed to reductive carboxylation, we used RNA interference (RNAi) to silence expression of IDH1 (isocitrate dehydrogenase 1 (NADP+, soluble), IDH2 (NADP+, mitochondrial) and IDH3 (NAD+, mitochondrial) in 143Bcytb cells and measured glutamine-derived ^{13}C labeling in citrate. Silencing either of the NADP+/NADPH dependent IDH isoforms, IDH1 or IDH2, reduced citrate m+5 in cells cultured with U-^{13}C-glutamine and silencing both at once further reduced citrate m+5 (Fig. 6b, c). Conversion of glutamine to glutamate was unaffected (Figure 6d). Silencing IDH3, the mitochondrial NAD/NADH-dependent isoform, had no effect on labeling (Figure 6 b, c). Thus, reductive carboxylation in 143Bcytb cells involves IDH1 and IDH2, but not IDH3.

We used immunofluorescence imaging of IDH1 and IDH2 to validate their sub-cellular localization in 143Bwt and 143BcytbB cells. IDH1 was found diffusely throughout the cytoplasm in both cell lines (Figure 7a). IDH2 protein was observed to co-localize with the mitochondrial-specific stain Mitotracker in both cell lines (Figure 7a). To independently validate these microscopy experiments, we also separated cystolic and mitochondrial fractions from 143Bwt and 143Bcytb and probed for IDH1 and IDH2 each in fraction. IDH1 was detected only in the cytoplasmic fraction and IDH2 was found only in the mitochondrial fraction, confirming the immunofluorescence experiments (Figure 7b). Together, these data indicate that reductive carboxylation requires either of the NADP/NADPH-dependent

isoforms IDH1 or IDH2. Additionally, these sub-cellular localization studies suggest that the reductive carboxylation reaction can occur in either the cytoplasm or mitochondrial compartments in 143Bcytb.

To determine whether IDH1 and IDH2 were required for growth, we stably silenced each enzyme using lentiviral RNAi. In 143Bwt cells, silencing either isoform reduced cell growth (Figure 8a,b), consistent with findings in other cancer cells with normal mitochondria(Ward et al., 2010). In 143Bcytb cells, a similar growth reduction occurred when either isoform was silenced (Figure 8 a,b). Thus both IDH1 and IDH2 support growth in cells that use glutamine-dependent reductive carboxylation.

Reductive carboxylation supports lipid synthesis

We next determined whether reductive glutamine metabolism contributed to lipogenesis, a biosynthetic activity required for cancer cell growth (Hatzivassiliou et al., 2005). Both 143Bwt and 143Bcytb cells produced fatty acids *de novo*, as indicated by incorporation of $^{3}H_2O$ into lipids (Figure 9a). The two cell lines were then cultured with ^{14}C-labelled lipogenic substrates to examine carbon preferences for lipogenesis (Figure 9 b-d). Both cell lines had an intact pathway of lipogenesis from exogenously supplied acetate. The enhanced labeling in 143Bcytb cells probably resulted from an increased specific activity of the intracellular two-carbon pool because of suppressed PDH. Lipids derived from 143Bcytb cells contained little radioactivity from glucose (Figure 9c), but abundant radioactivity from glutamine (Figure 9d), indicating a switch in the extent to which these nutrients supplied lipogenesis.

To quantify the contribution of glucose and glutamine to lipogenic acetyl-CoA, cells were cultured in medium containing either U-^{13}C-glucose and unlabelled glutamine, or U-^{13}C-glutamine and unlabelled glucose. Extracted lipids were analyzed by ^{13}C NMR. Because fatty acids are synthesized by the sequential addition of two-carbon units, analyzing ^{13}C–^{13}C coupling between the ω-1 and ω-2 carbons—which enter the fatty acyl-chain on different two-carbon units—enables calculation of ^{13}C

enrichment in lipogenic acetyl-CoA (DeBerardinis et al., 2007). In the ω-1 multiplet, ^{13}C–^{13}C coupling produces a triplet when two ^{13}C-labelled two carbon units are added in succession, whereas one labeled and one unlabelled unit produce a doublet (Figure 9e). Therefore ^{13}C labeling in lipogenic acetyl-CoA is proportional to the contribution of the triplet to the overall area of the ω-1 multiplet. In 143Bwt cells cultured with U-^{13}C-glucose, the ω-1 resonance was dominated by the triplet, which accounted for 65% of the total area (Figure 9f, left). Glutamine was a minor source of fatty acyl carbon, as the triplet accounted for only 15% of the area when the cells were cultured with U-^{13}C-glutamine (Figure 9f, right). This pattern was reversed in the 143Bcytb cells, with glutamine providing 67% of the lipogenic carbon (Figure 9g). Thus, reductive glutamine metabolism was the major pathway of fatty acid production in newly synthesized lipids during 143Bcytb growth.

Reductive carboxylation supports TCA cycle function in Fumarate Hydratase deficient cancer cells

Although most cancer cells have functional mitochondria, a subset of human tumors harbors mutations that impair mitochondrial metabolism (Mullen and DeBerardinis, 2012). Two major classes of mutations occur in genes required for function of the TCA cycle enzymes succinate dehydrogenase (SDHA, SDHB, SDHC, SDHD, SDH5) or fumarate hydratase (FH) (Yang et al., 2012). To test whether glutamine-dependent reductive carboxylation occurs in tumor cells harboring these mutations, we studied UOK262 cells derived from a renal tumor in a patient with hereditary leiomyomatosis renal cell carcinoma syndrome (HLRCC) (Yang et al., 2010). In this syndrome, affected individuals inherit one loss-of-function FH allele and their tumors display loss of heterozygosity for the wild type FH locus (Tomlinson 2002). UOK262 cells are defective in respiration and are devoid of FH enzyme activity (Yang et al., 2010) . They failed to survive culture in glucose-free medium containing galactose and glutamine (Figure 10a), a condition that forces cells to use mitochondrial metabolism to generate ATP (Rossignol et al., 2004). Lack of FH activity precludes the use of glutamine as a carbon source in the conventional

oxidative TCA cycle. Yet the UOK262 cells required glutamine to proliferate (Figure 10b). UOK262 cells stably expressing functional fumarate hydratase (UOK262FH) have recently been generated, allowing us to study the metabolic consequence of the add-back of functional FH in these cells (Tong et al., 2011). We quantified the levels of several TCA cycle intermediates in both vector controlled (UOK262EV) and UOK262FH cell lines. As expected, fumarate was found to be extremely elevated in UOK262EV cells; this large pool was mostly suppressed in UOK262FH cells (Figure 10c). Interestingly, despite lacking FH activity UOK262EV had small but detectable pools of malate and citrate (Figure 10d, e).

We studied the contribution of U-^{13}C-glucose and U-^{13}C-glutamine to the TCA cycle in UOK262EV and UOK262FH. Culture of these cells with U-^{13}C-glucose produced mass isotopomer data similar to 143Bcytb cells, with minimal formation of citrate m+2 in UOK262EV (Figure 11a). UOK262FH had substantially higher citrate m+2, indicating increased oxidative citrate formation. To study glutamine metabolism in these cell lines we cultured UOK262EV and UOK262FH with U-^{13}C-glutamine and analyzed ^{13}C incorporation in several TCA cycle intermediates. In UOK262EV, the most abundant mass isotopomer of citrate was m+5, indicating it was formed through the reductive pathway (Figure 11b). Alternatively, UOK262FH showed pronounced oxidative citrate formation, indicated by citrate m+4, but modest citrate m+5, indicating these cells still retain some degree of reductive metabolism. In both cell lines, fumarate was predominantly formed through oxidative glutamine metabolism, producing fumarate m+4 (Figure 11c). However, in UOK262EV a large fraction of the malate pool (m+3) was formed via citrate cleavage and subsequent reductive metabolism (Figure 11d). UOK262FH contained predominately malate m+4, indicating it was formed through oxidative TCA cycle activity. Lipid labeling in UOK262 using U-^{13}C-glucose or U-^{13}C-glutamine revealed that, like 143Bcytb cells, glutamine is the major carbon source for fatty acid synthesis in cells lacking functional FH activity (Figure 11e). Thus these FH deficient cancer cells produce TCA cycle intermediates using two distinct pathways to compensate for the loss of FH enzyme activity: oxidative metabolism of glutamine to fumarate, and glutamine-dependent reductive

carboxylation to produce citrate, acetyl-CoA for lipogenesis and remaining four-carbon TCA cycle intermediates. These data also indicate that reconstitution with functional FH is sufficient to revert UOK262 to oxidative TCA cycle function.

Reductive carboxylation supports the TCA cycle in Complex I deficient cells

We next tested if reductive carboxylation was present in other established models of mitochondrial dysfunction. We studied the metabolism of CCL16-B2 Chinese hamster cells which contain a truncating mutation in the *NDUFA1* gene, resulting in a severe defect of ETC Complex I activity and respiration (Au et al., 1999). We compared these cells to CCL16 cells stably expressing the saccharomyces ceevisiae NADH-quinone oxidoreductase (CCL16-*NDI1*), which has been shown to partially restore the respiration of these cells (Seo 1998). Culture of these cells with U-^{13}C-glutamine revealed that the reductive carboxylation pathway is the dominant pathway of citrate, fumarate and malate formation in CCL16 cells (Figure 12a-c). Partial restoration of Complex I activity in CCL16-NDI1 cells significantly enhanced fumarate, malate and citrate m+4, indicating oxidative TCA cycle function in these cells. These data indicate that glutamine-dependent reductive carboxylation is the dominant pathway of citrate formation in cells lacking functional Complex I activity.

Reductive carboxylation contributes to citrate production in TFAM deficient mouse keratinocytes

The Mitochondrial Transcription Factor A (TFAM) is required for the transcription and replication of mtDNA. Deficiency in TFAM causes reduced mtDNA content and reduced electron transport chain activity, leading to widespread mitochondrial dysfunction (Campbell et al., 2012). Based on the observations that dysfunction of either ETC Complex I or III induced reductive carboxylation, we studied whether lack of TFAM could also induce reductive carboxylation. We studied the metabolism of primary mouse keratinocytes containing or lacking the *TFAM* gene. Culture of these cells with U-^{13}C-glucose

revealed large citrate m+2 in both cell lines (Figure 13a). TFAM deficient cells had a substantially higher fraction of unlabeled citrate, indicating reduced overall incorporation of glucose carbon in these cells. Culture of these cells with U-^{13}C-glutamine indicated TFAM deficient cells had a modest increase in citrate m+5 compared with control cells (Figure 13b). These data indicate that reductive carboxylation contributes a small fraction of citrate in cells lacking TFAM but, overall, TFAM-deficient cells do not exhibit profound changes in glucose or glutamine metabolism.

Reductive carboxylation supports TCA cycle function in VHL deficient cells

The Von-Hippel-Lindau (VHL) tumor suppressor negatively regulates the expression of HIF-α and is frequently observed to be inactivated in tumors (Kaelin and Ratcliffe, 2008). Stabilization of HIF-α induces a pseudohypoxia gene expression signature which has been shown to decrease oxidative metabolism through inhibition of PDH activity (Majmundar et al., 2010). The consequences of this on TCA cycle function are unknown. To determine if glutamine-dependent reductive carboxylation is active under these circumstances, we studied the metabolism of the human clear-cell renal carcinoma cell line which lack functional VHL (786-O-EV) (Biswas et al., 2010). We compared these cells to 786-O stably expressing functional VHL (786-O-VHL) (Kucejova et al., 2011). To study the contribution of glucose to the TCA cycle in these two cell lines we cultured each with U-^{13}C-glucose. 786-O-EV had suppressed citrate m+2 compared to 786-O-VHL, indicating reduced entry of glucose carbon into the TCA cycle (Figure 14a). This is consistent with HIF negatively regulating oxidative metabolism, as 786-O-VHL had substantially higher citrate m+2. To examine the fate of glutamine metabolism we cultured these cells with U-^{13}C-glutamie. 786-O-EV cells cultured with U-^{13}C-glutamine revealed large citrate m+4 and modest citrate m+5, indicating that these cells generated citrate through both oxidative and reductive glutamine metabolism (Figure 14a-c). 786-O-VHL cells showed lower citrate m+5, indicating that introduction of functional VHL is sufficient to suppress reductive carboxylation activity. These results

indicate reductive carboxylation is active in cells lacking functional VHL, suggesting this pathway compensates for reduced glucose-dependent citrate formation.

Suppression of c-Myc in 132OS cells induces reductive carboxylation

The c-Myc transcription factor regulates transcription of a suite of genes involved in mitochondrial biogenesis and metabolism (Dang et al., 2009a). We studied the metabolism of c-Myc-dependent mouse osteogenic sarcoma cells (1320S) in which c-Myc expression can be suppressed following treatment with doxycycline; inactivation of c-Myc causes these cells to differentiate into osteocytes within 48 hours (Jain et al., 2002). We found that suppressing c-Myc resulted in a significant decrease in glucose consumption and lactate secretion, while no change was found in glutamine consumption (Figure 15b,c). To study the contribution of glucose to citrate formation following c-Myc suppression we cultured 132OS cells +/- doxycycline with U-^{13}C-glucose and analyzed incorporation of ^{13}C into citrate. Suppression of c-Myc resulted in a modest, decrease in citrate m+2 and m+4, indicating reduced glucose oxidation in the mitochondria of the osteocytes (Figure 15e). To determine the metabolic fate of glutamine following inactivation of c-Myc we cultured 132OS cells with U-^{13}C-glutamine in the absence or presence of doxycycline and assayed ^{13}C incorporation into citrate. Suppression of c-Myc resulted in decreased citrate m+4 and increased citrate m+5, indicating reduced oxidative TCA cycle function and enhanced reductive carboxylation activity (Figure 15f). These data indicate that reductive carboxylation can support TCA cycle activity under conditions of c-Myc inactivation.

Inhibitors of the ETC induce reductive carboxylation

We tested whether or not glutamine-dependent reductive carboxylation was unique to cells with permanent abnormalities in mitochondrial metabolism. We cultured 143Bwt cells and transformed

mouse embryonic fibroblasts (MEFs) with U-^{13}C-glutamine and subjected them to acute ETC inhibition using poisons of the ETC (Figure 16a). Exposure to inhibitors of complex I (rotenone or metformin) or complex III (antimycin) induced a dramatic decrease in citrate m+4 and large increase in citrate m+5, indicating a switch from oxidative to reductive TCA cycle activity in both cell lines (Figure 16b-d). Metformin is a widely prescribed antidiabetic agent that inhibits respiration through effects on complex I (Owen et al., 2000). To determine the physiological relevance of this concentration to that administered to patients, we assayed various doses of metformin for their ability to induce reductive carboxylation in 143Bwt cultured with U-^{13}C-glutamine. Interestingly, doses that mimicked plasma concentrations in patients with acute metformin toxicity and lactic acidosis induced reductive glutamine metabolism (Figure 16d).

To test how quickly reductive carboxylation could be induced following ETC inhibition we cultured 143Bwt cells with U-^{13}C-glutamine and rotenone and analyzed reductive carboxylation at one hour time points (Figure 17a). We identified reductive carboxylation activity as early as one hour following ETC inhibition. Next, to determine if the switch to reductive TCA cycle activity required new protein synthesis, we pre-treated 143Bwt cells with the protein synthesis inhibitor cycloheximide. We then cultured these cells with U-^{13}C-glutamine with or without rotenone (Figure 17b). Despite slightly lower metabolic activity in the presence of cycloheximide, rotenone induced a significant increase in citrate m+5 even in the cells unable to synthesize new proteins. These results indicate that ETC inhibitors rapidly induce reductive carboxylation through a mechanism that does not require new protein synthesis.

Discussion

Oxidative metabolism of glucose and glutamine in the mitochondria supports production of precursors for macromolecular synthesis in cancer cells (Deberardinis et al., 2008). Yet, some tumors harbor mutation in the TCA cycle or ETC that disable normal oxidative metabolism and it has been unknown how these cells generate precursors for macromolecular synthesis. We hypothesized that these cells generated biosynthetic intermediates through unique metabolic pathways.

In this study, we identified an unusual metabolic pathway common among cells with mitochondrial defects termed reductive carboxylation. This pathway was observed in several models of mitochondrial dysfunction, including those lacking activity of ETC Complex I and III or the TCA cycle enzyme FH. This pathway has been previously observed to contribute a small fraction of citrate in mammalian cells(Comte et al., 1997; Des Rosiers et al., 1994; Lemons et al., 2010; Ward et al., 2010; Yoo et al., 2008) In cells with mitochondrial defects, we found reductive carboxylation to be the major pathway of citrate formation. Additionally, inhibitors of ETC activity were found to acutely induce reductive carboxylation in cells lacking mitochondrial defects. This reaction was found to require the NADP/NADPH isoforms of IDH, suggesting it could occur in either the cytoplasm or mitochondria. Moreover, we found that reductive carboxylation in 143Bcytb required the activity of both isoforms, suggesting non-redundant roles of each IDH1 and IDH2. Cleavage of citrate derived through reductive carboxylation was found to generate the majority of the acetyl-coA used for lipid synthesis. Cleavage of citrate was also found to support the production of the four-carbon intermediates of the canonical TCA cycle. Together, these data indicate that cells with metabolic dysfunction use reductive glutamine metabolism to support production of important biosynthetic intermediates.

Reductive glutamine metabolism was also observed in cells lacking a primary metabolic disturbance. In 786-O cells lacking functional VHL, the reductive carboxylation pathway was found to contribute to a substantial fraction of citrate production. These cells have constitutive upregulation of

HIF-2α and induction of HIF-2α target genes in normoxic conditions (Biswas et al., 2010). Consistent with this pseudohypoxic state, we found these cells to have reduced glucose oxidation in the TCA cycle, presumably due to HIF-mediated inhibition of PDH activity. This suggests reductive carboxylation allows cells to compensate for reduced glucose-dependent citrate formation. UOK262 cells also have constitutive HIF activation and a pseudohypoxic gene expression signature (Sullivan et al., 2013; Yang et al., 2010), suggesting a role for HIF in regulating reductive carboxylation independent of the primary metabolic disturbance in these cells. Differentiation of 132OS cells following suppression of c-Myc was also found to induce modest reductive carboxylation activity. This is consistent with a previous report indicating that contact-inhibited fibroblasts exit the cell cycle and exhibit enhanced reductive carboxylation activity (Lemons et al., 2010). Similarly, *TFAM* knockout mouse keratinocytes were found to generate a small fraction of citrate through reductive carboxylation. TFAM regulates mtDNA gene transcription, making it an indirect regulator of overall ETC function. In this context, reductive carboxylation is likely the result of reduced ETC activity. Recently, reductive carboxylation has also been observed in cells growing under conditions of hypoxia (Metallo et al., 2012; Wise et al., 2011). Collectively, these results indicate that reductive carboxylation is a shared metabolic pathway among cells with mitochondrial defects or those with impaired mitochondrial function. Additionally, induction of reductive carboxylation following chemical inhibition of ETC activity suggests this pathway allows cells to cope with interferences of normal ETC activity.

The molecular mechanisms regulating this pathway are still unclear. We detected reductive carboxylation as early as one hour after chemical inhibition of ETC activity. Additionally, pre-treatment of cells with a protein synthesis inhibitor had no effect on this induction. Together, these results indicate that cells can rapidly switch from oxidative to reductive TCA cycle activity through a mechanism that does not require changes in gene expression or enhanced protein synthesis. One such mechanism could be a disturbance of the redox ratio. Inhibition of proper ETC activity (through poisons or genetic defects)

would prevent cells from recycling NADH, leading to a low NAD/NADH ratio. HIF-mediated suppression of PDH activity has also been shown to alter this ratio. In these cells, treatment with the PDH activator dichloroacetate (DCA) has been shown to ablate HIF-mediated reductive carboxylation in normoxia (Metallo et al., 2012). A low NAD/NADH ratio would create a reduced state in the mitochondria that might potentially favor reductive glutamine metabolism. First, this ratio could stimulate the mitochondrial NAD(P)-transhydrogenase, which transfers reducing equivalents from NADH to NADPH. This would be predicted to favor reductive, and not oxidative, citrate formation through NADPH-dependent IDH1 and IDH2. A reduced mitochondrial redox potential would also favor reductive TCA cycle reactions, such as conversion of OAA to malate, as this and several other TCA cycle reactions are freely reversible based on product/substrate and/or NAD/NADH ratios (Salway, 2004). This theory could be tested by studying the redox ratio in cells where reductive carboxylation reaction is active and inhibiting transhydrogenase function.

The reductive carboxylation pathway is an attractive therapeutic target for several reasons. First, in most tissues this pathway appears to serve a redundant role and is thus minimally engaged, if at all. However, in cells with metabolic defects (such as HLRCC) which are unable to engage the conventional metabolic pathways, reductive carboxylation serves as the primary, and potentially only, pathway of precursor production available. This suggests that inhibiting this activity *in vivo* would not interfere with the growth of normal cells and would be synthetically lethal only to cells with metabolic defects or cells in hypoxic regions of tumors. The most direct method to inhibit this pathway would be to target the IDH enzymes. We found that targeting either IDH1 or IDH2 suppressed growth of 143Bcytb and also 143Bwt cells, which do not use reductive carboxylation but none the less require IDH1/2 for growth. Thus, inhibiting IDH1 or IDH2 would not be a way to selectively kill tumor which grow through reductive carboxylation. Rather, studying the mechanisms regulating this pathway has the potential to expose metabolic vulnerabilities specific to cells with mitochondrial defects.

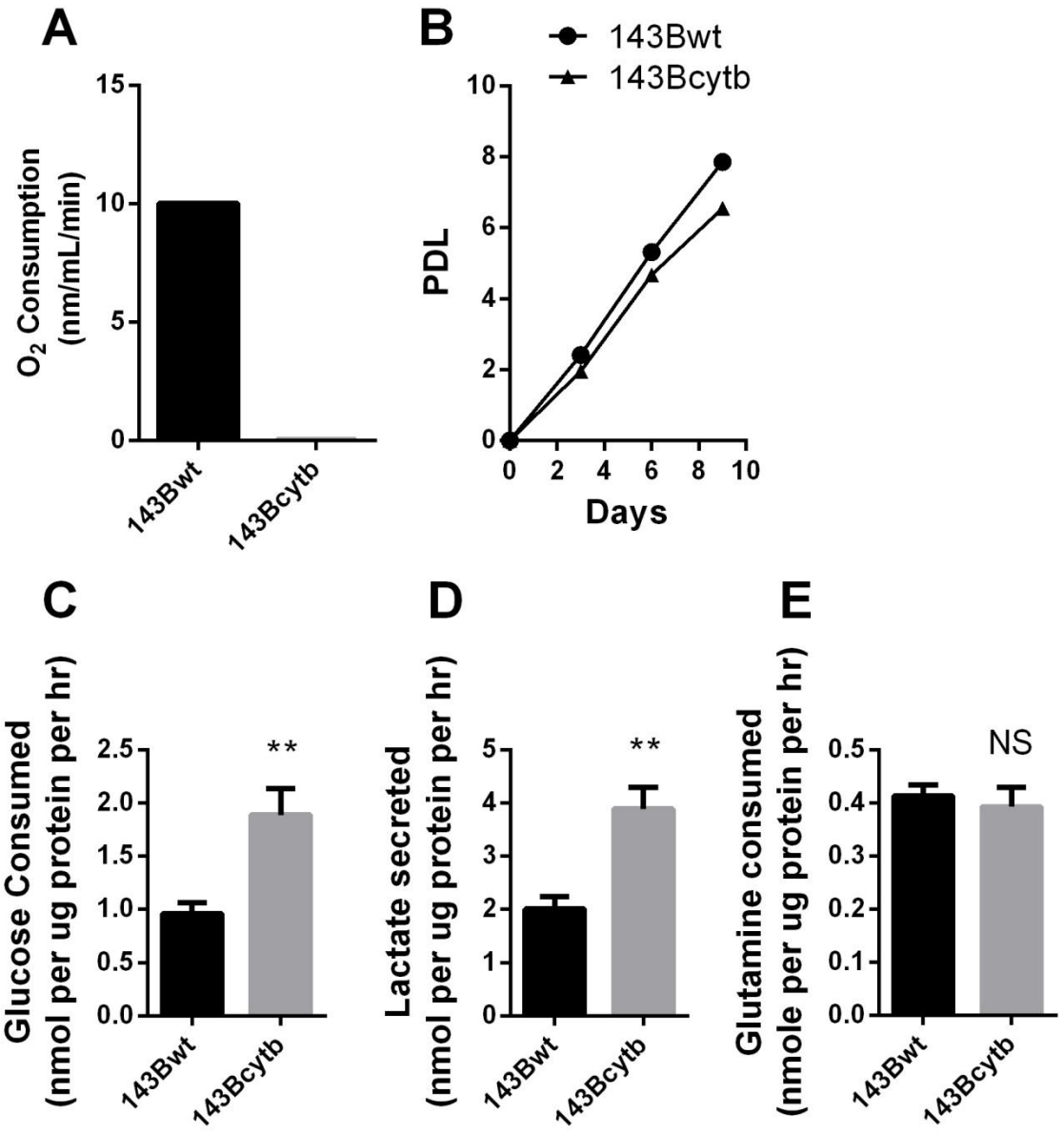

Figure 2.1. Metabolic characterization of 143B cells.
(a) Oxygen consumption rate of 143B cells. **(b)** Population doubling levels of 143Bwt and 143Bcytb cells. Doubling times were 28±1 and 33±2 hrs for 143Bwt and 143Bcytb cells, respectively. **(c- e)** Glucose utilization, lactate secretion and glutamine utilization in 143Bwt and 143Bcytb cells. Data are the average and s.d. for three independent cultures. *P,0.05; **P,0.005, Student's t-test

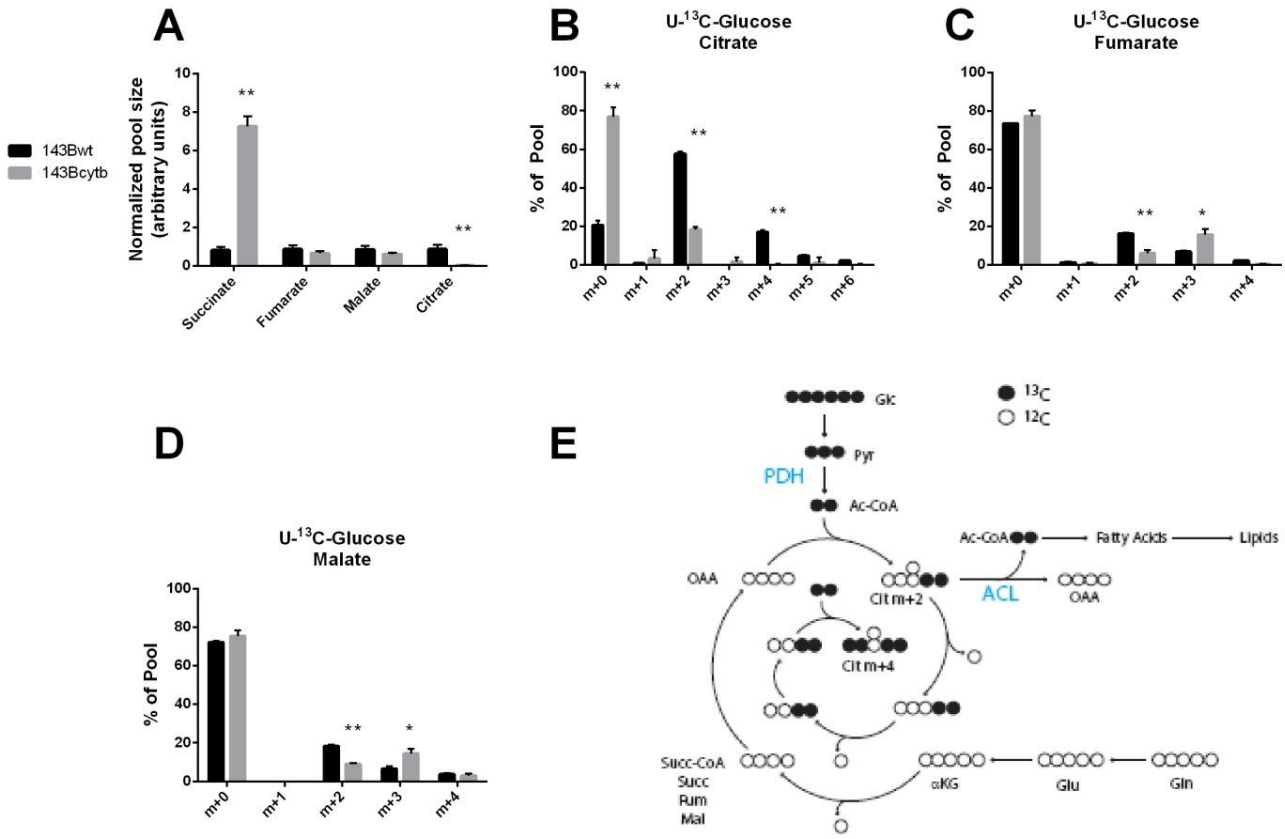

Figure 2.2. Cells lacking functional ETC activity have reduced glucose oxidation in the TCA cycle
(a) Relative pool sizes of succinate, fumarate, malate and citrate 143Bwt and 143Bcytb, normalized to 143Bwt. **(b, c, d)** Mass isotopomer distribution of citrate, fumarate and malate in cells cultured with U-^{13}C-glucose and unlabeled glutamine. **(e)** Schematic for metabolism of U-^{13}C-glucose. Metabolism of U-^{13}C-glucose produces uniformly ^{13}C-labeled pyruvate (Pyr) and, if pyruvate dehydrogenase (PDH) is active, uniformly ^{13}C -labeled acetyl-coA. In 143Bwt cells, a large flux from unlabeled glutamine (Gln) fills the TCA cycle from a-ketoglutarate to oxaloacetate (OAA). Thus, condensation of OAA with acetyl-coA produces citrate (cit) containing two ^{13}C -atoms (Citrate m+2). Much of this ^{13}C exits the cycle for use in lipid synthesis and other reactions, but some of it is oxidized within the TCA cycle to produce a modest amount of fumarate, malate and OAA m+2. If this condenses with labeled Ac-coA, citrate m+4 is produced. Data are the average and s.d. for three independent cultures. *P,0.05; **P,0.005, Student's t-test.

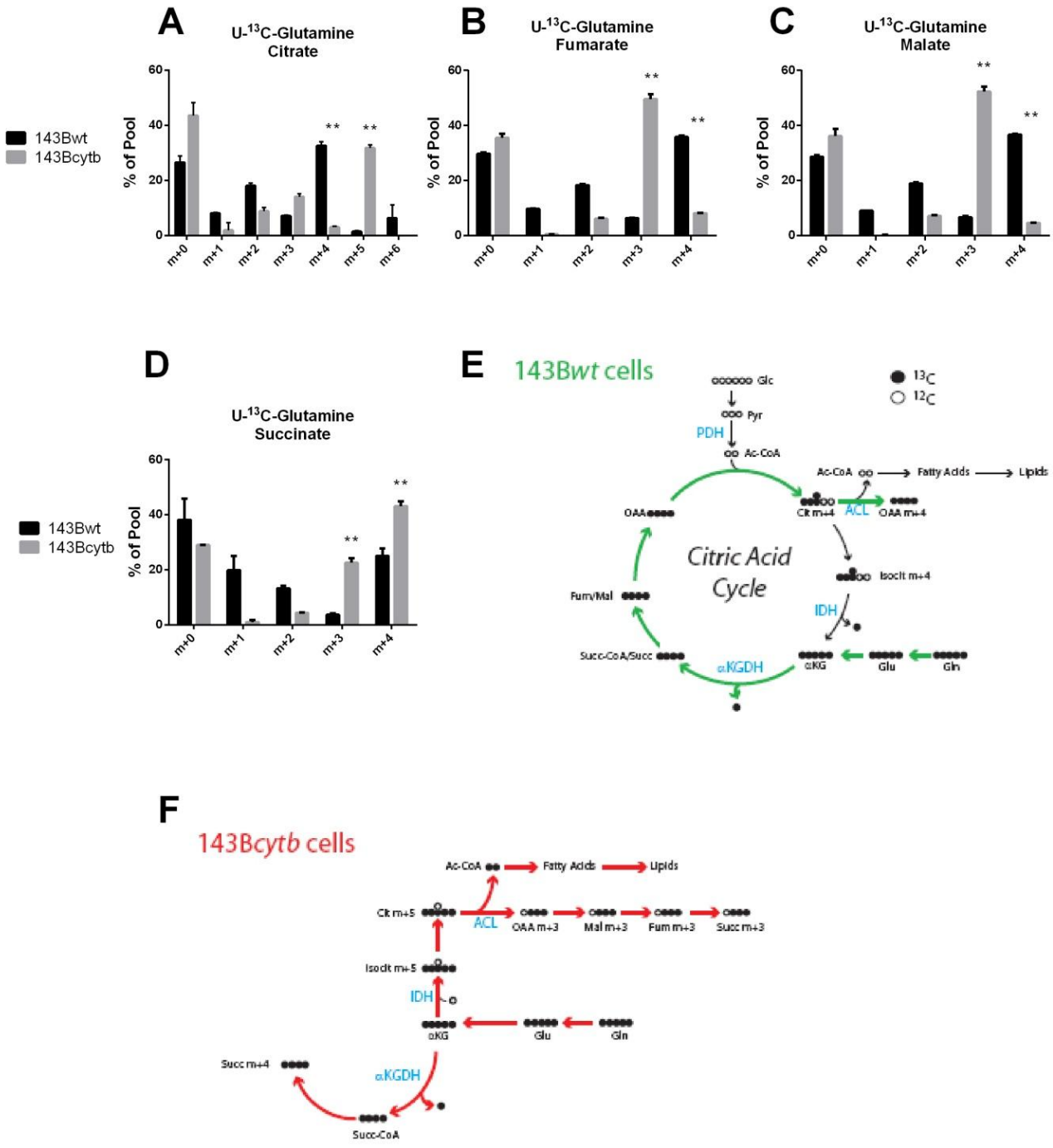

Figure 2.3: A reductive pathway of glutamine metabolism in cells lacking functional ETC activity.
d) Mass isotopomers distribution of citrate, fumarate and malate and succinate in cells cultured with U-^{13}C-glutamine and unlabeled glucose **(e,f)** Schematic for metabolism of U-^{13}C-glutamine in 143Bwt and 143Bcytb cells. In 143Bwt cells and other cells with normal TCA activity (top, green pathway), metabolism of U-^{13}C -glutamine produces uniformly ^{13}C-labeled TCA intermediates from α-ketoglutarate to oxaloacetate (αKG to OAA). Condensation of labeled OAA with glucose-derived (unlabeled) acetyl-coA produces Cit m+4, which can exit the cycle. Cleavage by ATP-citrate lyase (ACL) generates unlabeled

Figure 2.3 Continuted:
acetyl-coA, which is used for lipid synthesis, and OAA m+4, which can be metabolized further following any of several routes. Acetyl-CoA can also be produced from glutamine by oxidative decarboxylation of malate to pyruvate (not shown), followed by pyruvate dehydrogenase (PDH) activity. In 143Bcytb cells and other cells using reductive carboxylation (bottom, red pathway), glutamine-derived αKG is reduced to isocitrate/citrate m+5, incorporating one unlabeled carbon. Cleavage of Cit m+5 produces OAA m+3 (bearing the unlabeled carbon) and uniformly labeled acetyl-coA for lipid synthesis. Subsequent reductive metabolism of OAA m+3 produces additional m+3 TCA intermediates such as malate, fumarate and succinate (Mal, Fum, Succ). In 143Bcytb cells, there is also oxidative metabolism of αKG to succinate, producing a succinate pool that is a mixture of m+3 and m+4 isotopomers. Abbreviations: Glu, glutamate; Succ-CoA,succinyl-CoA; Isocit, isocitrate; αKGDH, αKG dehydrogenase. Data are the average and s.d. for three independent cultures. *P,0.05; **p,0.05, Student's t-test.

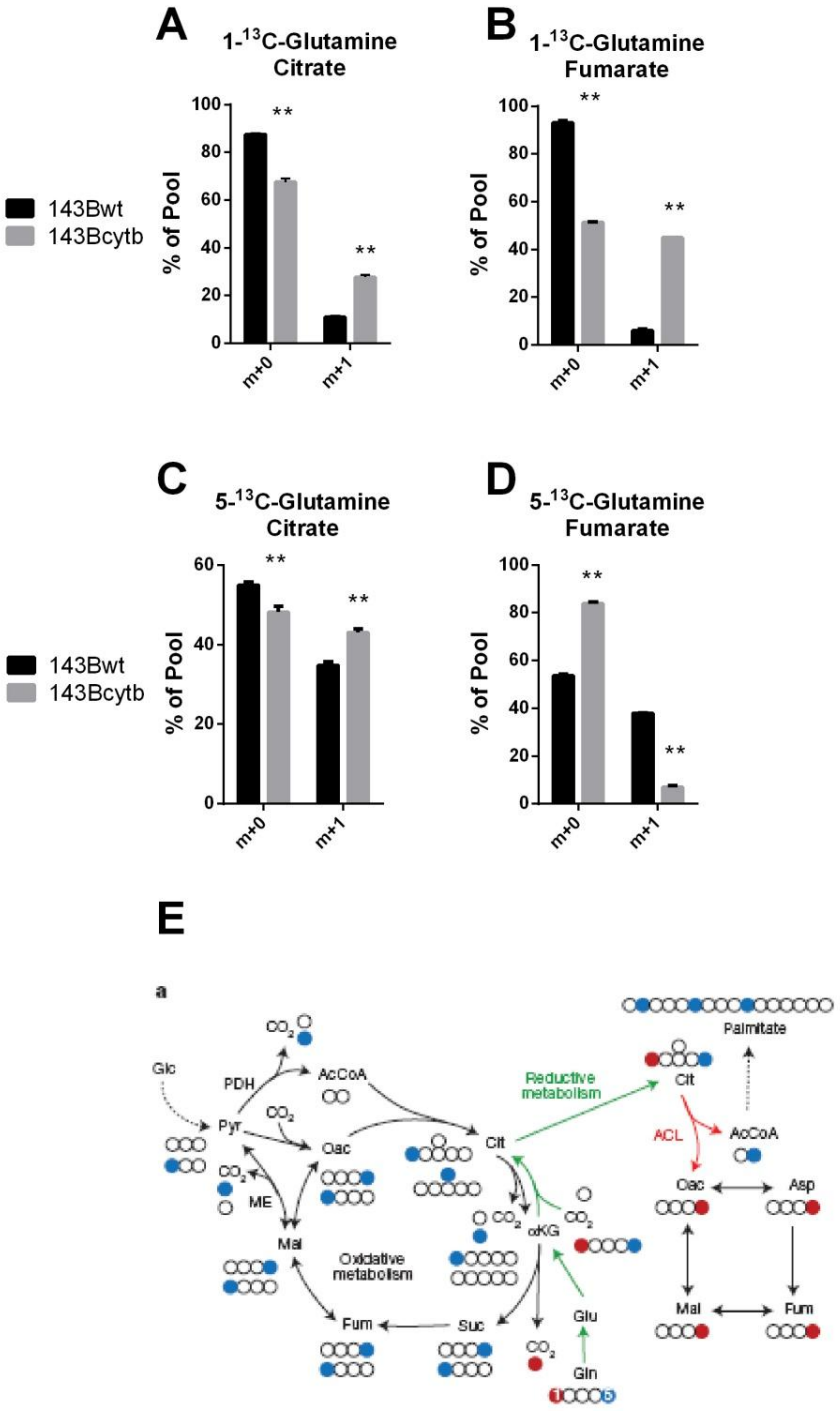

Figure 2.4. Validation of reductive carboxylation in 143Bcytb using alternative isotopically labeled nutrients

(a) Citrate and mass isotopomers m+0 and m+1 and **(b)** fumarate mass isotopomers m+0 and m+1 in 143Bcytb cells cultured with 1-^{13}C-glutamine and unlabeled glucose. **(c,d)** Citrate and fumarate mass isotopomers in 143Bcytb cells cultured with 5-^{13}C-glutamine and unlabeled glucose. **(e)** Schematic of 1-^{13}C-glutamine and 5-^{13}C-glutamine in 143B cells. 1-^{13}-C-glutamine (red circle) is metabolized to produce 1-^{13}C-αKG. Oxidative metabolism of 1-^{13}C-αKG releases the ^{13}C-label as CO_2. If reductive pathway is

Figure 2.4 Continuted:
active, 1-^{13}C-αKG is reduced to generate 1-^{13}C-citrate (green pathway). Cleavage of this citrate by ACL generates unlabeled acetyl-coA (AcCoA) and OAA, malate, and fumarate m+1. Metabolism of 5-^{13}C-glutmaine (blue position) is metabolized to produce 5-^{13}C-αKG. Oxidative TCA cycle activity this ^{13}C-label is retained on all the intermediates to generate citrate, fumarate m+1. Reductive metabolism generates 5-^{13}C-citrate which is cleaved. The ^{13}C-label is retained on acetyl-coA and is not incorporated into OAA, Mal, or Fum. Figure from (Metallo et al., 2012). Data are the average and s.d. for three independent cultures. *P,0.05; **P,0.005, Student's t-test.

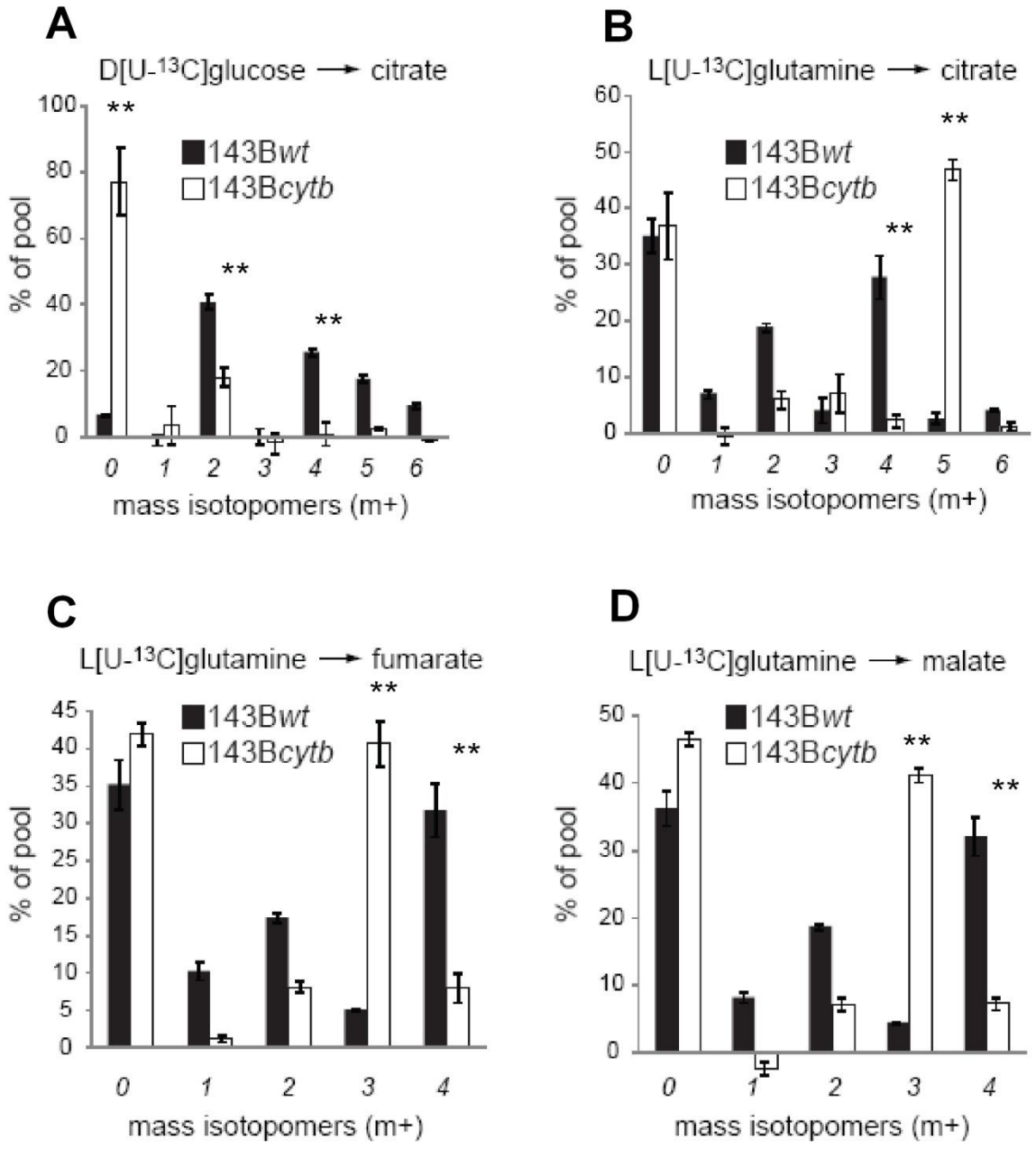

Figure 2.5. Glutamine-dependent reductive carboxylation in Roswell Park Memorial Institute (RPMI) Media

(a) Mass isotopomer distribution of citrate in 143Bwt and 143Bcytb cultured with U-^{13}C-glucose and unlabeled glutamine in RPMI media. **(b, c, d)** Mass isotopomer distribution of citrate, fumarate and malate in 143Bwt and 143Bcytb cultured with U-^{13}C-glutamine and unlabeled glucose in RPMI media. Data are the average and s.d. for three independent cultures. *P,0.05; **P,0.005, Student's t-test.

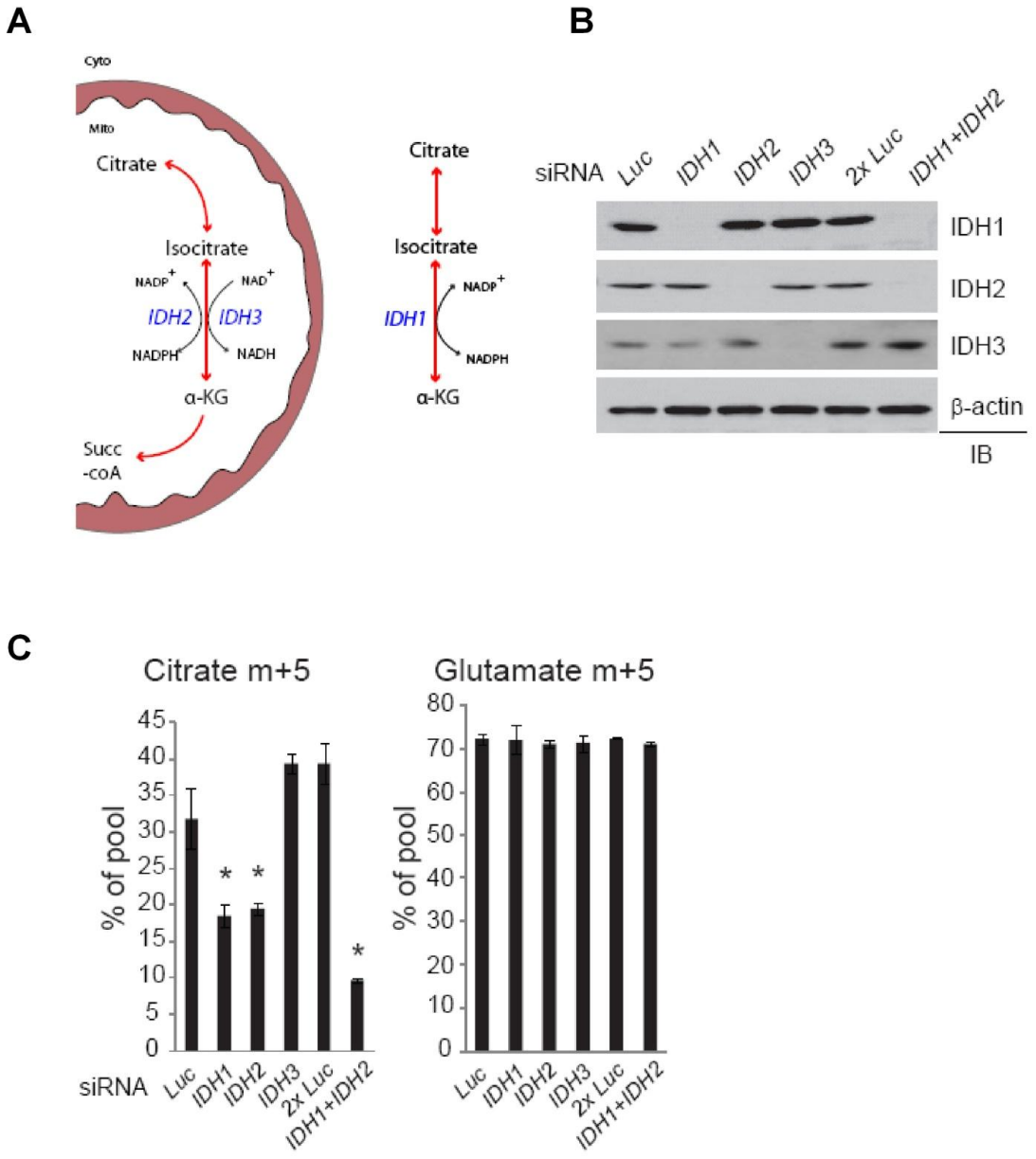

Figure 2.6. NADP/NADPH-dependent isoforms of isocitrate dehydrogenase contribute to reductive carboxylation 143Bcytb

(a) Schematic of isocitrate dehydrogenase (IDH) isoforms showing sub-cellular localization and co-factor preference. **(b)** Transient silencing of isocitrate dehydrogenase (IDH) proteins in 143Bcytb cells with short interfering RNAs (siRNAs) directed against IDH1, IDH2 or IDH3. An siRNA directed against luciferase (Luc) was used as a negative control. When IDH1 and IDH2 siRNAs were transfected concurrently (IDH1+IDH2), a transfection with the same nanomolar amount of Luc siRNA(2xLuc) was used as a negative control. **(c)** Mass isotopomer analysis of citrate and glutamate in 143Bcytb cells cultured with U-^{13}C-glutamine after silencing of IDH isoforms. Abbreviations: αKG, alphaketoglutarate; succ-coA, succinyl-coA. Data are the average and s.d. of three independent cultures. *P,0.05, Student's t-test.

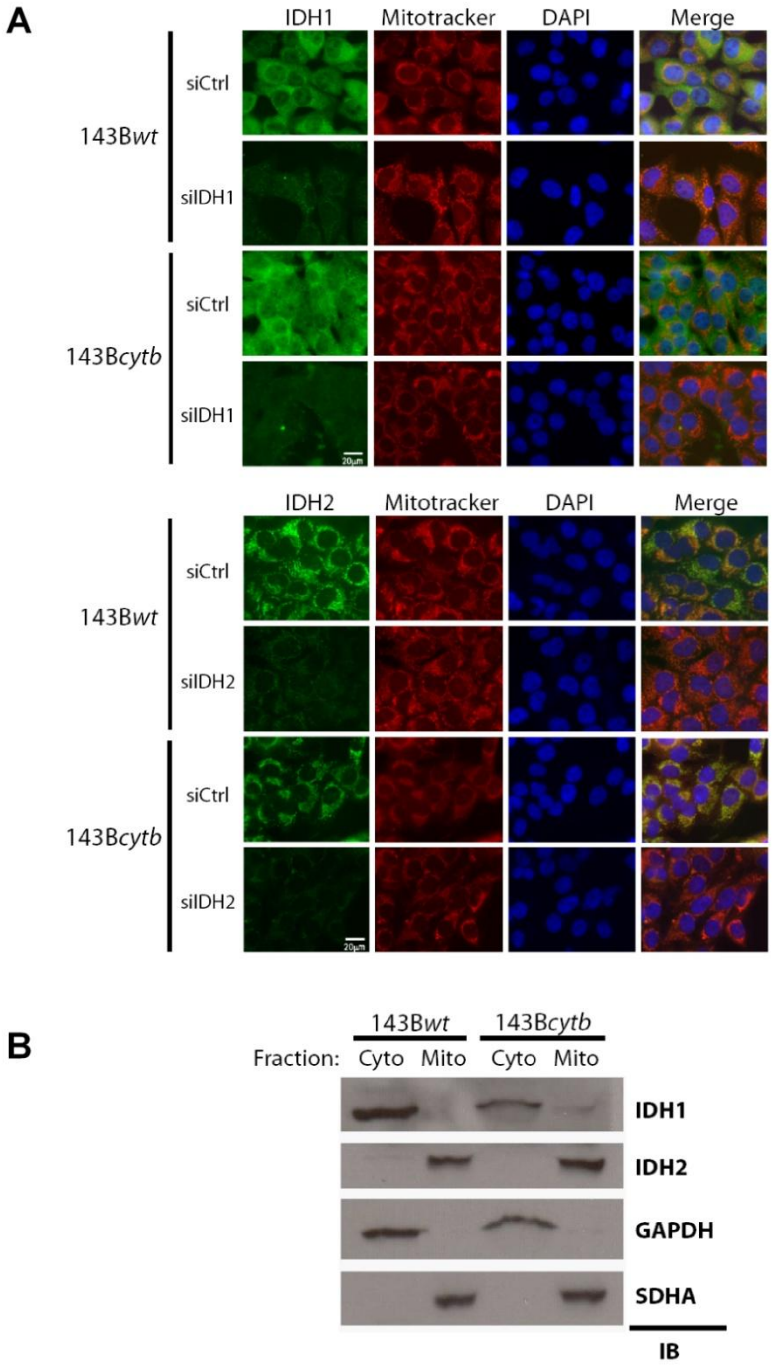

Figure 2.7.Sub-cellular localization of IDH1 and IDH2 are not altered in 143Bcytb cells
(a) Immunofluoresence of 143Bwt and 143Bcytb cells using antibodies against IDH1 (Top panels) or IDH2 (bottom panels). Cells were also transiently transfected with control (Ctrl) siRNAs or siRNAs directed against IDH1 or IDH2 to verify isoform specificity of the antibodies. **(b)** cytoplasmic and mitochondrial sub-cellular fractions of 143Bwt and 143Bcytb probed for IDH1, IDH2, glyceraldehydes-3-phosphate dehydrogenase (GAPDH, a cytoplasmic control) and succinate dehydrogenase subunit A (SDHA, a mitochondrial control). Abbreviations, DAPI; 4',6-Diamidino-2-Phenylindole, Dihydrochloride.

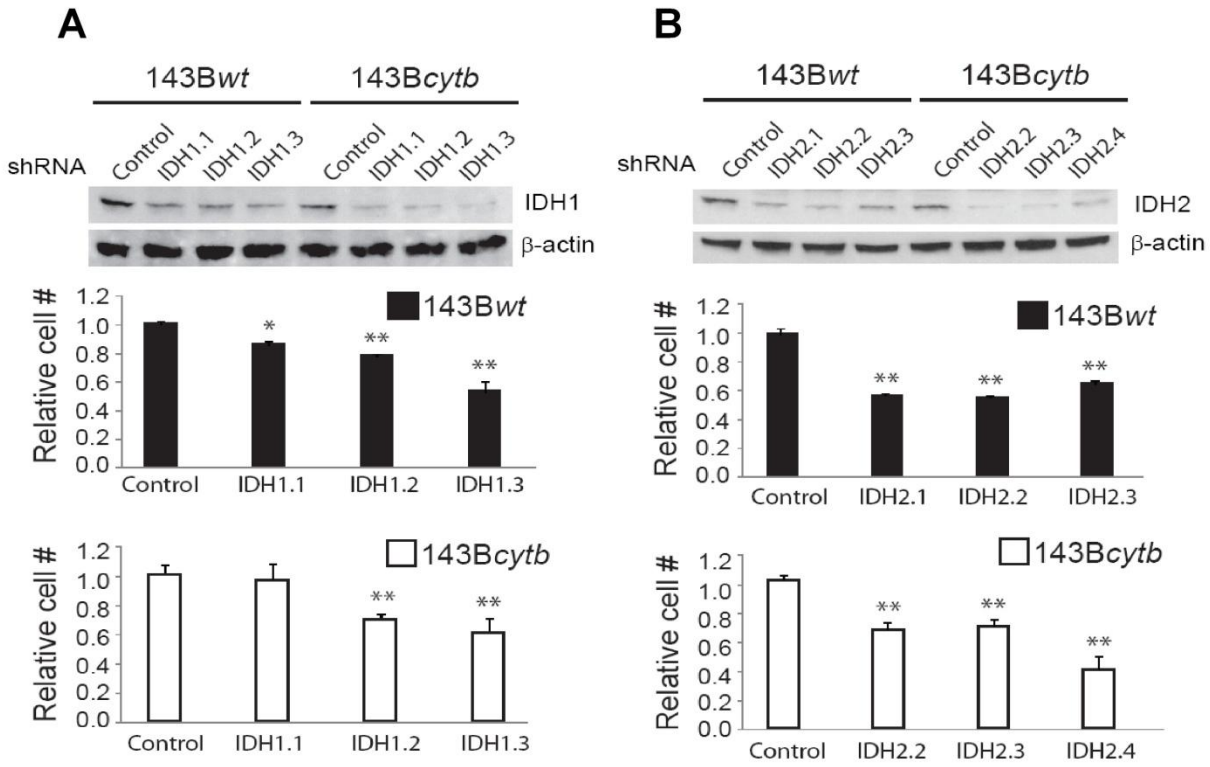

Figure 2.8. IDH1 and IDH2 are required for the growth of both 143Bwt and 143Bcytb
(a and b) Immunoblot showing protein expression of IDH1 or IDH2 and β-actin following stable silencing of IDH1 or IDH2 in 143Bwt and 143Bcytb. Three independent shRNAs targeting either IDH1 or IDH2 were used per cell line and compared against non-targeting shRNA. Plotted below are relative cell numbers of each pooled shRNA after growth over 72 hours. To calculate relative growth each hairpin, cell numbers were normalized to the control shRNA. Data are average and SEM of the mean for four individual cultures. *P,0.05; **P,0.005, Student's t-test.

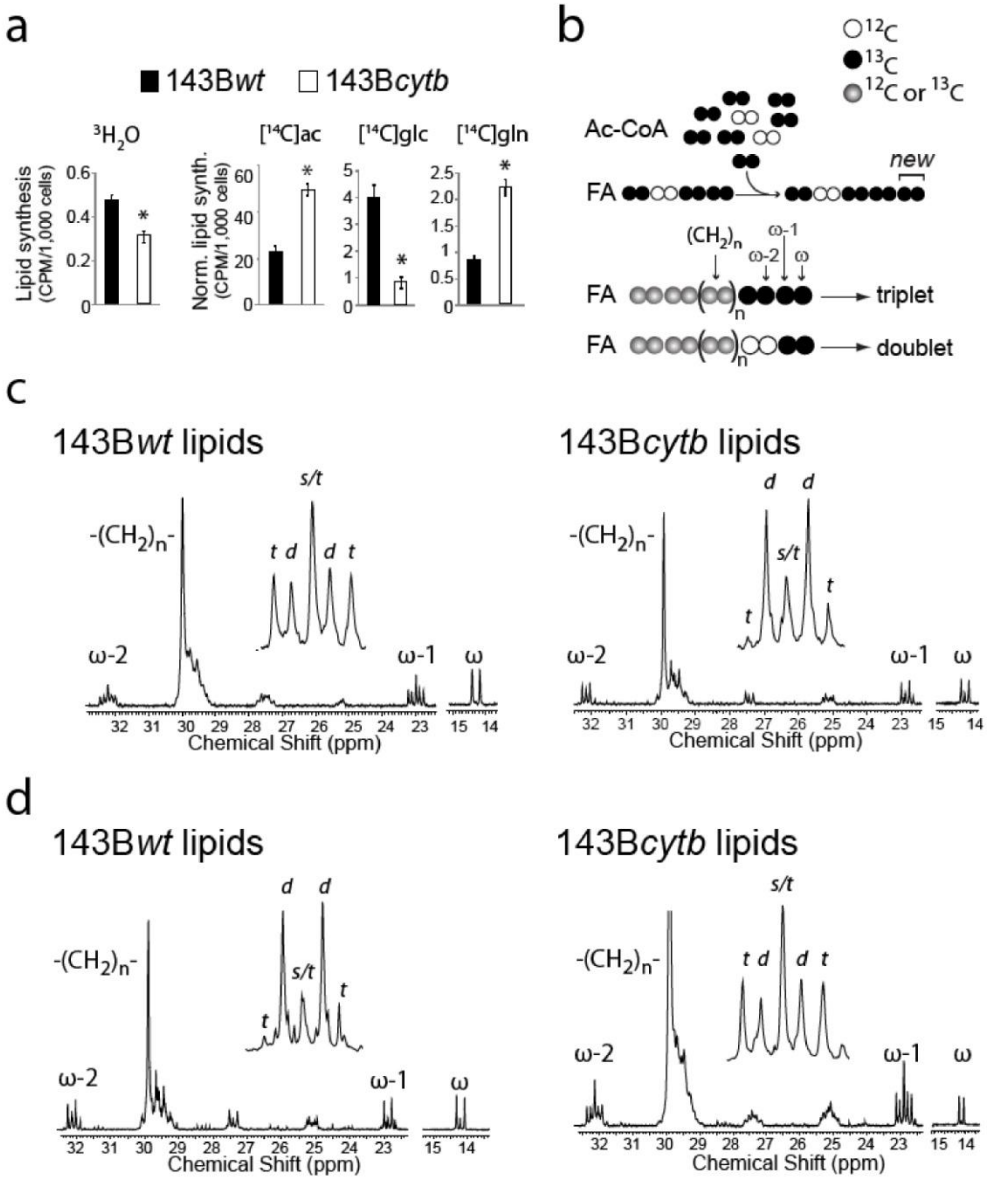

Figure 2.9. Glutamine is the major lipogenic precursor in 143Bcytb cells

(a) Total lipid synthesis measured in 143B cells cultured in medium containing $^{3}H_2O$ (21 vol.%) or ^{14}C tracers of acetate (5 mCi), glucose (10 mCi) or glutamine (10 mCi). Lipids were analyzed for ^{3}H or ^{14}C content by scintillation counting. In the ^{14}C experiments, raw counts per 10^3 cells were normalized to the absolute rate of fatty acid synthesis established using $^{3}H_2O$. **(b)** Schematic outlining synthesis of fatty acids (FA) from acetyl-CoA (Ac-CoA) and the source of the triplet and doublet at v21 in ^{13}C NMR spectroscopy. **(c)** ^{13}C NMR of lipids labeled with U-^{13}C-glucose or **(d)** U-^{13}C-glutamine. Insets are expansions of the ω-1 resonance. Abbreviations: s, singlet; d, doublet; t, triplet. *P,0.05, Student's t-test.

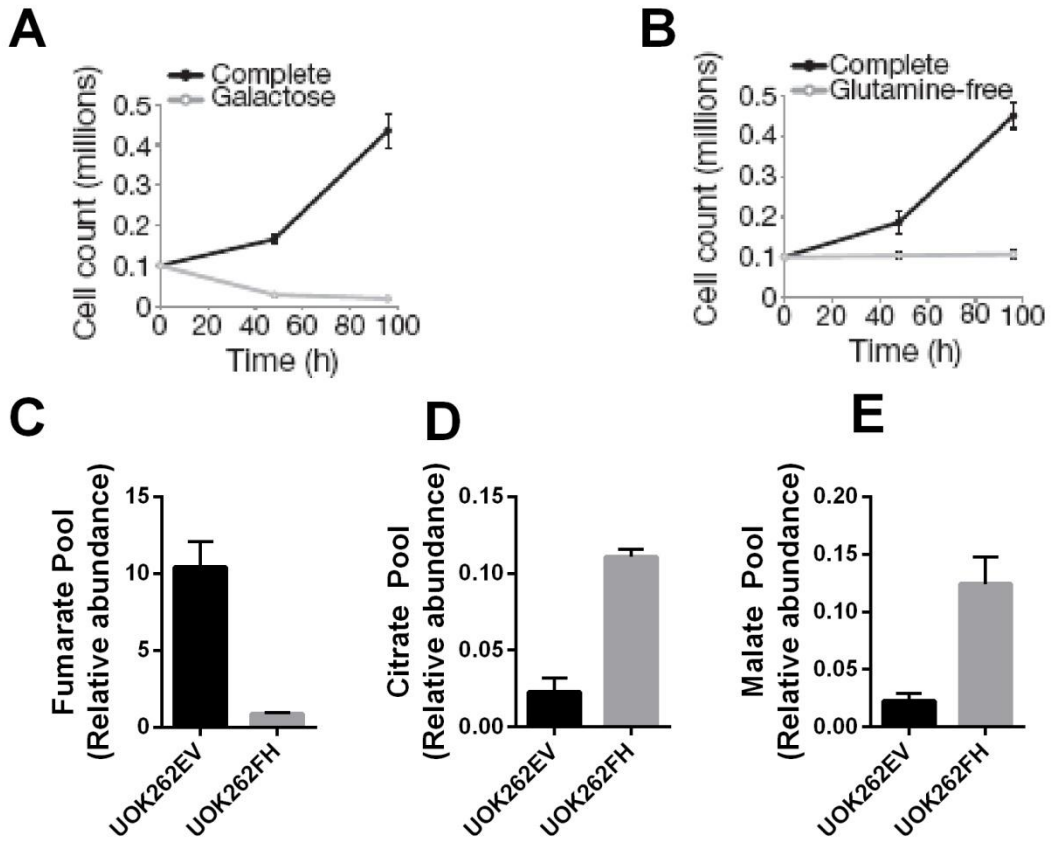

Figure 2.10. Characterization of FH deficient cells

(a) Growth of UOK262 cells in complete medium, in medium in which glucose was replaced with galactose, and in medium lacking glutamine **(b)**. **(c- e)** Relative pool sizes of fumarate, citrate and malate in UOK262-empty PCDNA3.1 vector (UOK262EV) and UOK262-expressing functional FH from PCDNA3.1 vector (UOK262FH). Data are the average and s.d. of three independent cultures

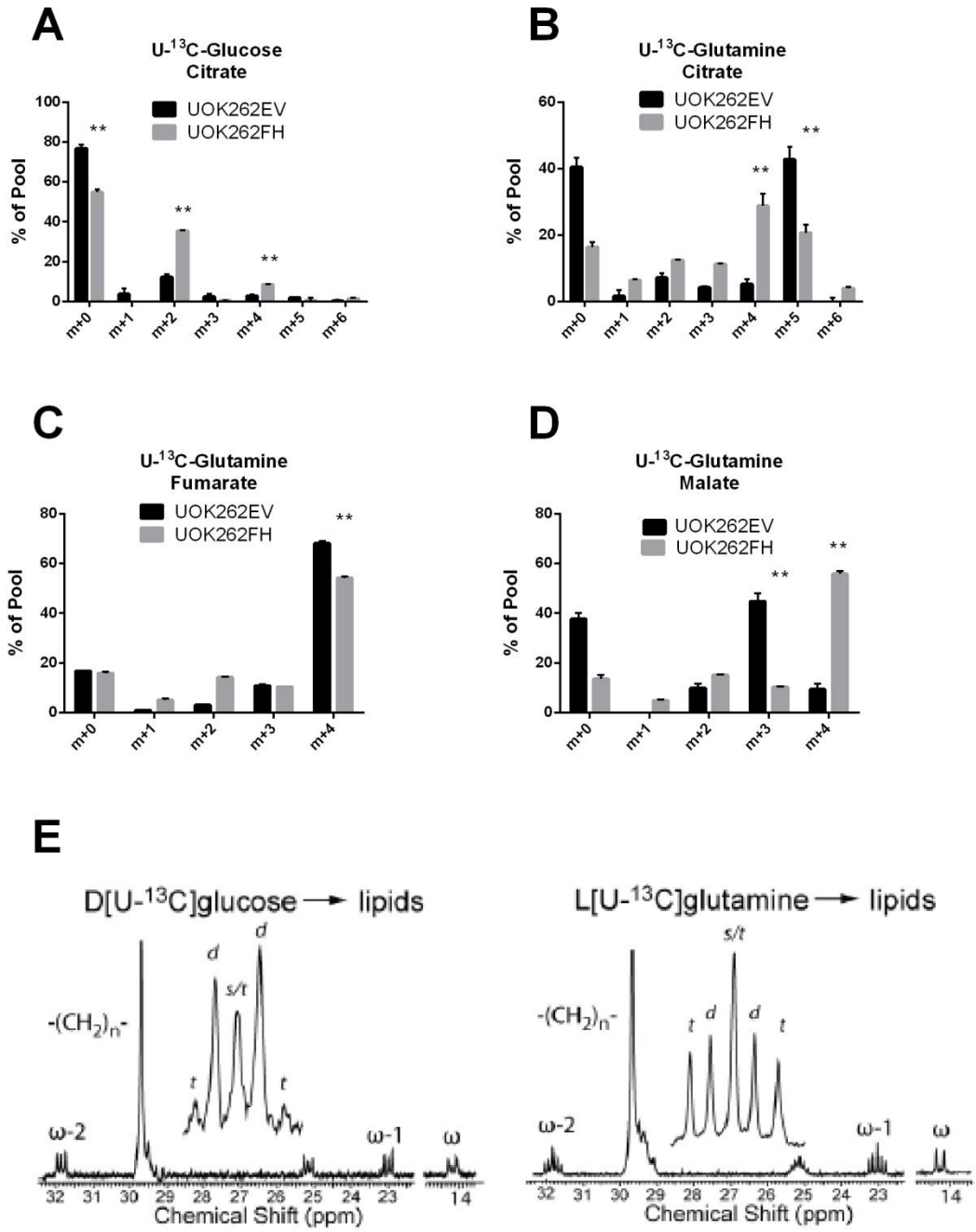

Figure 2.11: FH deficient cells, UOK262, use glutamine-dependent reductive carboxylation
(a) Mass isotopomer distribution of citrate in UOK262EV and UOK262FH following culture with U-^{13}C-glucose and unlabeled glutamine. **(b- d)** Mass isotopomers distribution of citrate, fumarate and malate following culture with U-^{13}C-glutamine and unlabeled glucose. **(e)** ^{13}C NMR of lipids labeled with U-^{13}C-glucose or U-^{13}C-glutamine. Insets are expansions of the ω-1 resonance. Labeling data are the average and s.d. of three independent cultures. *P,0.05, **P,0.005, Student's t-test. Lipid data are one representative experiment.

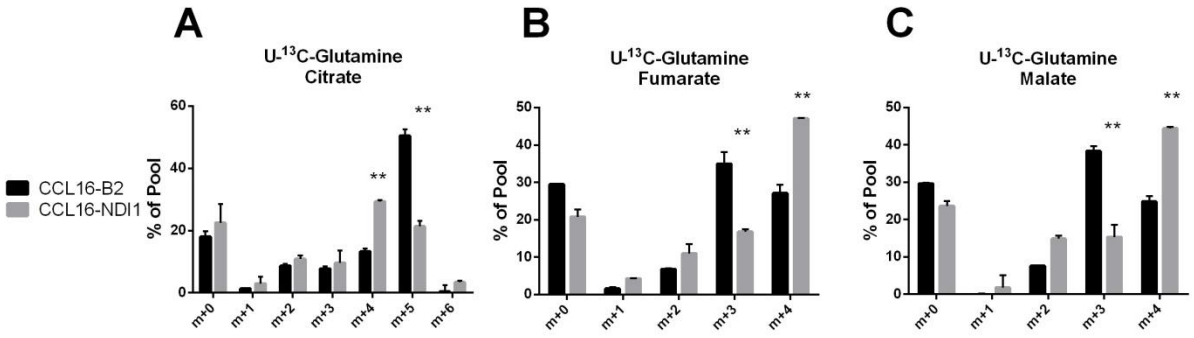

Figure 2.12. Complex I deficient cells, CCL16, use glutamine-dependent reductive carboxylation
(a, b, c) Mass isotopomer distributions of citrate, fumarate and malate in parental CCL16B2 and CCL16 cells expressing NDI1 (CCL16-NDI1) following culture with U-^{13}C-glutamine and unlabeled glucose. Data are the average and s.d. of three independent cultures. *P,0.05, **P,0.005, Student's t-test.

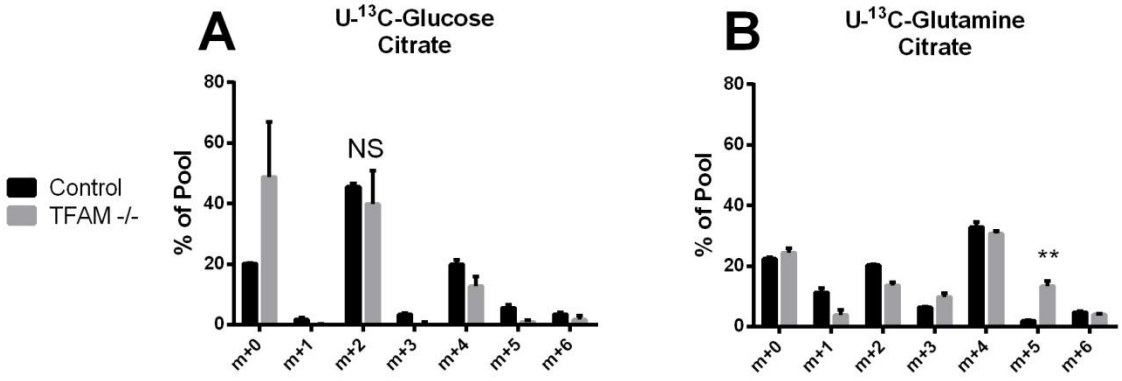

Figure 2.13: Knockout of Transcription Factor A (TFAM) in mouse keratinocytes induces glutamine-dependent reductive carboxylation

(a) Mass isotopomer distribution of citrate in primary (Control) and Mitochondrial Transcription Factor A (TFAM) knockout mouse keratinocytes (TFAM-/-) following culture with U-^{13}C-Glucose and unlabeled glutamine. **(b)** Mass isotopomer distribution of citrate following culture with U-^{13}C-Glutamine and unlabeled glucose. Data are the average and s.d. of three independent cultures. *P,0.05, **P,0.005, Student's t-test.

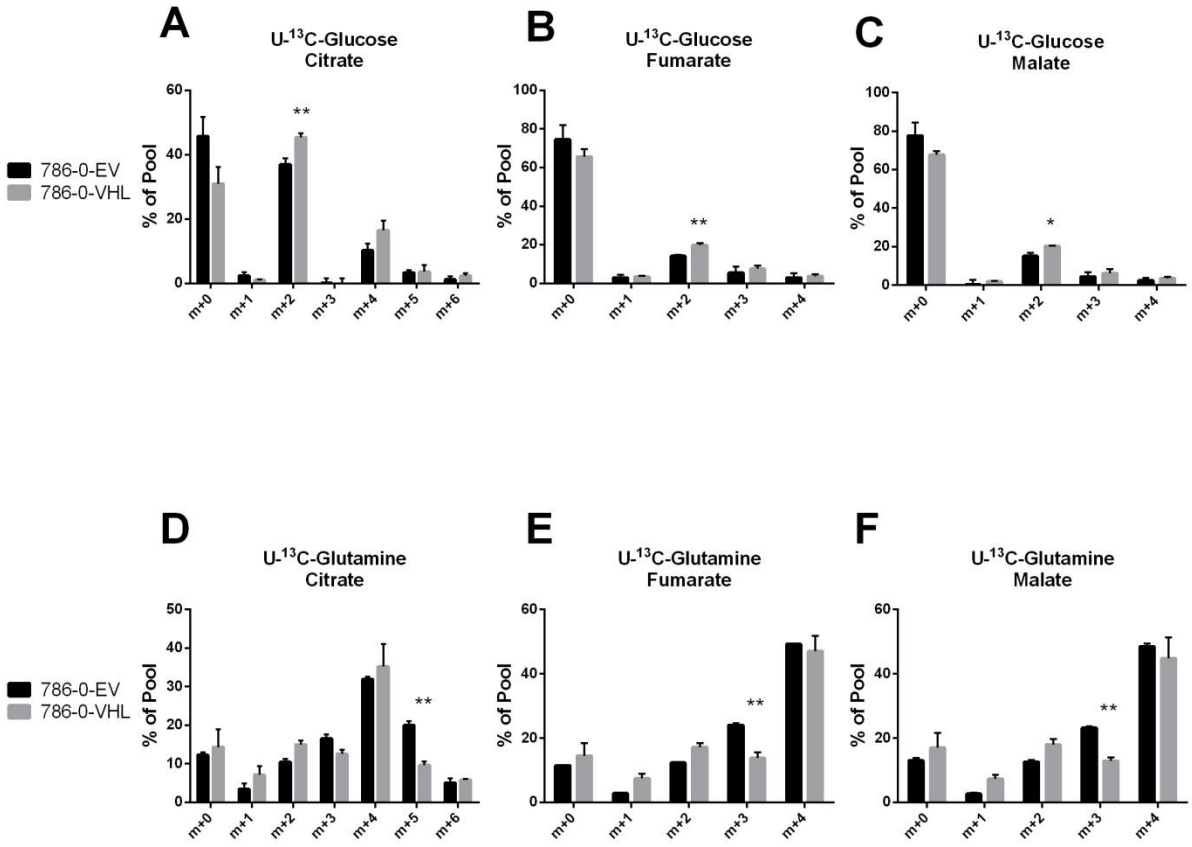

Figure 2.14. VHL deficient cells, 786-0, use glutamine-dependent reductive carboxylation
(a, b, c) Mass isotopomer distributions of citrate, fumarate and malate in parental 786-0-empty vector (786-0-EV) and 786-0 VHL-reconstituted (786-0-VHL) cells following culture with U-^{13}C-glucose and unlabeled glutamine. **(d, e, f)** Mass isotopomer distribution of citrate, fumarate and malate in 786-O-EV or 786-0-FH following culture with U-^{13}C-glutamine and unlabeled glucose. Data are the average and s.d. of three independent cultures. *P,0.05, **P,0.005, Student's t-test.

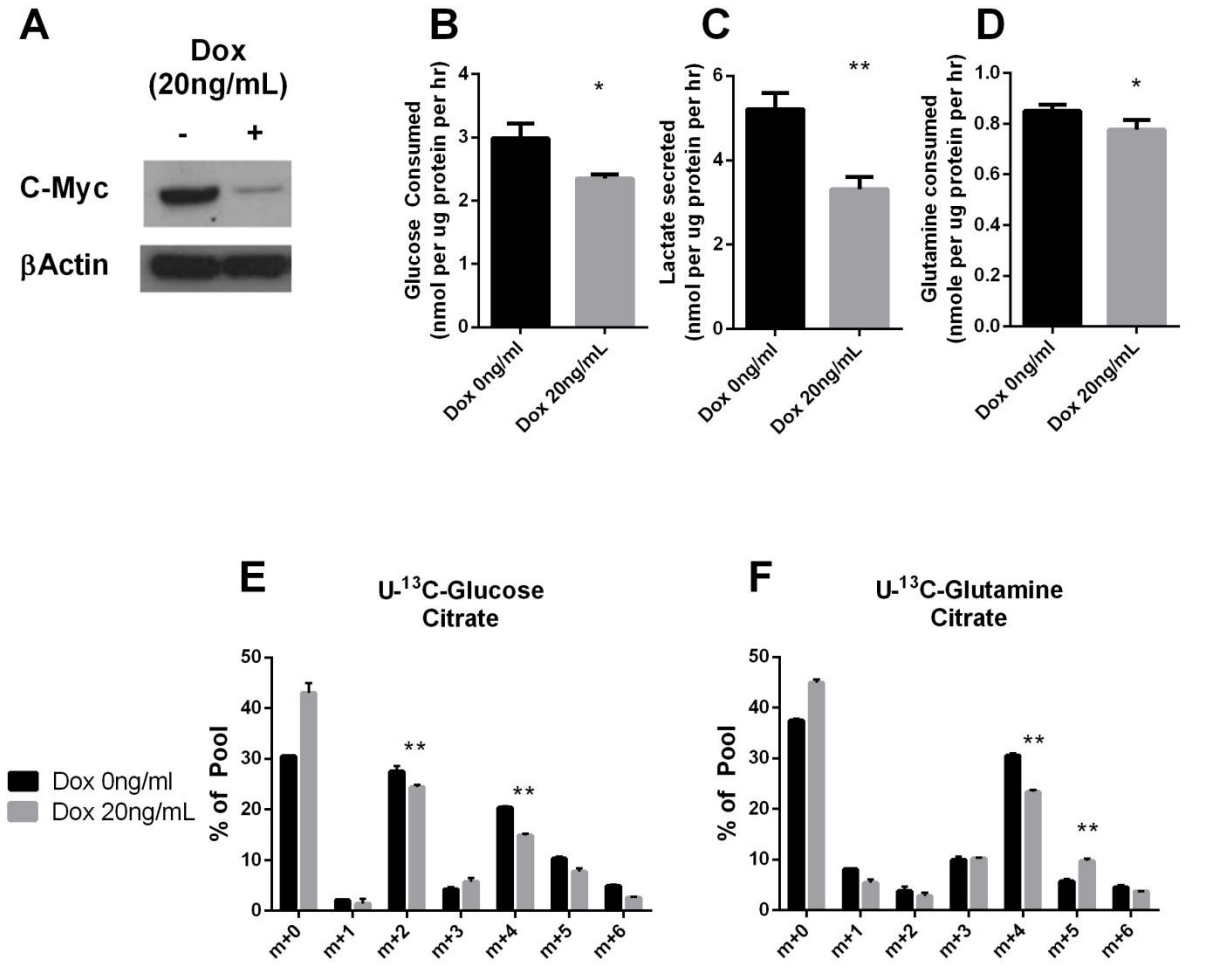

Figure 2.15: Suppression of c-Myc in mouse osteogenic sarcoma cells induces glutamine-dependent reductive carboxylation

(a) Western blot analysis following 48 hours of Doxycyclin (Dox) administration in mouse osteogenic sarcoma cells (132OS) (0ng/mL or 20ng/mL). **(b, c, d)** Glucose consumption, lactate secretion and glutamine consumption in control or Dox treated cells performed after 48hrs of Dox administration. **(e)** Mass isotopomer distribution of citrate in control or Dox treated cells cultured with U-^{13}C-glucose and unlabeled glutamine or U-^{13}C-glutamine and unlabeled glucose **(f)**. Data are the average and s.d. of three independent cultures. *P,0.05, **P,0.005, Student's t-test.

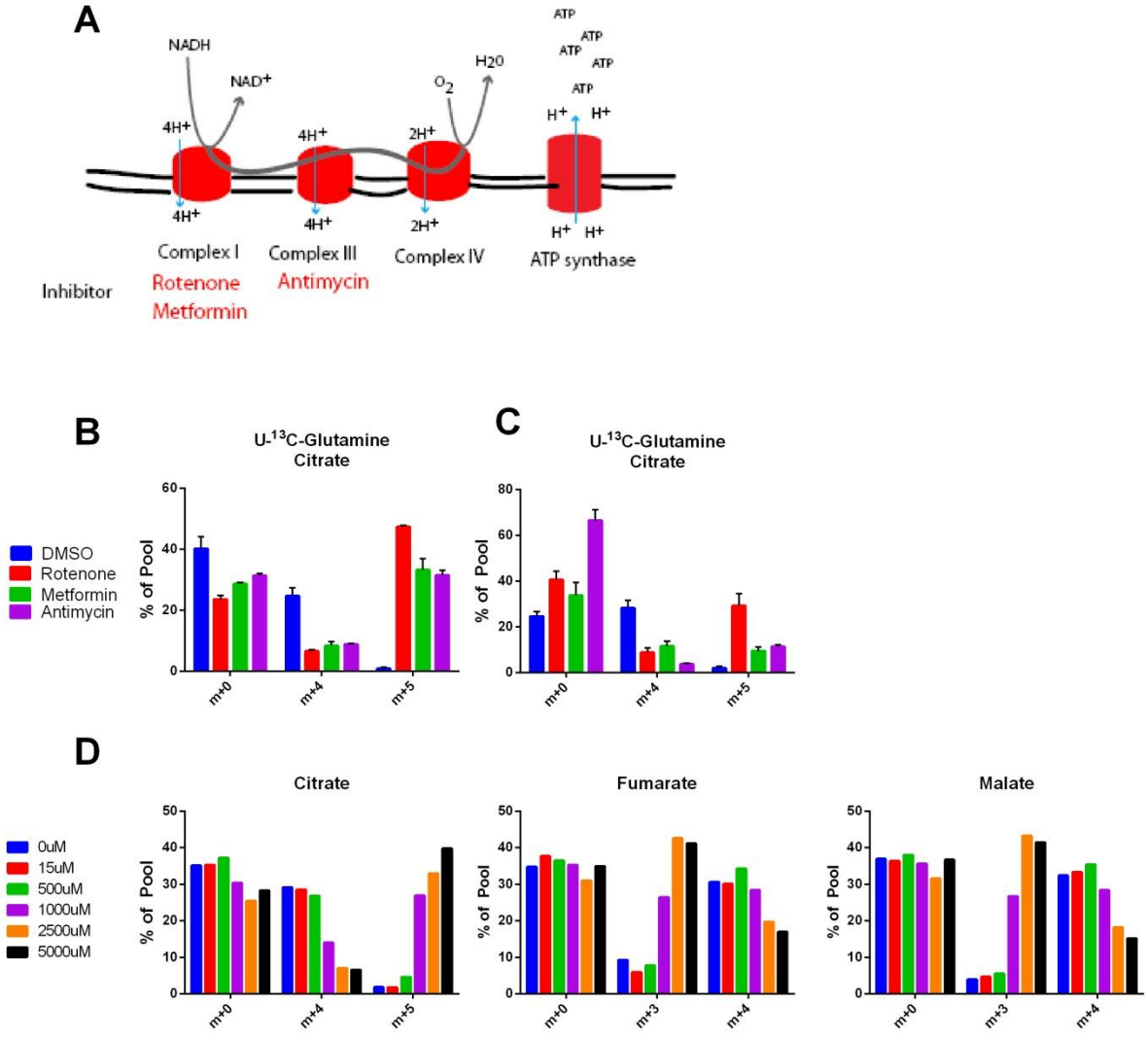

Figure 2.16. Chemical inhibition of ETC activity in cells induces reductive carboxylation
(a) Schematic of inhibitors of the electron transport chain. **(b and c)** 143Bwt cells cultured with U-^{13}C-glutamine and unlabeled glucose and either vehicle (DMSO), rotenone, metformin or antimycin. Shown are citrate mass isotopomers m+0, m+4, m+5 and fumarate mass isotopomers m+0, m+3, m+4. Data are the average and s.d. of three independent cultures. *P,0.05, **P,0.005, Student's t-test. **(d)** Mass isotopomers distribution of citrate in mouse embryonic fibroblasts (MEFs) cultured with U-^{13}C-glutamine and unlabeled glucose and either vehicle (DMSO), metformin, rotenone or antimycin at the indicated concentrations. **(e)** Mass isotopomer distributions of citrate in 143Bwt cells cultured with increasing doses of metformin.

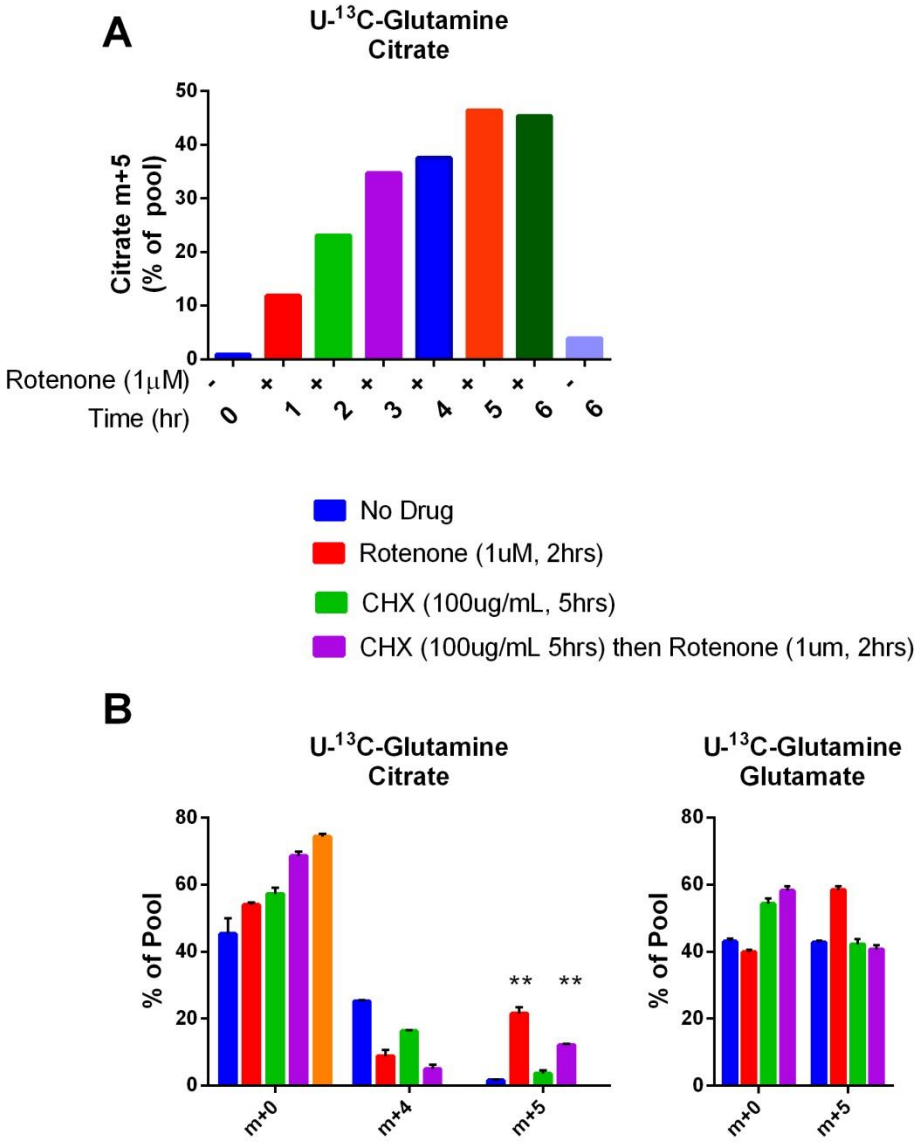

Figure 2.17: Induction of RC by rotenone is rapid and does not require new protein synthesis
(a) 143Bwt cells cultured with U-^{13}C-glutamine and unlabeled glucose with or without rotenone, for the indicated duration. Data are the citrate m+5 as a percentage of the total citrate pool of one culture.
(b) Mass isotopomers distribution of citrate and glutamate in 143Bwt cells. Blue bars and red bars are cells which were cultured with U-^{13}C-glutamine and unlabeled glucose which either received no drug (No Drug) or were incubated with roteone (1ug/mL), respectively. Green and purple bars are cells pretreated with 100 μg/mL cycloheximide (CHX) in unlabeled nutrients for five hours. Following this, both cells were cultured with U-^{13}C-glutamine and unlabeled glucose and CHX with or without rotenone for two hours (1ug/mL). Data are the average and s.d. of three independent cultures. *P,0.05, **P,0.005, Student's t-test.

Methods

Cell culture, growth and viability.

143Bwt, 143Bcytb, CCL16-B2, CCL16-NDI1, and UOK262 cells were cultured with DMEM supplemented with penicillin/streptomycin, 10% fetal bovine serum (FBS), L-glutamine (6mM), uridine (100ug/mL) and sodium-pyruvate (1mM). For experiments using UOK262EV and UOK262FH, this media was supplemented with G418 (300ug/mL) (Weinberg 2010; Brunelle 2005; Yang 2010; Tong 2011). Mouse embryonic fibroblasts (MEFs) and 132OS cells were cultured in Dulbecco's modified Eagle medium (DMEM) with 10% FBS, penicillin/streptomycin and L-glutamine (6mM). Primary mouse keratinocytes (TFAM $^{+}/^{+}$ and TFAM $^{-}/^{-}$) were grown in DMEM with low calcium (0.07mM) supplemented with uridine (100ug/mL) (Hamanaka 2013). 786-O-EV and 786-O-VHL were grown in Roswell Park Memorial Institute (RPMI) media supplemented with 10% FBS, penicillin/streptomycin, D-Glucose (25mM), L-Glutamine (4mM), sodium-pyruvate (1mM). To maintain vectors, cells were cultured with Puromycin (1ug/mL) and hygromycin (250ug/mL) (Kucejova 2011). Doubling times of 143Bs were calculated by repeatedly allowing sub-confluent cultures to reach confluence, then trypsinizing, counting and re-plating at low confluence.

Nutrient utilization and secretion

Concentrations of glucose, lactate and glutamine in tissue culture medium were measured from 0.7mL aliquots of cell culture media using a NOVA BioProfile Basic4 chemical analyzer. Rates of consumption/secretion were calculated by determining the change in metabolite concentration over 6 hr, converting this change into nmoles consumed or secreted, and normalizing to protein content.

Oxygen consumption

Oxygen consumption of 143Bwt and 143Bcytb were measured using an Oxygraph (Hansatech) with 10x10^6 cells suspended in 0.5mL of regular growth media. Oxygen sensor was calibrated using 1.5mL of regular growth media and oxygen consumption of each cell line was determined using entire 0.5mL volume of cells. Rate of oxygen utilization was monitored for at least three minute to calculate average. Potassium cyanide (KCN) was used to inhibit respiration. Oxygen consumption was calculated by subtracting the average rate of oxygen utilization after KNC treatment from the uninhibited respiration rate.

Generation of UOK262 PCDNA3.1 empty vector cell line

CDNA3.1 empty vector plasmid was transfected with Fugene (Promega) to UOK262 cells. To isolate stable integration of the plasmid cells were continuously grown in G418 (300ug/mL).

Mass isotopomer distribution and mass spectrometry

Nutrients labeled with ^{13}C were purchased from Cambridge Isotope Laboratories. All ^{13}C studies were performed in medium containing 10% dialyzed FBS and prepared so that 100% of either the glucose or glutamine pool was labeled with ^{13}C, and the other pool was unlabelled. DMEM lacking both glucose and glutamine was prepared from powder (Sigma) and supplemented with penicillin/streptomycin, sodium pyruvate (1mM) and uridine (100ug/mL). Media was then supplemented with either 15mM U-^{13}C-glucose and 2mM unlabelled glutamine, or 15mM unlabelled glucose and 2mM of either U-^{13}C-, 1-^{13}C- or 5-^{13}C-glutamine. For experiments with RPMI, glutamine free RPMI (11mM unlabelled glucose) was supplimented with 2mM U-^{13}C glutamine. All experiments were done from cells grown in 60- or 100-mm dishes until 80% confluent, then rinsed with PBS and cultured with ^{13}C-containing medium for the indicated time (usually 6 h). The cells were then washed with saline and metabolites were extracted by freeze-thawing three times in 0.5 ml of a cold 1:1 mixture of methanol:water. Macromolecules and

debris were removed by centrifugation, an internal standard was added (50nmol of 2-oxobutyrate), and the supernatants with aqueous metabolites were evaporated completely and derivatized for 30 min at 42°C in 100 ml of a trimethylsilyl donor (Tri-Sil, Thermo). Metabolites were analyzed using an Agilent 6970 gas chromatograph networked to an Agilent 5973 mass selective detector. Retention times and mass fragmentation signatures of all metabolites were validated using pure standards. To determine relative metabolite abundance across samples, the area of the total ion current peak for the metabolite of interest was compared to that of the internal standard and normalized for protein content. The mass isotopomer distribution analysis measured the fraction of each metabolite pool that contained every possible number of ^{13}C atoms; that is, a metabolite could contain 0, 1, 2,…n ^{13}C atoms, where n= the number of carbons in the metabolite. For each metabolite, an informative fragment ion containing all carbons in the parent molecule was analyzed using MSDChem software (Agilent), integrating the abundance of all mass isotopomers from m+0 to m+n, where m the mass of the fragment ion without any ^{13}C. Fragment ions monitored were: Glutamate (363-368); Succinate (247-251); Fumarate (245-249); Malate (335-339); Citrate (465-471). The abundance of each mass isotopomer was then corrected mathematically to account for natural abundance isotopes using Cormat (Fernandez et al., 1996) and finally converted into a percentage of the total pool.

^{14}C-Lipid synthesis assays

All radioisotopes were from Perkin-Elmer. Culture with $^{3}H2O$ was used to measure total lipid synthesis by preparing high-glucose DMEM from powder (Sigma) and supplementing with 2mM L-glutamine and 10% FBS. The $^{3}H2O$ was added during preparation of this medium to a final content of 21% of the total volume. The ^{14}C assays also used high-glucose DMEM with 2mM L-glutamine, 10% FBS and tracer quantities of [1,2-^{14}C]acetate (5 mCi, 4.4 mM), D[U-^{14}C]glucose (10 mCi, 1.7 mM) or L[U-^{14}C]glutamine (10 mCi, 1.9 mM). In all radioisotope assays, cells were grown to 80–90% confluence then cultured for

18 h in medium containing the label. Following this, cells were counted and divided into three equal aliquots with 3x10^6 cells each. Cells were washed twice with PBS and lysed with Triton-X 100 (0.5%). Lipids were extracted in Methanol, chloroform and water and were then dried. Lipids were then re-suspended in chloroform and transferred to liquid scintillation vials.

^{13}C Lipid Synthesis assays

For ^{13}C NMR experiments, cells were plated at approximately 50% confluence in 10-cm dishes and allowed to proliferate exponentially in complete DMEM containing 10% FBS, penicillin/streptomycin, uridine and pyruvate which was supplemented with either 15mM D[U-^{13}C]glucose and 2mM unlabelled glutamine, or 15mM unlabelled glucose and 2mM L[U-^{13}C]glutamine. Cells were grown and expanded until two confluent 15-cm dishes were obtained. Glucose and glutamine concentrations were monitored in the medium to ensure that neither nutrient was depleted during expansion of the culture. Cells were then washed with PBS, split with trypsin and re-suspended with media and transferred to glass tubes. Cells were washed twice with PBS and pelleted. To extract lipids, cold 50% methanol was added and probe sonicator was used to lyse cells. Chloroform was added to this and the bottom (organic) phase was extracted and entire sample was re-extracted and combined with the first. Lipids were dried down on heat block and resuspend in ternary mixture of CDCL3, CD3OD, EDTA (0.2M in D20) at a ratio of 400:320:160 and analyzed by ^{13}C NMR using a Varian ANOVA 14.1 T spectrometer equipped with a 3-mmbroadband probe with the observe coil tuned to 13C (150MHz). Relevant peak areas were determined using ACDLabs SpecManager (Advanced Chemistry Development).

RNA interference.

Transient gene silencing experiments were performed using commercial siRNA pools (siGENOME, Thermo) directed against IDH1, IDH2, IDH3 (catalogue numbers MU-008294-00, MU-004013-00 and

MU-008753-00, respectively); Luciferase (Luc) served as a negative control. For the simultaneous silencing of IDH1 and IDH2, individual siRNAs rather than pools were used (IDH1: 59-GGACUUGGCUGCUUGC AUU-39; IDH2: 59-CAAGAACUAUGACGGAGAU-39).Specifically, 0.3x10^6 cells were transfected with DharmaFECT transfection reagent #3 (Thermo) in normal growth media lacking penicillin/streptomycin and allowed to adhere to dishes. After 24hrs media was replaced with regular growth media. Metabolic assays and protein abundance performed 72 hours later. For metabolic assays, cells were washed twice with PBS and incubated with L[U-^{13}C]glutamine for two hours before extraction of metabolites with 50% methanol for mass isotopomer distribution analysis. To monitor protein abundances cells were lysed in RIPA buffer and protein separated on NuPAGE® Novex® 4-12% Bis-Tris gel (Invitrogen). Protein was transferred to Immobilon transfer membranes (Millipore) and detected using commercial antibodies against IDH1, IDH2, or IDH3 (Santa Cruz Biotech). Silencing used lentiviral-mediated shRNAs from the Mission shRNA pLKO.1-puro library (Sigma). Cells were infected with each lentivirus using the manufacturer-supplied protocol, and pools of puromycin-resistant cells were used for subsequent experiments. Pools with the best silencing of IDH1 or IDH2 were used in the growth assay.

Sub-cellular localization studies

143Bwt and 143Bcytb cells were transfected with siRNA as described above. After 72 h, the transfected cells were incubated in medium containing 1 mM Mitotracker Deep Red FM (Invitrogen) for 30 min. The cells were then fixed with 3.7% formaldehyde in PBS for 15 min, permeabilized with 0.5% (v/v) Triton X-100 for 5 min, and blocked with 1% bovine serum albumin for 5 min. Immunofluorescence used commercial antibodies against IDH1 (Santa Cruz Biotechnology) or IDH2 (Abcam) followed by anti-goat or anti-mouse secondary antibodies conjugated to Alexa Fluor-488. Cells were stained with primary and secondary antibodies for one hour at room temperature and mounted on Vectashield mounting

medium containing DAPI (Vector Laboratories). Images were acquired using an LD Plan-Neofluar 403/1.3 DIC objective on a Zeiss Axioplan 2E imaging deconvolution microscope. Mitochondrial fractions were isolated by differential centrifugation as previously described26.

132OS Cells

For metabolic experiments in 132OS cells, cells were seeded at 0.25x10^6 cells/6cm dishes with or without Doxycycline (20ng/mL). After 48hrs, metabolic assays were preformed as described above.

Chapter Three

Oxidative metabolism of αKG supports reductive citrate formation

Introduction

In growing cancer cells, oxidative metabolism of glucose and glutamine in the mitochondria provide precursors needed for *de novo* synthesis of proteins, nucleic acids and lipids. Yet, a subset tumors harbor genetic mutations in the electron transport chain (ETC) or tricarboxylic acid cycle (TCA) that disable normal oxidative mitochondrial function (Mullen and DeBerardinis, 2012). We demonstrated that cells with metabolic defects engage an unusual pathway of glutamine metabolism termed reductive carboxylation that allows them to generate biosynthetic precursors required for growth.

There is very little known about the mechanism(s) regulating the reductive carboxylation pathway. Recent i*n vitro* studies of IDH1 have indicated that a high ratio of NADPH/$NADP^+$ and low citrate concentration strongly influence the reductive carboxylation reaction (Leonardi et al., 2012). This is supported by *in vivo* data indicating that reductive carboxylation in VHL deficient tumor cells is associated with a high NADPH/NADP ratio and a low concentration of citrate (Gameiro et al., 2013a). Others have reported that the reductive reaction can be modulated by changing the ratio of citrate to αKG (Fendt et al., 2013). Collectively, these reports indicate that reductive carboxylation can be modulated through either alteration of the balance of substrate/products or cofactors. Here, we used metabolomics and metabolic flux analysis to study several models of reductive carboxylation in order to gain insight into the mechanisms regulating this pathway.

Results

Shared metabolomic features among cell lines engaged in reductive carboxylation

To identify conserved metabolic features associated with reductive carboxylation, we analyzed metabolite abundance in isogenic pairs of cell lines in which one member displayed substantial reductive carboxylation and the other did not. We used a pair of previously described cybrids derived from 143B osteosarcoma cells, in which one cell line contained wild-type mitochondrial DNA (143Bwt) and the other contained a mutation in cytb (143Bcytb), severely reducing complex III function (Rana et al., 2000; Weinberg et al., 2010). The 143Bwt cells primarily use oxidative metabolism to supply the TCA cycle while the 143Bcytb cells use a combination of oxidative metabolism and reductive carboxylation (Mullen et al., 2012) The other pair contained UOK262 cells, a renal carcinoma cell line with loss of FH UOK262EV, and a derivative cell line in which wild-type FH had been re-expressed (UOK262FH). Metabolites were extracted from all four cell lines and analyzed by triple-quadrupole mass spectrometry. We profiled the relative abundance of approximately 100 metabolites from glycolysis, the pentose phosphate pathway, one-carbon/nucleotide metabolism, the TCA cycle, amino acid degradation, and other pathways. Each metabolite was normalized to protein content, and relative abundance was determined between cell lines from each pair (Table-1).

We performed hierarchical clustering (Figure 1a) and principal component analysis (Figure 1b) and found greater metabolomic similarities between members of each pair than between the cell lines using reductive carboxylation. We analyzed these results using fairly stringent cutoffs for fold changes and probability in order to identify metabolites that were significantly altered in 143Bcytb or UOK262EV, respectively (Figure 1c,d). Predictably, in the UOK262 pair malate was found to have the most negative fold change in UOK262EV compared to UOK262FH. Interestingly, fumarate did not have the largest

positive fold change in UOK262EV, possibly due to incomplete rescue of FH enzymatic activity in UOK262FH.

Of the metabolites altered in 143B and UOK262, only three displayed similar directions of difference in the two cell lines using reductive carboxylation. Proline, a nonessential amino acid derived from glutamate in an NADPH-dependent biosynthetic pathway, was suppressed in 143Bcytb and UOK262 cells (Figure 2a). Succinate, the TCA cycle intermediate was substantially elevated in both cell lines (Figure 2b). Finally, 2-hydroxyglutarate, the reduced form of αKG, was substantially elevated in both these cell lines (Figure 2c). Further analysis revealed that both the L- and D- enantiomers of this metabolite were increased in 143Bcytb cells (Figure 2d). Two studies have reported reductive carboxylation reaction to be a function of an altered ratio of citrate to αKG (citrate/αKG). Specifically, it was found that induction of reductive carboxylation, through either chemical inhibition of ETC function, hypoxia or pseudo-hypoxia states caused by mutations in VHL, were associated with a low citrate/αKG ratio (Fendt et al., 2013; Gameiro et al., 2013b). In these cases, it was postulated that elevated αKG and low citrate levels induced reverse activity of IDH through mass action effect of αKG. To determine if this ratio was similarly altered in our models of reductive carboxylation, we quantitatively analyzed these two metabolites in 143B and UOK262 cells. Both 143Bcytb and UOK262EV cells had lower citrate/αKG ratios than their oxidative partners, consistent with the published reports (Figure 2e). Additionally, we analyzed the ratio of total NAD to NADH in both 143B and UOK262 pairs. 143Bcytb and UOK262EV were found to have low NAD/NADH ratios (Figure 2f).

The Citrate/αKG ratio is a feature, but not a regulator of reductive carboxylation

To more definitively evaluate whether the citrate/αKG ratio was the cause of reductive carboxylation or a consequence of it, we used RNAi to transiently silence the E1 subunit of the αKG metabolizing enzyme alpha ketoglutarate dehydrogenase (αKGDH; gene symbol *OGDH*) in 143Bwt cells

(Figure 3a). Based on the fact that these cells use oxidative glutamine metabolism, we predicted that inhibiting this enzyme would lead to a low citrate/αKG ratio by elevating αKG and reducing citrate (through suppression of glutamine-dependent anaplerosis). As predicted, we found that transient knockdown of *OGDH* in 143Bwt cells resulted in a significant decrease in the citrate/αKG ratio (Figure 3b). To determine if this altered ratio was sufficient to induce reductive carboxylation, we cultured these cells with U-^{13}C-glutamine. We observed a suppression of citrate formed through oxidative metabolism (citrate m+4) yet no increase in reductive citrate formation (citrate m+5) (Figure 3c). Additionally, we analyzed the NAD/NADH ratio in both these cells. OGDH knockdown was associated with an increase in the NAD/NADH ratio, consistent with suppression of oxidative metabolism in these cells (Figure 3d). Together, the data demonstrate that a reduced citrate/αKG ratio was not sufficient to induce reductive carboxylation in the 143B model, implying that additional factors beyond mass action account for the induction of this pathway.

Oxidative glutamine metabolism is the primary route of succinate formation

Next, we examined the other high priority metabolites that emerged from our metabolomics analysis. The TCA cycle intermediate succinate was found to be elevated over three fold in both 143Bcytb and UOK262EV (Figure 2b). Succinate accumulation has previously been reported in the context of FH-deficiency, including UOK262 cells and mouse renal cells lacking lack FH activity (Frezza et al., 2011). Additionally, we previously reported that the succinate pool in 143Bcytb cells is produced through simultaneous oxidative and reductive glutamine metabolism. To characterize the relative contributions of these two pathways, we cultured 143Bwt and 143Bcytb with U-^{13}C-glutamine and monitored time-dependent ^{13}C incorporation in succinate and other TCA cycle intermediates. Oxidative metabolism of glutamine generates succinate, fumarate and malate containing four glutamine-derived ^{13}C molecules on the first turn of the cycle (m+4). Alternatively, reductive metabolism results in the

incorporation of three ^{13}C molecules in these intermediates (m+3). As expected, oxidative glutamine metabolism was the predominant source of succinate, fumarate and malate in 143Bwt cells (Figure 4a-c). In 143Bcytb, fumarate and malate were produced almost exclusively through reductive metabolism (Figure 4d-f). Surprisingly, analysis of the succinate formation indicated that the majority of the pool was formed primarily through oxidative glutamine metabolism, with a minor contribution from the reductive carboxylation pathway. Notably, this oxidatively-derived succinate was detected prior to that formed through reductive carboxylation. Thus, 143Bcytb cells produce TCA cycle intermediates through bidirectional metabolism of αKG. In the reductive pathway, glutamine-derived αKG is metabolized through IDH1/2 to citrate, OAA, malate, fumarate and succinate. Concurrently, αKG is also diverted into two oxidative TCA cycle reactions, terminating with succinate.

Pyruvate carboxylation contributes to the TCA cycle in cells using reductive carboxylation

Because of the persistence of oxidative metabolism, we determined the extent to which other routes of metabolism besides reductive carboxylation contributed to the production of TCA cycle intermediates. We observed that culture of 143Bcytb cells with U-^{13}C-glucose produced citrate m+3, suggesting these cells exhibited upregulated pyruvate carboxylase (PC) activity (Mullen et al., 2012). In this pathway, glucose-derived pyruvate is carboxylated by PC to generate OAA, which can then be converted to other TCA cycle intermediates (Cheng et al., 2011). To determine amount of citrate and OAA formed through the PC pathway, we cultured 143Bwt and 143Bcytb with 3,4-^{13}C-glucose and analyzed ^{13}C incorporation in TCA cycle intermediates. In this labeling scheme, glycolysis generates 1-^{13}C-pyruvate; this label is retained in OAA if pyruvate is carboxylated by PC, but is removed as CO_2 by PDH. Both cell lines contained label in malate and other TCA cycle intermediates from [3,4-^{13}C]glucose, but the fractional contribution was significantly greater in 143Bcytb (Figure 5a). Importantly, although PC was active in 143Bcytb cells, the apparent glucose-dependent labeling of citrate via PC was small relative

to the total citrate pool and to the previously reported contribution from glutamine-dependent reductive carboxylation (Mullen et al., 2012). Next, we choose to study the effect of PC suppression on reductive carboxylation. We used two independent shRNA hairpins to stably silence *PC* expression in 143Bcytb cells (Figure 5b). Culture of these cells with 3,4-^{13}C-glucose revealed a decrease in PC-dependent labeling in malate, validating the pathway was suppressed (Figure 5c). Culture of these cells with U-^{13}C-glutamine revealed an increase in citrate m+5 (Figure 5d), suggesting that in the absence of PC activity the fractional contribution of reductive carboxylation increased. Together, these demonstrate that the PC pathway contributes a minor fraction of citrate in 143Bcytb cells.

Oxidative metabolism of αKG is required for reductive carboxylation.

In tumors with mutations in the succinate dehydrogenase (SDH) complex, large accumulations of succinate are associated with epigenetic modifications of DNA and histone proteins that promote malignancy (Kaelin and McKnight, 2013; Killian et al., 2013). Given these signaling properties, we tested the hypothesis that succinate accumulation was required for the induction of reductive carboxylation in 143Bcytb cells. To test this, we inhibited the last enzymatic step in the oxidative pathway, the succinate-forming enzyme succinyl-coA synthetase (SCC). We used RNAi directed against the gene encoding the alpha subunit of succinyl-CoA synthetase (*SUCLG1*) (Figure 6a). Silencing *SUCLG1* greatly reduced succinate levels, indicating that the pathway was sufficiently suppressed. Additionally, this also confirmed that the oxidative, and not reductive pathway, was the major route of succinate formation in 143Bcytb cells (Figure 6b). We cultured these cells with U-^{13}C-glutamine to determine what effect suppression of this pathway had on reductive carboxylation. Knockdown of *SUCLG1* had no effect on the labeling pattern of citrate from U-^{13}C-glutamine (Figure 6c). Based on this result, we concluded that the large succinate pool was dispensable for reductive carboxylation in 143Bcytb.

We next tested whether the proximal step in the oxidative pathway, αKGDH, was required for reductive carboxylation. We transiently silenced expression of the E1 component of the αKG dehydrogenase complex (*OGDH*), which catalyzes the oxidative decarboxylation of αKG to succinyl-CoA (Figure 6d). *OGDH* silencing greatly diminished succinate abundance, validating effective suppression of the pathway (Figure 6e). Surprisingly, culture of these cells with U-^{13}C-glutamine revealed a decrease in the fraction of citrate m+5 resulting from reductive carboxylation. Coupled with the decrease in the citrate pool size, this indicated a substantial decrease in the contribution of reductive carboxylation when *OGDH* was silenced (Figure 6f). This was surprising, as we predicted inhibiting oxidative αKG metabolism would enhance reductive citrate formation.

αKGDH and NNT maintain a redox state favorable for reductive carboxylation

Previous work has shown that reductive glutamine metabolism under hypoxia is dependent on the activity of nicotinamide nucleotide transhydrogenase (NNT, gene symbol *NNT*) to generate NADPH for the reductive carboxylation reaction (Gameiro et al., 2013a; Sazanov and Jackson, 1994). NNT is a mitochondrial transmembrane protein which catalyses the transfer of an H^+ from NADH to NADP using the proton gradient to generate NADPH. Because of this activity, it has well established roles in redox homeostasis and defense from reactive oxygen species (Rydstrom, 2006). To determine if NNT activity was required for reductive carboxylation in 143Bcytb cells, we used RNAi to transiently silence *NNT* and assayed reductive carboxylation using U-^{13}C-glutamine. Consistent with previous reports, silencing *NNT* significantly impaired reductive citrate formation (Figure 7a,b).

Previous reports have not identified the source of NADH required for the forward reaction of NNT. Based on the observation that αKGDH is required for reductive carboxylation, we hypothesized that this step was the source of NADH for NNT function. To test this, we transiently silenced *OGDH* or *NNT* and examined the ratio of total intracellular NAD to NADH (Figure 7c). Knockdown of *OGDH*

resulted in a significant increase in the ratio of NAD/NADH, indicating a decrease in the relative amount of NADH. Conversely, *NNT* knockdown decreased the ratio, indicating an increase in the relative amount of NADH. These data indicate that αKG dehydrogenase is an important source of NADH, and NNT a re-generator of NAD in 143Bcytb. We propose a model whereby oxidative metabolism of αKG, through αKGDH, contributes NADH which supports NADPH generation by NNT (Figure 7d).

Discussion

Cancer cell growth requires the production of acetyl-coA for myriad biological functions. This is highlighted by the observation that, even in the context of several mitochondrial perturbations, tumor cells have unique mechanisms to generate acetyl-coA (Metallo et al., 2012; Mullen et al., 2012; Wise et al., 2011). In this study we used a combination of global metabolomic profiling and metabolic flux to identify mechanisms regulating reductive carboxylation. Our analysis revealed that the metabolomic signature of 143Bcytb was more similar to 143Bwt than it was to UOK262EV, suggesting the reductive carboxylation pathway is not a defining feature of the metabolome in these cells. This could be due to a combination of at least two factors. One, these cancer cells were derived from different tissue, osteosarcoma and renal cell carcinoma, respectively of unrelated patients. Thus, although they are both cancer cells using the same reductive pathway, they may still retain metabolic features of their tissue-of-origin. On top of this, these cells do not share the same primary metabolic disturbance, as loss of ETC activity and FH dysfunction are distinct metabolic abnormalities. Additionally, high fumarate may be able to independently account for a large portion of the difference in the metabolome, as high fumarate is sufficient to drastically alter gene expression (Yang et al., 2012). Thus, the relatively few shared metabolic features of these two different models are potentially relevant to other models of reductive carboxylation.

We identified that elevated succinate is a common feature of cells engaged in the reductive carboxylation pathway. In these cells, we found that succinate was primarily formed through oxidative, and not reductive, glutamine metabolism. Our loss of function studies of this pathway found that that flux through αKGDH, but not the production of succinate *per se,* was necessary for maximal reductive carboxylation, as knockdown of SUCLG1 suppressed succinate formation but had no effect on reductive citrate formation. Specifically, flux through this pathway was found to be an important source of NADH

in 143Bcytb cells, as inhibition of αKGDH resulted in a significant increase in the NAD/NADH ratio. This is consistent with *in vitro* studies of IDH1, which have shown that reductive carboxylation is strongly influenced by the redox potential (Leonardi et al., 2012). Similarly, we observed 143Bcytb and UOK262EV to have low NAD/NADH ratios compared to their oxidative counterpart. Like other reports, the mitochondrial transhydrogenase NNT was found to be an important mediator of reductive carboxylation. We observed that knockdown of NNT decreased the NAD/NADH ratio; indicating NNT also mediates the NAD/NADH ratio. These data are consistent with a model whereby oxidative flux through αKGDH generates NADH that is dissipated by NNT to support NADPH-dependent reductive carboxylation. Interestingly, the reductive carboxylation pathway is not engaged in mouse FH-deficient renal cell lines (Ternette et al., 2013). In these mouse cell lines, fumarate was found to be significantly more elevated than in patient-derived human cells. Consequently, this was associated with fumarate-dependent succination of the mitochondrial aconitase. Consequently, these cells can catalyze the reductive carboxylation reaction but are unable to generate citrate.

In vitro, reductive carboxylation is also negatively regulated, to a lesser extent than NADP, by isocitrate (Leonardi et al., 2012). Previous reports have postulated that reductive carboxylation is mediated by a low ratio of citrate to αKG (Fendt et al., 2013; Gameiro et al., 2013b). We observed this ratio to be low in both our models of reductive carboxylation, but we identified a situation where a low citrate/αKG ratio was not associated with reductive carboxylation. In this case, we induced a low citrate/αKG ratio in cells which use oxidative metabolism. Despite lowering the ratio ten-fold, this was not sufficient to stimulate reductive carboxylation. Rather, this was found to only decrease oxidative glutamine metabolism and significantly increase the NAD/NADH ratio. In the context of these previous reports, our data indicate that the citrate/αKG ratio is not sufficient to independently regulate reductive carboxylation. Rather, the citrate/αKG ratio appears to be a feature that is permissive for reductive

carboxylation (as isocitrate negatively regulates the reaction) but induction does not occur unless there are changes in the cellular redox potential.

In addition to high intracellular succinate, we identified that 143Bcytb and UOK262EV have elevated pools of 2-HG. Interestingly, this was found to be predominantly composed of L-2HG, which is the same enantiomer that has been observed to accumulate in patients with loss of function mutations in L-2HGDH and also predisposes these individuals to brain tumors (Kranendijk et al., 2012). Similarly, 2-HG has been previously observed, to a small degree, to accumulate in cells under conditions of hypoxia, although the specific enantiomer was not reported (Wise et al., 2011). Importantly, 2-HG is detectable in the serum of individuals with acute myeloid leukemia (AML) with somatic mutations in IDH2 (Ward et al., 2010). Thus, reductive carboxylation-dependent increase in 2-HG may be a novel way to monitor tumors which use this pathway in vivo.

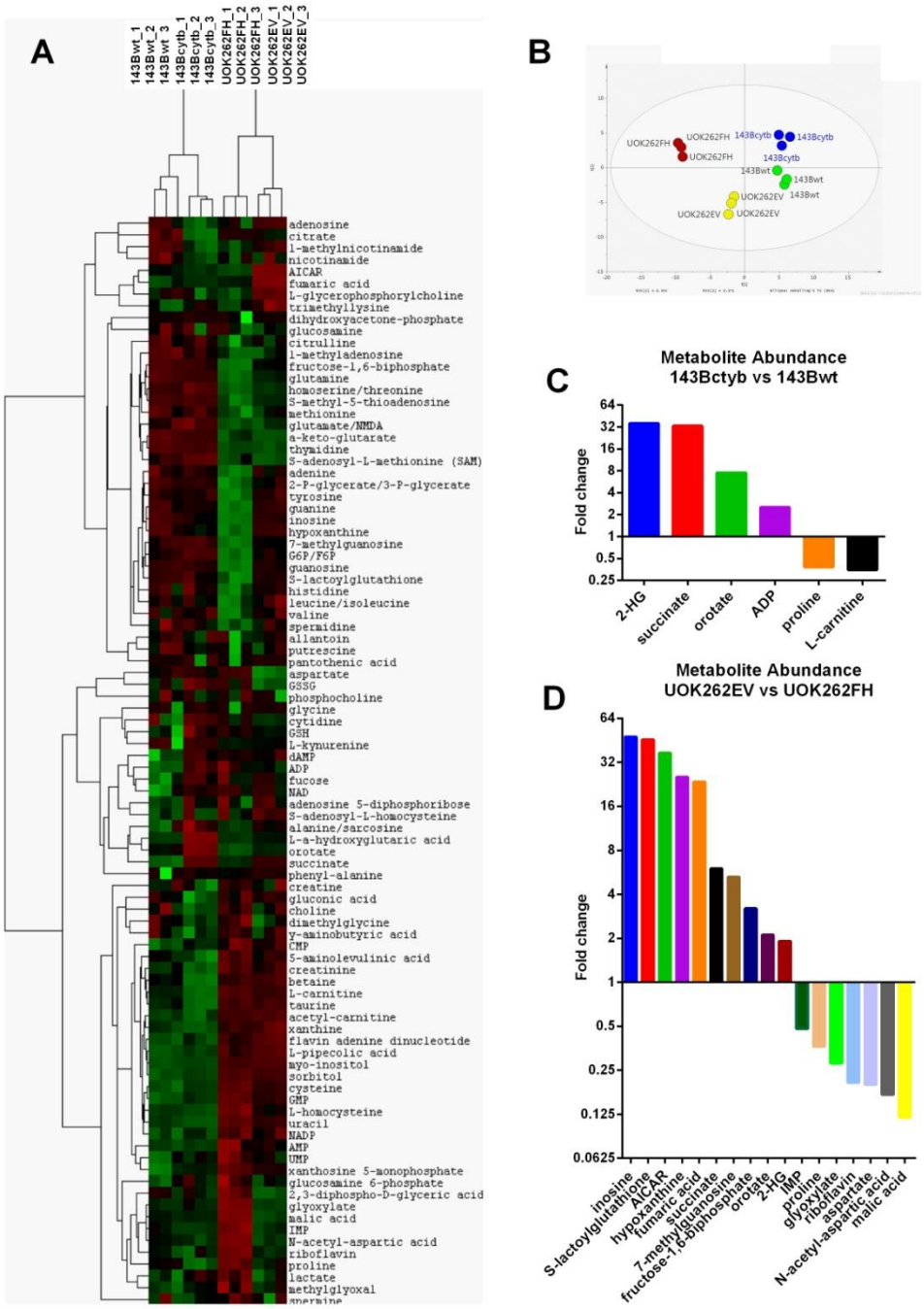

Figure 3.1: Metabolic features of reductive carboxylation

(a) Heatmap of relative changes in metabolite concentrations between 143Bwt, 143Bcytb, UOK262FH, UOK262EV. Color indicates the degree of change in metabolite abundance. **(b)** Principal component analysis (PCA) plot showing 143B and UOK262 pairs. **(c)** Fold change of significantly altered metabolites in 143Bcytb versus 143Bwt or **(d)** UOK262EV versus UOK262FH. Only the metabolites with greater than 2-fold change in expression and statistical significance of $p \leq 0.009$ were reported.

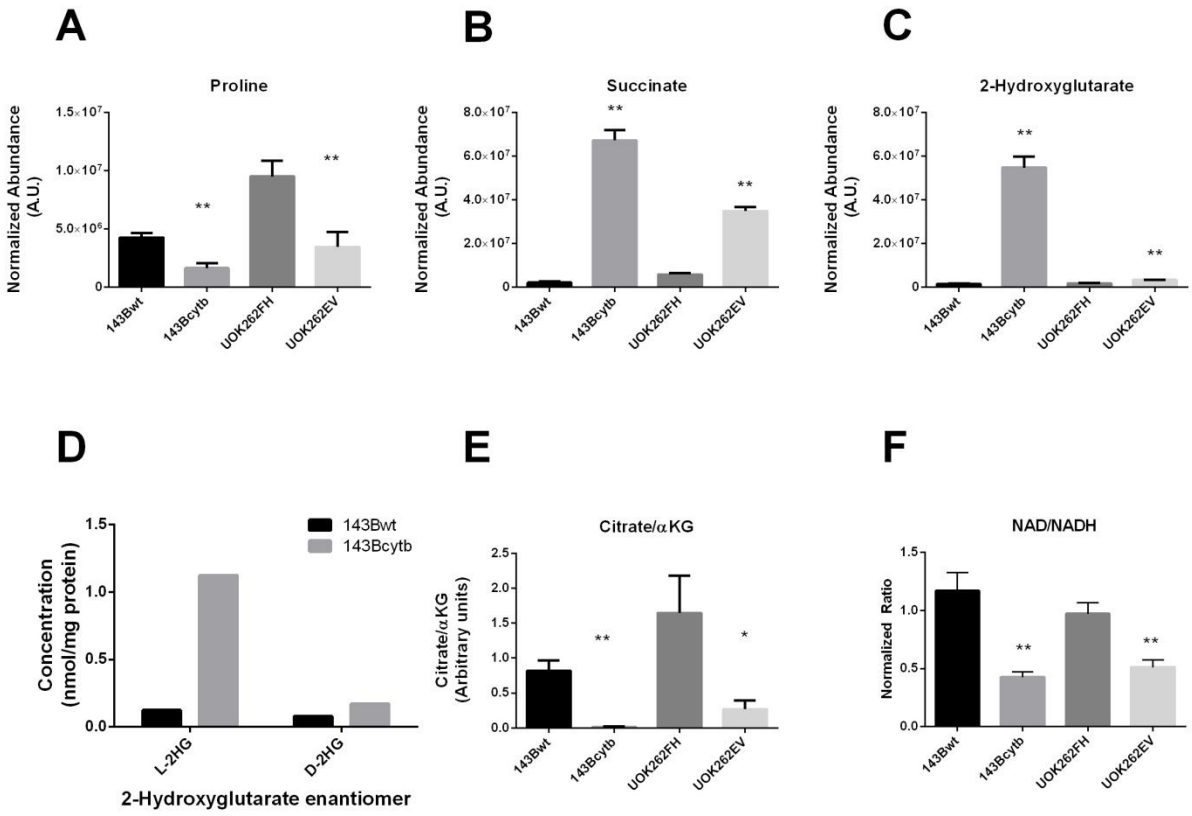

Figure 3.2: Metabolic biomarkers of reductive carboxylation

(a-c) Relative abundance of proline, succinate and 2-hydroxyglutarate in 143B and UOK262 cells measured by LC/MS. **(d)** Abundance of either L- or D-2HG in 143Bwt and 143Bcytb. **(e)** Citrate-αKG ratio in 143B and UOK262 cells. To calculate the ratio, absolute concentrations of citrate and αKG were measured from 143B or UOK262 cells. **(f)** Ratio of total NAD to NADH in 143B and UOK262 cells; values were normalized to 143Bwt. Data are the average and s.d. for three independent samples. *P,0.05; **P,0.005, Student's t-test.

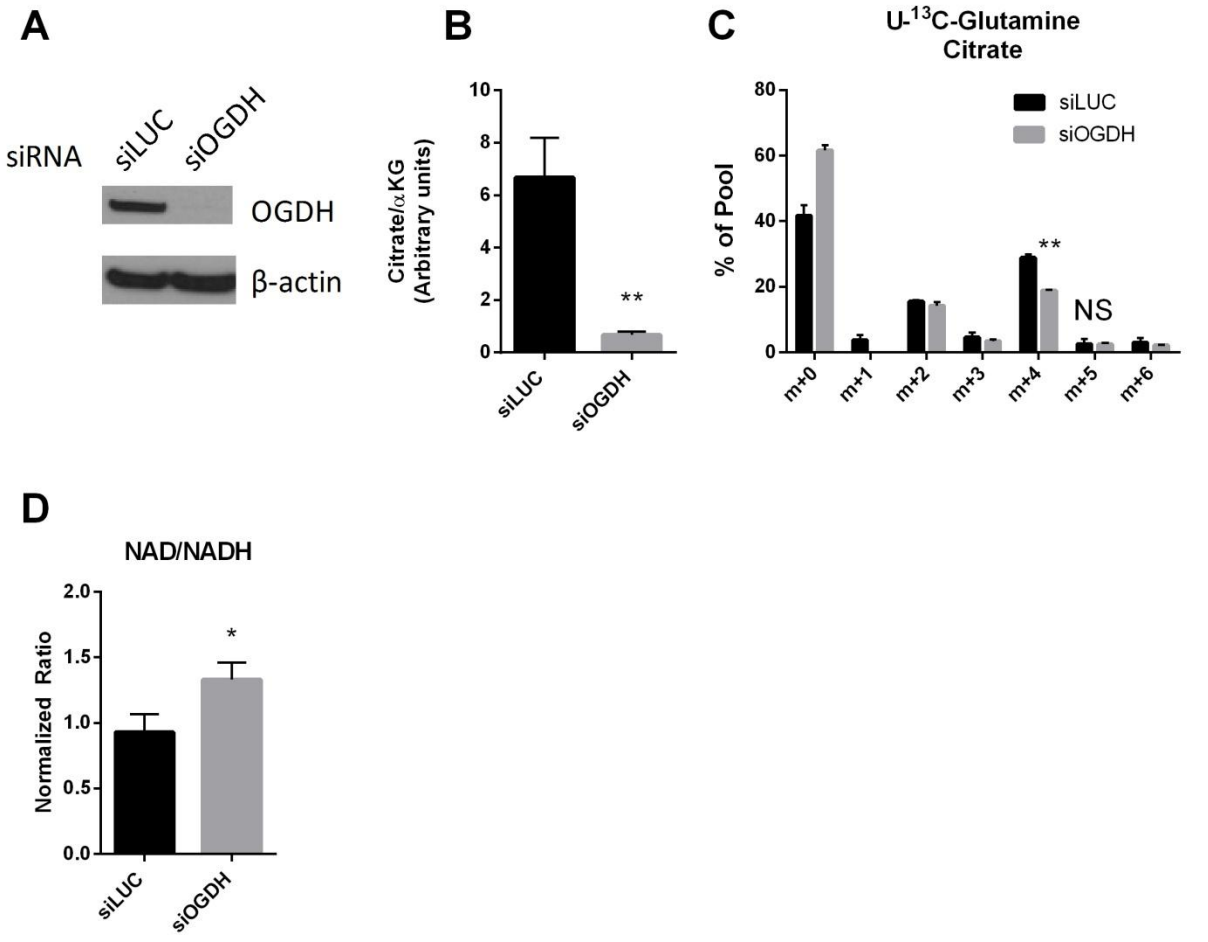

Figure 3.3: Inducing a low citrate/αKG ratio does not induce reductive carboxylation

(a) Western blot showing abundance of αKGDH (OGDH) and β-actin following transient transfection with siRNAs directed against luciferase (*LUC*, a negative control) or *OGDH* in 143Bwt cells. **(b)** Citrate-αKG ratio determined by quantifying absolute abundance of citrate and αKG after siRNA knockdown of *LUC* or *OGDH* in 143Bwt. **(c)** Mass isotopomer distribution of citrate in 143Bwt cells cultured with U-^{13}C-glutamine and unlabeled glucose. **(d)** Ratio of total NAD to NADH following transient knockdown of *LUC* or *OGDH* in 143Bwt cells; values were normalized to LUC. Data are the average and s.d. for three independent cultures. *P,0.05; **P,0.005, Student's t-test.

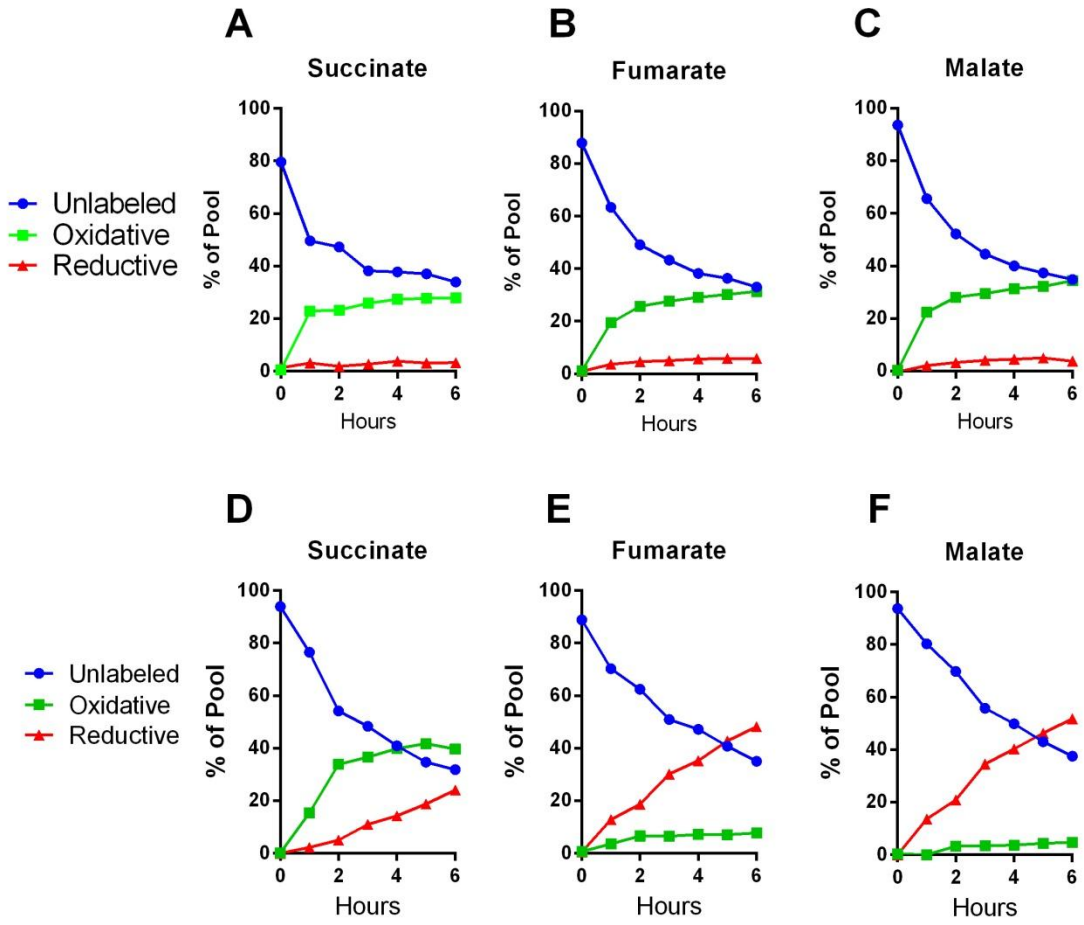

Figure 3.4. 143Bcytb cells form succinate through oxidative TCA cycle activity

(a-c) Succinate, fumarate and malate formation in 143Bwt cells cultured with U-^{13}C-glutamine and unlabeled glucose. Cells were indicated for the indicated period of time. Metabolites formed through oxidative glutamine metabolism contain four-^{13}C-carbons, while those formed through reductive metabolism contain three-^{13}-carbons. Unlabeled corresponds to the percent of the respective metabolite pool which contained no ^{13}C-label. **(d-f)** Succinate, fumarate and malate formation in 143Bcytb cells cultured with U-^{13}C-glutamine and unlabeled glucose.

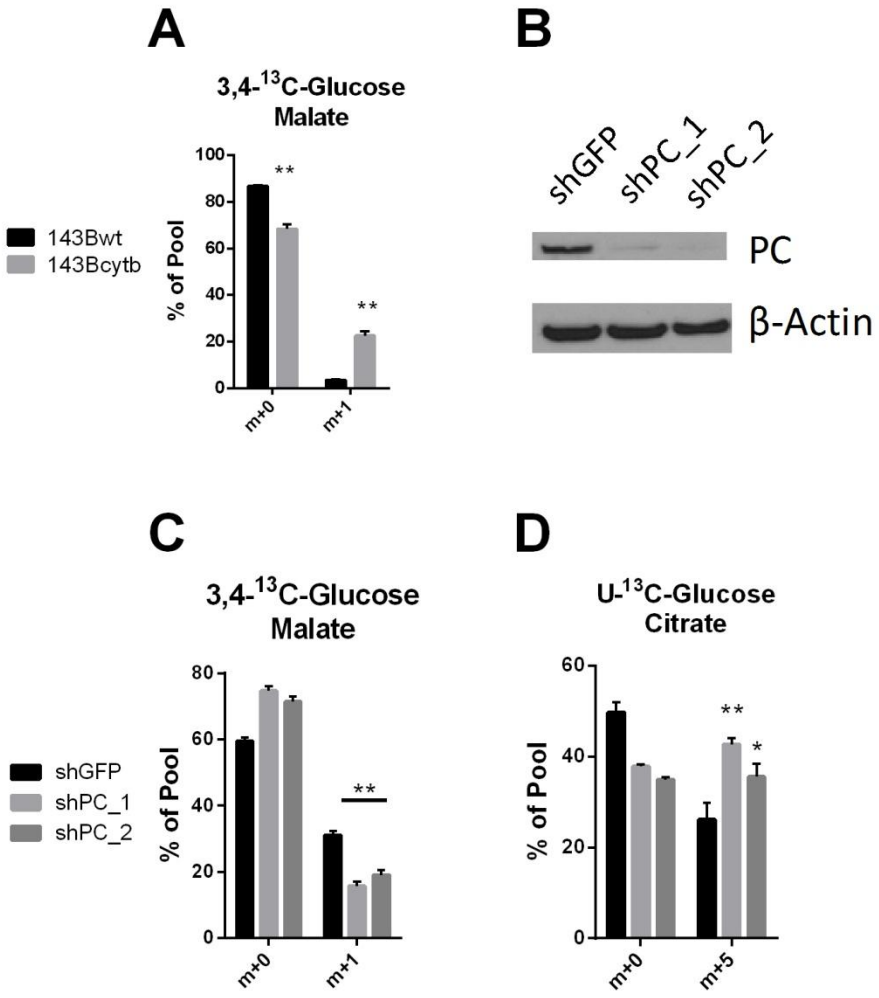

Figure 3.5: Pyruvate carboxylase activity is not required for reductive citrate formation

(a) Mass isotopomer distribution showing malate m+0 and m+1 in 143Bwt and 143Bcytb following culture with 3,4-^{13}C-glucose and unlabeled glutamine. **(b)** Western blot analysis of pyruvate carboxylase (PC) protein abundance following stable knockdown of either GFP or two independent hairpins targeting PC in 143Bcytb. **(c)** Mass isotopomer distribution of malate showing m+0 and m+1 in 143Bcytb stable knockdown cells following culture with 3,4-^{13}C-glucose and unlabeled glutamine. **(d)** Mass isotopomer distribution of citrate showing m+0 and m+5 in 143Bcytb stable knockdown cells following culture with U-^{13}C-glutamine and unlabeled glucose.

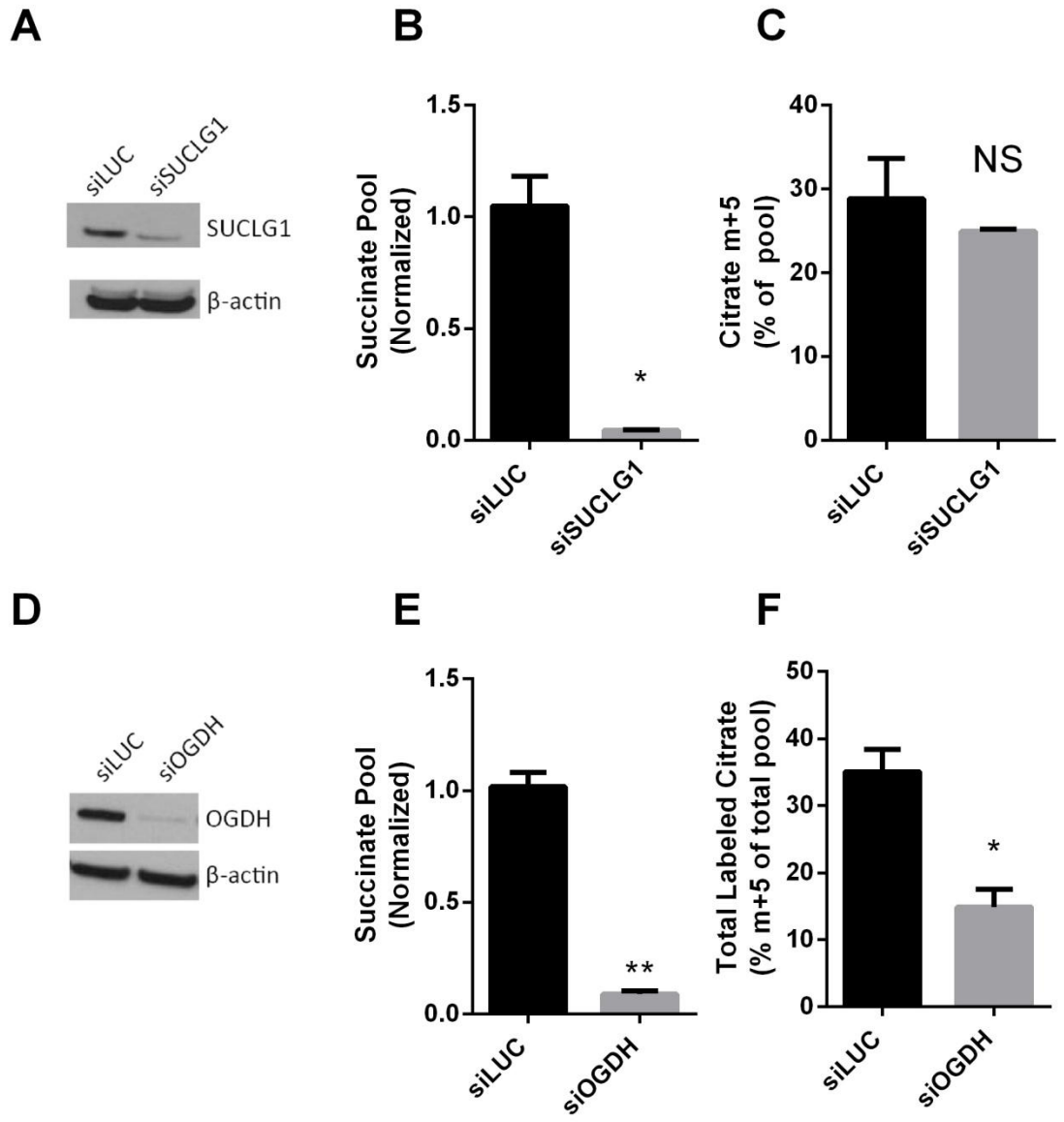

Figure 3.6: αKGDH activity is required for optimal reductive carboxylation

(a) Western blot analysis of succinyl-coA synthetase (SUCLG1) in 143Bcytb cells following transient knockdown of *LUC* or *SUCLG1*. **(b)** Succinate pool size following transient knockdown of *LUC* or *SUCLG1* in 143Bcytb. **(c)** Citrate m+5 following culture of these cells with U-^{13}C-glutamine and unlabeled glucose. **(d)** Western blot analysis of OGDH following transient knockdown of *LUC* or *OGDH* in 143Bcytb. **(e)** Succinate pool size following transient knockdown of *LUC* or *OGDH*. **(f)** Reductive citrate formation measured by multiplying the percent citrate m+5 by the relative citrate pool size. Data are the average and s.d. for three independent cultures. *P,0.05; **P,0.005, Student's t-test.

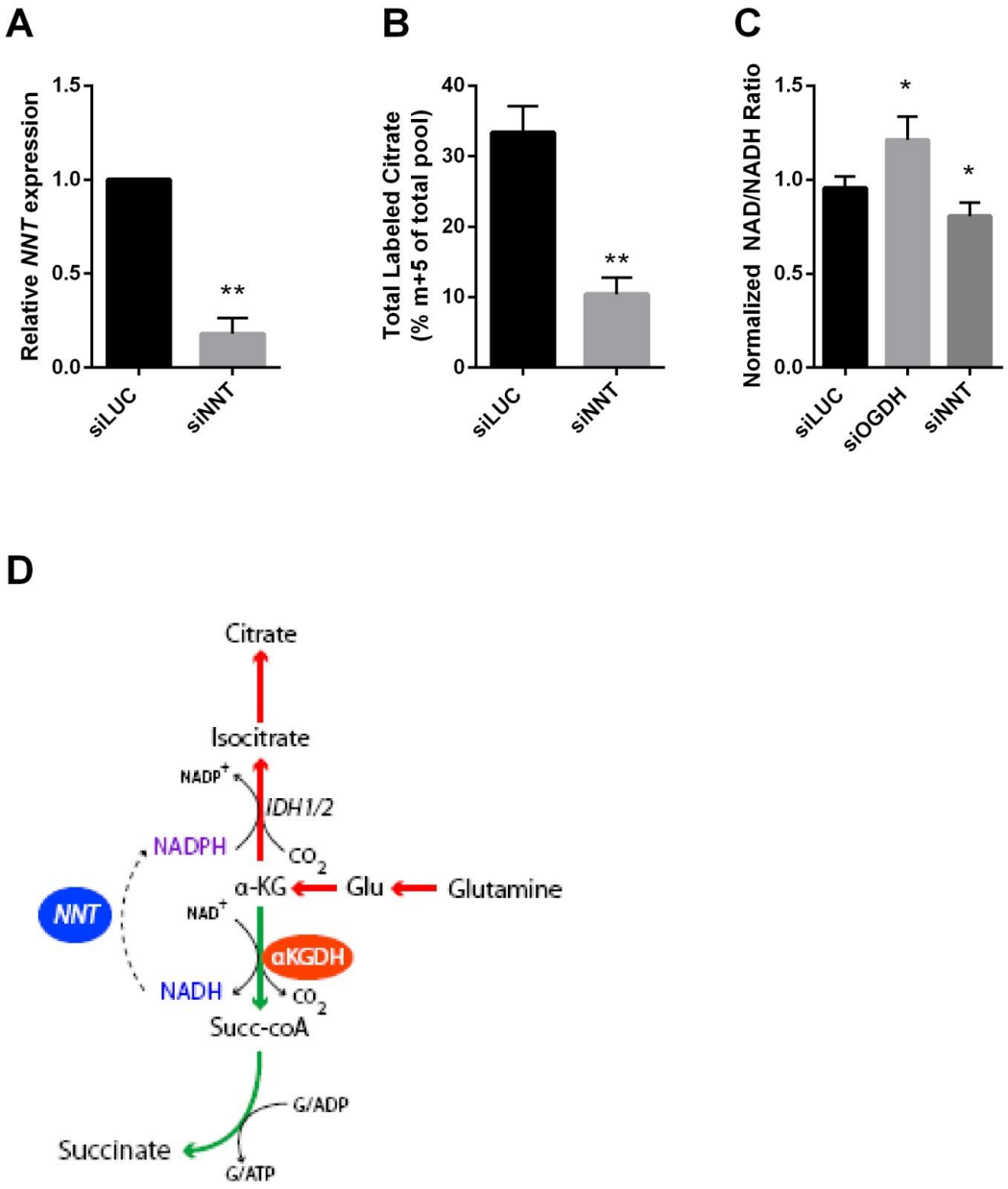

Figure 3.7: αKGDH and NNT maintain a redox state favorable for reductive carboxylation

(a) Quantitative PCR analysis of NNT transcript abundance following transient knockdown of *LUC* or *NNT* in 143Bcytb cells. **(b)** Reductive citrate formation in 143Bcytb cells following culture with U-^{13}C-glutamine and unlabeled glucose measured by multiplying the percent citrate m+5 by the relative pool size. **(c)** Ratio of total NAD to NADH following transient knockdown of *LUC, OGDH* or *NNT* in 143Bcytb cells. Values were normalized to LUC. Data are the average and s.d. for three independent cultures. *P,0.05; **P,0.005, Student's t-test. (d) Model. Flux through αKGDH generates succinate and NADH, which is dissipated by NNT to generate NADPH to sustain reductive carboxylation.

Table 3-1.Metabolites altered in 143Bcytb vs 143Bwt and UOK262EV vs UOK262FH

Metabolite	143B: cytb vs wt	UOK262: EV vs FH	143B: pvalue	UOK262: pvalue
1-methyladenosine	0.65955835	1.308599561	0.034014289	0.418260492
1-methylnicotinamide	0.695174311	1.281163997	0.009141829	0.012802799
2,3-diphospho-D-glyceric acid	0.862678483	0.225971499	0.632044832	0.027093379
2-P-glycerate/3-P-glycerate	0.919621852	1.764168178	0.263634007	0.029116626
5-aminolevulinic acid	0.65983081	0.779546947	0.05268571	0.077947437
7-methylguanosine	1.259301274	5.247050252	0.366583237	0.003506846
acetyl-carnitine	0.645030947	1.375665406	0.334189784	0.13139126
adenine	0.903410826	2.183664675	0.596810988	0.035917027
adenosine	0.329877367	2.027272114	0.083205198	0.068821442
adenosine 5-diphosphoribose	2.601797411	1.142075907	0.238831428	0.844646009
ADP	2.533304153	0.623669307	0.008690502	0.241572401
AICAR	0.477824925	37.0990315	0.0847738	0.003191316
a-keto-glutarate	0.843720416	0.852493765	0.059141421	0.387272184
alanine/sarcosine	1.899709995	1.44406455	0.114104004	0.021186379
allantoin	0.94527233	1.088826917	0.50470151	0.521696946
AMP	1.036188635	0.661784443	0.456551384	0.189216535
aspartate	0.974888557	0.199677238	0.919170243	0.000273229
betaine	0.529427791	1.092646995	0.00203185	0.276132958
choline	0.576591214	0.800435057	0.263354666	0.350779923
citrate	0.074201447	0.586591687	0.036999849	0.102900389
citrulline	0.980024707	1.300712692	0.867547066	0.144849358
CMP	1.32166406	0.826294618	0.038744969	0.372039116
creatine	0.676087359	0.946114238	0.308575298	0.866278249
creatinine	0.80341447	0.899702887	0.086617663	0.250085835
cysteine	1.619060894	0.497183363	0.053136619	0.014087219
cytidine	1.297922781	0.118602076	0.799574838	0.182419132
dAMP	1.501977261	1.012565434	0.027045382	0.871499755
dihydroxyacetone-phosphate	1.30770705	1.534841586	0.073417455	0.43892481
dimethylglycine	0.77963223	0.741250491	0.10223263	0.065733661
flavin adenine dinucleotide	1.174642288	1.32507394	0.386866983	0.037626587
fructose-1,6-biphosphate	0.779752368	3.203152313	0.097403421	0.001303717
fucose	1.757442085	0.978770421	0.025540063	0.925700686
fumaric acid	1.044817083	23.57590288	0.930423486	0.002380483
G6P/F6P	1.183320902	1.655435897	0.030825064	0.009049082
gluconic acid	0.600110649	0.958749185	0.01951517	0.780757729
glucosamine	0.908293	0.958527754	0.660276838	0.823331894

Metabolite	143B: cytb vs wt	UOK262: EV vs FH	143B: pvalue	UOK262: pvalue
glutamate/NMDA	1.11677624	1.096246815	0.388865113	0.320397237
glutamine	0.886824601	1.454236894	0.086969802	0.000995316
glycine	1.332886434	1.19633222	0.596279323	0.73592408
glyoxylate	1.153582658	0.278607443	0.418017003	0.001301368
GMP	1.200039586	0.782077578	0.021320354	0.003336177
GSH	1.394874773	0.898825223	0.066992718	0.059612198
GSSG	1.867041634	0.478878916	0.034357332	0.079437754
guanine	0.499502827	28.83714831	0.25453034	0.019033343
guanosine	0.757277017	40.78885063	0.260867318	0.022683899
histidine	1.10861333	1.936197981	0.683619712	0.005484339
homoserine/threonine	1.177835376	1.287279709	0.07290582	0.006623856
hypoxanthine	0.24697327	25.4099626	0.106663053	0.004780494
IMP	0.866462939	0.479858788	0.246856082	0.002987805
inosine	0.278611254	47.90302737	0.048209258	0.002001538
lactate	1.231101855	0.771723917	0.038772316	0.044245388
L-a-hydroxyglutaric acid	35.90446191	1.909749455	0.002941926	0.000657109
L-carnitine	0.350060576	0.684415909	1.22221E-05	0.010210906
leucine/isoleucine	0.999070023	1.595202075	0.992711298	0.050006161
L-glycerophosphorylcholine	0.789874835	1.984012565	0.323123214	0.001759751
L-homocysteine	0.882982832	0.572758483	0.023080782	0.007033033
L-kynurenine	1.253047626	1.517311867	0.675738459	0.028624016
L-pipecolic acid	1.230535507	1.21489968	0.047917673	0.261559192
malic acid	0.926998517	0.118996851	0.450107731	0.000136816
methionine	0.992188281	1.34807725	0.954727462	0.126376724
methylglyoxal	1.155959392	0.753401384	0.049923736	0.110387864
myo-inositol	1.264876602	1.276234398	0.110179213	0.036903805
N-acetyl-aspartic acid	0.70354951	0.1699442	0.048096698	3.18086E-05
NAD	1.814810848	0.942433926	0.114577424	0.767392564
NADP	1.13664757	0.879608219	0.241501017	0.389793656
nicotinamide	0.597184428	1.101934406	0.052369644	0.716627673
orotate	7.542633464	2.112675497	0.008069337	0.002473884
pantothenic acid	1.598146797	2.430516862	0.540865066	0.096223257
phenyl-alanine	1.319837745	1.749835221	0.601543187	0.016234292
phosphocholine	0.937323378	0.917888784	0.521842501	0.514684634
proline	0.382875396	0.36365299	0.001164002	0.004568047
putrescine	0.926135286	1.052880833	0.254209734	0.611209544
riboflavin	1.048931847	0.206104498	0.916460573	0.003804086
S-adenosyl-L-homocysteine	1.493967056	1.296728012	0.472941799	0.442520265

Metabolite	143B: cytb vs wt	UOK262: EV vs FH	143B: pvalue	UOK262: pvalue
S-lactoylglutathione	1.007596261	45.82194154	0.992259578	0.00547164
S-methyl-5-thioadenosine	1.033581403	2.165645747	0.713944473	0.053674284
sorbitol	1.528167607	0.737862167	0.046663827	0.102946744
spermidine	0.694986018	2.555800901	0.495553199	0.102130527
spermine	0.875322809	0.768432947	0.694731789	0.363470751
succinate	33.18847576	6.00052675	0.001622313	0.000315858
taurine	0.484013501	0.956966907	0.030274913	0.630691206
thymidine	0.717927569	0.945058318	0.090865247	0.809117601
trimethyllysine	1.576000728	2.261273766	0.091354673	0.057557195
tyrosine	1.004178958	2.359381736	0.968906439	0.011444443
UMP	1.242744696	0.633590055	0.28121995	0.078140547
uracil	0.692856497	0.630976445	0.039190329	0.004979344
valine	1.041892123	1.729589608	0.795759109	0.040611085
xanthine	0.702040824	1.484393732	0.108886103	0.160722517
xanthosine 5-monophosphate	1.889501589	0.526883285	0.109291637	0.038400931
y-aminobutyric acid	0.659216399	0.882505689	0.251971557	0.592890528

Methods

Cell Culture

143Bwt and 143Bcytb cells were cultured with DMEM supplemented with penicillin/streptomycin, 10% fetal bovine serum (FBS), L-glutamine (6mM), uridine (100ug/mL) and sodium-pyruvate (1mM). For experiments using UOK262EV and UOK262FH, this media was supplemented with G418 (300ug/mL) (Weinberg 2010; Tong 2011).

Mass isotopomer distribution and mass spectrometry

Nutrients labeled with ^{13}C were purchased from Cambridge Isotope Laboratories. All ^{13}C studies were performed in medium containing 10% dialyzed FBS and prepared so that 100% of either the glucose or glutamine pool was labeled with ^{13}C, and the other pool was unlabelled. DMEM lacking both glucose and glutamine was prepared from powder (Sigma) and supplemented with penicillin/streptomycin, sodium pyruvate (1mM) and uridine (100ug/mL). Media was then supplemented with either 15mM U-^{13}C- or 3,4-^{13}C-glucose and 2mM unlabelled glutamine, or 15mM unlabelled glucose and 2mM U-^{13}C-glutamine. All experiments were done from cells grown in 60mm dishes until 80% confluent, then rinsed with PBS and cultured with ^{13}C-containing medium for the indicated time (usually 6hrs). The cells were then washed with saline and metabolites were extracted by freeze-thawing three times in 0.5 ml of a cold 1:1 mixture of methanol:water. Macromolecules and debris were removed by centrifugation, an internal standard was added (50nmol of 2-oxobutyrate), and the supernatants with aqueous metabolites were evaporated completely and derivatized for 30 min at 42°C in 100 ml of a trimethylsilyl donor (Tri-Sil, Thermo). Metabolites were analyzed using an Agilent 6970 gas chromatograph networked to an Agilent 5973 mass selective detector. Retention times and mass fragmentation signatures of all metabolites were validated using pure standards.

To determine relative metabolite abundance across samples, the area of the total ion current peak for the metabolite of interest was compared to that of the internal standard and normalized for protein content. The mass isotopomer distribution analysis measured the fraction of each metabolite pool that contained every possible number of ^{13}C atoms; that is, a metabolite could contain 0, 1, 2,…n ^{13}C atoms, where n= the number of carbons in the metabolite. For each metabolite, an informative fragment ion containing all carbons in the parent molecule was analyzed using MSDChem software (Agilent), integrating the abundance of all mass isotopomers from m+0 to m+n, where m the mass of the fragment ion without any ^{13}C. Fragment ions monitored were: Glutamate (363-368); Succinate (247-251); Fumarate (245-249); Malate (335-339); Citrate (465-471). The abundance of each mass isotopomer was then corrected mathematically to account for natural abundance isotopes using Cormat (Fernandez 1996) and finally converted into a percentage of the total pool.

Relative and quantitative measurements of metabolite levels

For relative measurements of metabolites cells were incubated with DMEM with 10% dialyzed serum supplemented with unlabeled glucose and glutamine at a concentration of 15mM and 2mm, respectively. After two hours cells were washed twice with cold saline and metabolites were extracted with 50% methanol. For quantitative measurements of citrate, succinate or αKG, precise concentrations of ^{13}C-labeled citrate, αKG and succinate were added to the extracts. For all samples, metabolites were extracted through three freeze-thaw cycles followed by centrifugation. Supernatant was dried and then reconstituted in 0.03% formic acid in water. This was followed by LC/MS quantification.

RNAi

Transient gene silencing experiments were done using siRNA oligos targeting SUCLG1, OGDH or NNT (siGenome, Thermo) were transfected to 143B cells with DharmaFECT transfection reagent (Thermo);

oligos targeting luciferase was as a negative control (siGenome, Thermo). All experiments took place 72 hours later and were carried out as described above. Cells were cultured with ^{13}C-nutrients for two hours. For stable gene silencing, lentiviral-mediated shRNAs targeting PC from the Mission shRNA pLKO.1-puro library (Sigma) were used to infect 143Bcytb cells according to supplied protocol. 143B cells were infected with individual shRNA hairpin and table integrants were selected with Puromycin (Invitrogen).

To monitor protein abundances cells were lysed in RIPA buffer and protein separated on NuPAGE® Novex® 4-12% Bis-Tris gel (Invitrogen). Protein was transferred to Immobilon transfer membranes (Millipore). Protein was detected using commercially available antibodies against SUCLG1 (Cell Signaling), OGDH (Sigma) or PC (Santa Cruz Biotechnology). NNT knockdown was quantified using RT-QPCR. Briefly, RNA was extracted in Trizol (Invitrogen) and isolated according to manufactures protocol. CDNA was generated using iScript synthesis kit (Biorad) and transcript abundance was measured on Thermo QPCR instrument.

Generation of UOK262 PCDNA3.1 Empty Vector cell line

PCDNA3.1 empty vector plasmid was transfected with Fugene (Promega) to UOK262 cells. To isolate stable integration of the plasmid cells were continuously grown in G418 (Invitrogen).

NADH Ratio

NAD/NADH ratio was measured using a commercially available kit (Biovisison, K337-100). Procedure for extraction and measurements were done according to manufacturer's protocol. Briefly, cells were incubated two hours with DMEM supplemented with 10% dialyzed FBS and unlabeled glucose and

glutamine at a concentration of 15mM and 2mM, respectively. After this cells were washed twice with saline and fresh saline was added so cells could be scraped off the dishes and pelleted. Next, NAD and NADH were extracted in the supplied Extraction Buffer. Samples were subjected to two freeze-thaws and centrifuged. Aliquots of each sample were heated at 60C for 30 minutes to decompose of NAD. Following this, samples were loaded to Costar 96well plate and manufacture-supplied Cycling Buffer added and absorbance read at OD_{450}.

Chapter Four

Discussion and future directions

Warburg postulated nearly 60 years ago that human cancers were the result of mitochondrial defects (Warburg, 1956). Subsequent studies have shown this to be untrue and have highlighted the importance of functional mitochondrial activities for tumor cell growth. However, over the last ten years we have learned of several tumors which are metabolic outliers, and are the direct result of mitochondrial dysfunction. In my view, these tumors are a touchstone in the discussion of the importance of metabolic pathways in tumor cell growth. At one time, these tumors may have been the basis for why some believed the study of cancer metabolism was unimportant, as cellular transformation can occur even in the context of severe metabolic dysfunction. We and others believed these tumors were important outliers which, by their very nature, demonstrated the relevance of metabolic pathways to cancer biology. We hypothesized that, in the context of such unusual metabolic disturbances, these tumors were relying on novel and/or unusual metabolic pathways for growth. Studying these outliers has given us new insight into the mechanisms supporting growth in rare tumors and has depended our understanding of metabolic pathways in common tumors.

These findings are important for the metabolism field. First, the TCA cycle has changed little since it was first discovered (Krebs, 1970). Our work has revealed contexts where this pathway can operate in a novel and highly unusual fashion through mechanisms that are still largely unknown. Furthermore, we found this mode of metabolism can be induced in cells using common drugs. The reductive carboxylation reaction itself is also highly interesting. The other known mammalian carboxylases, which include acetyl-coA carboxylaes, propionyl-CoA carboxylase, 3-methylcrotonyl-CoA carboxylase, geranyl-CoA carboxylase, pyruvate carboxylase, and urea carboxylase, are all biotin dependent enzymes (Tong, 2013). This raises the possibility that IDH1 and IDH2 associate with biotin or a biotin-associated enzyme in order to catalyze the carboxylation reaction. This appears to be unlikely however, as the reductive carboxylation can occur *in vitro* with pure IDH extracts (Leonardi et al., 2012). None the less, this highlights a unique feature of the reaction mechanism. Additionally, reductive

carboxylation is dependent on different isoforms in different cell types; the mechanisms regulating this have not been defined. Moreover, we do not understand the metabolic adaptations that allow this pathway to be fully engaged in normal cells. For example, treatment with the ETC Complex I inhibitor rotenone acutely induces reductive glutamine metabolism yet these cells do not proliferate; defining the adaptations which allow cells to fully engage this pathway will be informative. Moreover, we know almost nothing about the function of this pathway in normal growth and development *in vivo*. Thus, the reductive carboxylation pathway is a rich source of unanswered basic science questions.

Secondly, this work highlights the importance of biosynthetic metabolism for cell growth. One outcome of this study was that we would find cells with metabolic defects to not engage any alternative pathways of precursor production. The observation that, even in the context of severe mitochondrial dysfunction, cells engage an unconventional pathway underscores the importance of biosynthetic metabolism to cell growth. Additionally, this pathway appears to provide metabolic flexibility to cells without a primary metabolic defect. This is important for periods of reduced ETC activity, such as during hypoxia. Lastly, the existence of this pathway underscores glutamine's role as an important tumor nutrient.

Thirdly, this pathway has therapeutic potential. The gold standard for cancer treatment is to identify activities which are both exclusive to tumors and also required for their growth, so as to avoid toxicity to normal. Reductive carboxylation is one such cancer-specific activity, as it appears to be limited exclusively to tumor cells with metabolic defects or under conditions of hypoxia. Presently however, we lack synthetically lethal targets. One way to identify novel targets would be a gene expression analysis of multiple cell lines which uses reductive carboxylation. This would potentially provide shared gene expression signatures of cells which engage this pathway and may inform ways to selectively target theses cells. Alternatively, an RNAi or small molecule-based screen in isogenic paired

cell lines could identify components of this pathway which would be synthetically lethal to these cells. Doing the screen in isogenic pairs would have the added advantage of identifying genuine, synthetically-lethal hits and would reduce off-target hits. This also has the potential to uncover additional vulnerabilities which may be associated with reductive carboxylation. Beyond reductive carboxylation, cancer metabolism is an exciting field. Weekly, we are learning of new ways in which metabolic activities are regulated and dysregulated in cancer. Collectively, I think this has the potential to transform both the diagnosis and treatment of patients and will likely impact other areas of biology beyond cancer.

Several years ago, Yuri Lazebnik commented on the then nascent field of apoptosis in a piece titled "Can a biologist fix a radio? – Or, what I learned while studying apoptosis", which I feel is highly relevant to this discussion. Lazebnik noted that, at the time, the field of apoptosis was at a feverish stage in which every issue of *Cell, Science* or *Nature* had publications related to apoptosis; not unlike the current stage of the cancer metabolism field. He likened this stage to a Klondike gold rush, where an unexpected finding "makes many realize that the previously mysterious process can be dissected with available tools and, importantly, that this effort may result in a miracle drug" (Lazebnik, 2002). However, Lazebnik's piece is a cautionary tale, as he notes that all fields eventually hit a wall and reach "a stage at which models, that seemed so complete, fall apart, predictions that were considered so obvious are found to be wrong, and attempts to develop wonder drugs largely fail" (Lazebnik, 2002). I assume the field of cancer metabolism will be no different. I believe the recent work on IDH1/2 mutations in tumors is incredibly important and should serve as a model for future studies in the cancer metabolism field. In less than five years, mutations in IDH1/2 were discovered, the neomorphic enzyme activity identified, mechanisms of 2-HG defined, and inhibitors against the mutant enzyme developed. This has yielded important insights into the basic science of cancer biology and has the potential improve clinical outcomes. For the future success of this field, I believe there needs to be ever increasing emphasis on translating our basic science discoveries into therapeutic treatment strategies.

Reference

Adam, J., Hatipoglu, E., O'Flaherty, L., Ternette, N., Sahgal, N., Lockstone, H., Baban, D., Nye, E., Stamp, G.W., Wolhuter, K.*, et al.* (2011). Renal cyst formation in Fh1-deficient mice is independent of the Hif/Phd pathway: roles for fumarate in KEAP1 succination and Nrf2 signaling. Cancer cell *20*, 524-537.

Adhikary, S., and Eilers, M. (2005). Transcriptional regulation and transformation by Myc proteins. Nature reviews Molecular cell biology *6*, 635-645.

Alderson, N.L., Wang, Y., Blatnik, M., Frizzell, N., Walla, M.D., Lyons, T.J., Alt, N., Carson, J.A., Nagai, R., Thorpe, S.R.*, et al.* (2006). S-(2-Succinyl)cysteine: a novel chemical modification of tissue proteins by a Krebs cycle intermediate. Archives of biochemistry and biophysics *450*, 1-8.

Amary, M.F., Bacsi, K., Maggiani, F., Damato, S., Halai, D., Berisha, F., Pollock, R., O'Donnell, P., Grigoriadis, A., Diss, T.*, et al.* (2011). IDH1 and IDH2 mutations are frequent events in central chondrosarcoma and central and periosteal chondromas but not in other mesenchymal tumours. The Journal of pathology *224*, 334-343.

Astuti, D., Latif, F., Dallol, A., Dahia, P.L., Douglas, F., George, E., Skoldberg, F., Husebye, E.S., Eng, C., and Maher, E.R. (2001). Gene mutations in the succinate dehydrogenase subunit SDHB cause susceptibility to familial pheochromocytoma and to familial paraganglioma. American journal of human genetics *69*, 49-54.

Au, H.C., Seo, B.B., Matsuno-Yagi, A., Yagi, T., and Scheffler, I.E. (1999). The NDUFA1 gene product (MWFE protein) is essential for activity of complex I in mammalian mitochondria. Proceedings of the National Academy of Sciences of the United States of America *96*, 4354-4359.

Avramis, V.I., and Tiwari, P.N. (2006). Asparaginase (native ASNase or pegylated ASNase) in the treatment of acute lymphoblastic leukemia. International journal of nanomedicine *1*, 241-254.

Bardella, C., Olivero, M., Lorenzato, A., Geuna, M., Adam, J., O'Flaherty, L., Rustin, P., Tomlinson, I., Pollard, P.J., and Di Renzo, M.F. (2012). Cells lacking the fumarase tumor suppressor are protected from apoptosis through a hypoxia-inducible factor-independent, AMPK-dependent mechanism. Molecular and cellular biology *32*, 3081-3094.

Bauer, D.E., Hatzivassiliou, G., Zhao, F., Andreadis, C., and Thompson, C.B. (2005). ATP citrate lyase is an important component of cell growth and transformation. Oncogene *24*, 6314-6322.

Bayley, J.P., Launonen, V., and Tomlinson, I.P. (2008). The FH mutation database: an online database of fumarate hydratase mutations involved in the MCUL (HLRCC) tumor syndrome and congenital fumarase deficiency. BMC medical genetics *9*, 20.

Baysal, B.E., Ferrell, R.E., Willett-Brozick, J.E., Lawrence, E.C., Myssiorek, D., Bosch, A., van der Mey, A., Taschner, P.E., Rubinstein, W.S., Myers, E.N.*, et al.* (2000). Mutations in SDHD, a mitochondrial complex II gene, in hereditary paraganglioma. Science *287*, 848-851.

Baysal, B.E., McKay, S.E., Kim, Y.J., Zhang, Z., Alila, L., Willett-Brozick, J.E., Pacak, K., Kim, T.H., and Shadel, G.S. (2011). Genomic imprinting at a boundary element flanking the SDHD locus. Human molecular genetics *20*, 4452-4461.

Bensaad, K., Tsuruta, A., Selak, M.A., Vidal, M.N., Nakano, K., Bartrons, R., Gottlieb, E., and Vousden, K.H. (2006). TIGAR, a p53-inducible regulator of glycolysis and apoptosis. Cell *126*, 107-120.

Berwick, D.C., Hers, I., Heesom, K.J., Moule, S.K., and Tavare, J.M. (2002). The identification of ATP-citrate lyase as a protein kinase B (Akt) substrate in primary adipocytes. The Journal of biological chemistry *277*, 33895-33900.

Biswas, S., Troy, H., Leek, R., Chung, Y.L., Li, J.L., Raval, R.R., Turley, H., Gatter, K., Pezzella, F., Griffiths, J.R.*, et al.* (2010). Effects of HIF-1alpha and HIF2alpha on Growth and Metabolism of Clear-Cell Renal Cell Carcinoma 786-0 Xenografts. Journal of oncology *2010*, 757908.

Cairns, R.A., Harris, I.S., and Mak, T.W. (2011). Regulation of cancer cell metabolism. Nature reviews Cancer *11*, 85-95.

Campbell, C.T., Kolesar, J.E., and Kaufman, B.A. (2012). Mitochondrial transcription factor A regulates mitochondrial transcription initiation, DNA packaging, and genome copy number. Biochimica et biophysica acta *1819*, 921-929.

Cantor, J.R., and Sabatini, D.M. (2012). Cancer cell metabolism: one hallmark, many faces. Cancer discovery *2*, 881-898.

Cavalli, L.R., Varella-Garcia, M., and Liang, B.C. (1997). Diminished tumorigenic phenotype after depletion of mitochondrial DNA. Cell growth & differentiation : the molecular biology journal of the American Association for Cancer Research *8*, 1189-1198.

Cervera, A.M., Bayley, J.P., Devilee, P., and McCreath, K.J. (2009). Inhibition of succinate dehydrogenase dysregulates histone modification in mammalian cells. Molecular cancer *8*, 89.

Chatterjee, A., Mambo, E., and Sidransky, D. (2006). Mitochondrial DNA mutations in human cancer. Oncogene *25*, 4663-4674.

Cheng, T., Sudderth, J., Yang, C., Mullen, A.R., Jin, E.S., Mates, J.M., and DeBerardinis, R.J. (2011). Pyruvate carboxylase is required for glutamine-independent growth of tumor cells. Proceedings of the National Academy of Sciences of the United States of America *108*, 8674-8679.

Chowdhury, R., Yeoh, K.K., Tian, Y.M., Hillringhaus, L., Bagg, E.A., Rose, N.R., Leung, I.K., Li, X.S., Woon, E.C., Yang, M.*, et al.* (2011). The oncometabolite 2-hydroxyglutarate inhibits histone lysine demethylases. EMBO reports *12*, 463-469.

Comte, B., Vincent, G., Bouchard, B., and Des Rosiers, C. (1997). Probing the origin of acetyl-CoA and oxaloacetate entering the citric acid cycle from the 13C labeling of citrate released by perfused rat hearts. The Journal of biological chemistry *272*, 26117-26124.

Cook, R.J. (2000). Defining the steps of the folate one-carbon shuffle and homocysteine metabolism. The American journal of clinical nutrition *72*, 1419-1420.

Cory, J.G., and Cory, A.H. (2006). Critical roles of glutamine as nitrogen donors in purine and pyrimidine nucleotide synthesis: asparaginase treatment in childhood acute lymphoblastic leukemia. In Vivo *20*, 587-589.

Dang, C.V., Le, A., and Gao, P. (2009a). MYC-induced cancer cell energy metabolism and therapeutic opportunities. Clinical cancer research : an official journal of the American Association for Cancer Research *15*, 6479-6483.

Dang, L., White, D.W., Gross, S., Bennett, B.D., Bittinger, M.A., Driggers, E.M., Fantin, V.R., Jang, H.G., Jin, S., Keenan, M.C.*, et al.* (2009b). Cancer-associated IDH1 mutations produce 2-hydroxyglutarate. Nature *462*, 739-744.

de Koning, T.J., Snell, K., Duran, M., Berger, R., Poll-The, B.T., and Surtees, R. (2003). L-serine in disease and development. The Biochemical journal *371*, 653-661.

DeBerardinis, R.J., and Cheng, T. (2010). Q's next: the diverse functions of glutamine in metabolism, cell biology and cancer. Oncogene *29*, 313-324.

DeBerardinis, R.J., Mancuso, A., Daikhin, E., Nissim, I., Yudkoff, M., Wehrli, S., and Thompson, C.B. (2007). Beyond aerobic glycolysis: transformed cells can engage in glutamine metabolism that exceeds the requirement for protein and nucleotide synthesis. Proceedings of the National Academy of Sciences of the United States of America *104*, 19345-19350.

Deberardinis, R.J., Sayed, N., Ditsworth, D., and Thompson, C.B. (2008). Brick by brick: metabolism and tumor cell growth. Current opinion in genetics & development *18*, 54-61.

Delhommeau, F., Dupont, S., Della Valle, V., James, C., Trannoy, S., Masse, A., Kosmider, O., Le Couedic, J.P., Robert, F., Alberdi, A.*, et al.* (2009). Mutation in TET2 in myeloid cancers. The New England journal of medicine *360*, 2289-2301.

DeNicola, G.M., Karreth, F.A., Humpton, T.J., Gopinathan, A., Wei, C., Frese, K., Mangal, D., Yu, K.H., Yeo, C.J., Calhoun, E.S.*, et al.* (2011). Oncogene-induced Nrf2 transcription promotes ROS detoxification and tumorigenesis. Nature *475*, 106-109.

Deprez, J., Vertommen, D., Alessi, D.R., Hue, L., and Rider, M.H. (1997). Phosphorylation and activation of heart 6-phosphofructo-2-kinase by protein kinase B and other protein kinases of the insulin signaling cascades. The Journal of biological chemistry *272*, 17269-17275.

Des Rosiers, C., Fernandez, C.A., David, F., and Brunengraber, H. (1994). Reversibility of the mitochondrial isocitrate dehydrogenase reaction in the perfused rat liver. Evidence from isotopomer analysis of citric acid cycle intermediates. The Journal of biological chemistry *269*, 27179-27182.

Elstrom, R.L., Bauer, D.E., Buzzai, M., Karnauskas, R., Harris, M.H., Plas, D.R., Zhuang, H., Cinalli, R.M., Alavi, A., Rudin, C.M.*, et al.* (2004). Akt stimulates aerobic glycolysis in cancer cells. Cancer research *64*, 3892-3899.

Fendt, S.M., Bell, E.L., Keibler, M.A., Olenchock, B.A., Mayers, J.R., Wasylenko, T.M., Vokes, N.I., Guarente, L., Vander Heiden, M.G., and Stephanopoulos, G. (2013). Reductive glutamine metabolism is a function of the alpha-ketoglutarate to citrate ratio in cells. Nature communications *4*, 2236.

Fernandez, C.A., Des Rosiers, C., Previs, S.F., David, F., and Brunengraber, H. (1996). Correction of 13C mass isotopomer distributions for natural stable isotope abundance. Journal of mass spectrometry : JMS *31*, 255-262.

Figueroa, M.E., Abdel-Wahab, O., Lu, C., Ward, P.S., Patel, J., Shih, A., Li, Y., Bhagwat, N., Vasanthakumar, A., Fernandez, H.F*., et al.* (2010). Leukemic IDH1 and IDH2 mutations result in a hypermethylation phenotype, disrupt TET2 function, and impair hematopoietic differentiation. Cancer cell *18*, 553-567.

Frezza, C., Zheng, L., Folger, O., Rajagopalan, K.N., MacKenzie, E.D., Jerby, L., Micaroni, M., Chaneton, B., Adam, J., Hedley, A*., et al.* (2011). Haem oxygenase is synthetically lethal with the tumour suppressor fumarate hydratase. Nature *477*, 225-228.

Fu, T.F., Rife, J.P., and Schirch, V. (2001). The role of serine hydroxymethyltransferase isozymes in one-carbon metabolism in MCF-7 cells as determined by (13)C NMR. Archives of biochemistry and biophysics *393*, 42-50.

Gaglio, D., Soldati, C., Vanoni, M., Alberghina, L., and Chiaradonna, F. (2009). Glutamine deprivation induces abortive s-phase rescued by deoxyribonucleotides in k-ras transformed fibroblasts. PloS one *4*, e4715.

Gameiro, P.A., Laviolette, L.A., Kelleher, J.K., Iliopoulos, O., and Stephanopoulos, G. (2013a). Cofactor balance by nicotinamide nucleotide transhydrogenase (NNT) coordinates reductive carboxylation and glucose catabolism in the tricarboxylic acid (TCA) cycle. The Journal of biological chemistry *288*, 12967-12977.

Gameiro, P.A., Yang, J., Metelo, A.M., Perez-Carro, R., Baker, R., Wang, Z., Arreola, A., Rathmell, W.K., Olumi, A., Lopez-Larrubia, P*., et al.* (2013b). In vivo HIF-mediated reductive carboxylation is regulated by citrate levels and sensitizes VHL-deficient cells to glutamine deprivation. Cell metabolism *17*, 372-385.

Gao, P., Tchernyshyov, I., Chang, T.C., Lee, Y.S., Kita, K., Ochi, T., Zeller, K.I., De Marzo, A.M., Van Eyk, J.E., Mendell, J.T*., et al.* (2009). c-Myc suppression of miR-23a/b enhances mitochondrial glutaminase expression and glutamine metabolism. Nature *458*, 762-765.

Geisbrecht, B.V., and Gould, S.J. (1999). The human PICD gene encodes a cytoplasmic and peroxisomal NADP(+)-dependent isocitrate dehydrogenase. The Journal of biological chemistry *274*, 30527-30533.

Gonzalez, E., and McGraw, T.E. (2009). The Akt kinases: isoform specificity in metabolism and cancer. Cell Cycle *8*, 2502-2508.

Gottlob, K., Majewski, N., Kennedy, S., Kandel, E., Robey, R.B., and Hay, N. (2001). Inhibition of early apoptotic events by Akt/PKB is dependent on the first committed step of glycolysis and mitochondrial hexokinase. Genes & development *15*, 1406-1418.

Green, A., and Beer, P. (2010). Somatic mutations of IDH1 and IDH2 in the leukemic transformation of myeloproliferative neoplasms. The New England journal of medicine *362*, 369-370.

Greenhouse, W.V., and Lehninger, A.L. (1976). Occurrence of the malate-aspartate shuttle in various tumor types. Cancer research *36*, 1392-1396.

Hamanaka, R.B., and Chandel, N.S. (2009). Mitochondrial reactive oxygen species regulate hypoxic signaling. Current opinion in cell biology *21*, 894-899.

Hanahan, D., and Weinberg, R.A. (2000). The hallmarks of cancer. Cell *100*, 57-70.

Hao, H.X., Khalimonchuk, O., Schraders, M., Dephoure, N., Bayley, J.P., Kunst, H., Devilee, P., Cremers, C.W., Schiffman, J.D., Bentz, B.G*., et al.* (2009). SDH5, a gene required for flavination of succinate dehydrogenase, is mutated in paraganglioma. Science *325*, 1139-1142.

Hatzivassiliou, G., Zhao, F., Bauer, D.E., Andreadis, C., Shaw, A.N., Dhanak, D., Hingorani, S.R., Tuveson, D.A., and Thompson, C.B. (2005). ATP citrate lyase inhibition can suppress tumor cell growth. Cancer cell *8*, 311-321.

Hedeskov, C.J. (1968). Early effects of phytohaemagglutinin on glucose metabolism of normal human lymphocytes. The Biochemical journal *110*, 373-380.

Hensen, E.F., Jordanova, E.S., van Minderhout, I.J., Hogendoorn, P.C., Taschner, P.E., van der Mey, A.G., Devilee, P., and Cornelisse, C.J. (2004). Somatic loss of maternal chromosome 11 causes parent-of-origin-dependent inheritance in SDHD-linked paraganglioma and phaeochromocytoma families. Oncogene *23*, 4076-4083.

Hu, W., Zhang, C., Wu, R., Sun, Y., Levine, A., and Feng, Z. (2010). Glutaminase 2, a novel p53 target gene regulating energy metabolism and antioxidant function. Proceedings of the National Academy of Sciences of the United States of America *107*, 7455-7460.

Hume, D.A., Radik, J.L., Ferber, E., and Weidemann, M.J. (1978). Aerobic glycolysis and lymphocyte transformation. The Biochemical journal *174*, 703-709.

Ishikawa, K., Imanishi, H., Takenaga, K., and Hayashi, J. (2012). Regulation of metastasis; mitochondrial DNA mutations have appeared on stage. Journal of bioenergetics and biomembranes *44*, 639-644.

Issa, J.P. (2004). CpG island methylator phenotype in cancer. Nature reviews Cancer *4*, 988-993.

Jain, M., Arvanitis, C., Chu, K., Dewey, W., Leonhardt, E., Trinh, M., Sundberg, C.D., Bishop, J.M., and Felsher, D.W. (2002). Sustained loss of a neoplastic phenotype by brief inactivation of MYC. Science *297*, 102-104.

Kaelin, W.G., Jr., and McKnight, S.L. (2013). Influence of metabolism on epigenetics and disease. Cell *153*, 56-69.

Kaelin, W.G., Jr., and Ratcliffe, P.J. (2008). Oxygen sensing by metazoans: the central role of the HIF hydroxylase pathway. Molecular cell *30*, 393-402.

Killian, J.K., Kim, S.Y., Miettinen, M., Smith, C., Merino, M., Tsokos, M., Quezado, M., Smith, W.I., Jr., Jahromi, M.S., Xekouki, P*., et al.* (2013). Succinate dehydrogenase mutation underlies global epigenomic divergence in gastrointestinal stromal tumor. Cancer discovery *3*, 648-657.

Kim, J.W., Tchernyshyov, I., Semenza, G.L., and Dang, C.V. (2006). HIF-1-mediated expression of pyruvate dehydrogenase kinase: a metabolic switch required for cellular adaptation to hypoxia. Cell metabolism *3*, 177-185.

Kirito, K., Hu, Y., and Komatsu, N. (2009). HIF-1 prevents the overproduction of mitochondrial ROS after cytokine stimulation through induction of PDK-1. Cell Cycle *8*, 2844-2849.

Koivunen, P., Hirsila, M., Remes, A.M., Hassinen, I.E., Kivirikko, K.I., and Myllyharju, J. (2007). Inhibition of hypoxia-inducible factor (HIF) hydroxylases by citric acid cycle intermediates: possible links between cell metabolism and stabilization of HIF. The Journal of biological chemistry *282*, 4524-4532.

Koivunen, P., Lee, S., Duncan, C.G., Lopez, G., Lu, G., Ramkissoon, S., Losman, J.A., Joensuu, P., Bergmann, U., Gross, S.*, et al.* (2012). Transformation by the (R)-enantiomer of 2-hydroxyglutarate linked to EGLN activation. Nature *483*, 484-488.

Kranendijk, M., Struys, E.A., Salomons, G.S., Van der Knaap, M.S., and Jakobs, C. (2012). Progress in understanding 2-hydroxyglutaric acidurias. Journal of inherited metabolic disease *35*, 571-587.

Kranendijk, M., Struys, E.A., van Schaftingen, E., Gibson, K.M., Kanhai, W.A., van der Knaap, M.S., Amiel, J., Buist, N.R., Das, A.M., de Klerk, J.B.*, et al.* (2010). IDH2 mutations in patients with D-2-hydroxyglutaric aciduria. Science *330*, 336.

Krebs, H.A. (1970). The history of the tricarboxylic acid cycle. Perspectives in biology and medicine *14*, 154-170.

Kucejova, B., Pena-Llopis, S., Yamasaki, T., Sivanand, S., Tran, T.A., Alexander, S., Wolff, N.C., Lotan, Y., Xie, X.J., Kabbani, W.*, et al.* (2011). Interplay between pVHL and mTORC1 pathways in clear-cell renal cell carcinoma. Molecular cancer research : MCR *9*, 1255-1265.

Kuhajda, F.P. (2000). Fatty-acid synthase and human cancer: new perspectives on its role in tumor biology. Nutrition *16*, 202-208.

Laplante, M., and Sabatini, D.M. (2012). mTOR signaling in growth control and disease. Cell *149*, 274-293.

Lazebnik, Y. (2002). Can a biologist fix a radio?--Or, what I learned while studying apoptosis. Cancer cell *2*, 179-182.

Lee, S., Nakamura, E., Yang, H., Wei, W., Linggi, M.S., Sajan, M.P., Farese, R.V., Freeman, R.S., Carter, B.D., Kaelin, W.G., Jr*., et al.* (2005). Neuronal apoptosis linked to EglN3 prolyl hydroxylase and familial pheochromocytoma genes: developmental culling and cancer. Cancer cell *8*, 155-167.

Lemons, J.M., Feng, X.J., Bennett, B.D., Legesse-Miller, A., Johnson, E.L., Raitman, I., Pollina, E.A., Rabitz, H.A., Rabinowitz, J.D., and Coller, H.A. (2010). Quiescent fibroblasts exhibit high metabolic activity. PLoS biology *8*, e1000514.

Leonardi, R., Subramanian, C., Jackowski, S., and Rock, C.O. (2012). Cancer-associated isocitrate dehydrogenase mutations inactivate NADPH-dependent reductive carboxylation. The Journal of biological chemistry *287*, 14615-14620.

Letouze, E., Martinelli, C., Loriot, C., Burnichon, N., Abermil, N., Ottolenghi, C., Janin, M., Menara, M., Nguyen, A.T., Benit, P*., et al.* (2013). SDH mutations establish a hypermethylator phenotype in paraganglioma. Cancer cell *23*, 739-752.

Liu, W., Le, A., Hancock, C., Lane, A.N., Dang, C.V., Fan, T.W., and Phang, J.M. (2012). Reprogramming of proline and glutamine metabolism contributes to the proliferative and metabolic responses regulated by oncogenic transcription factor c-MYC. Proceedings of the National Academy of Sciences of the United States of America *109*, 8983-8988.

Liu, Y.C., Li, F., Handler, J., Huang, C.R., Xiang, Y., Neretti, N., Sedivy, J.M., Zeller, K.I., and Dang, C.V. (2008). Global regulation of nucleotide biosynthetic genes by c-Myc. PloS one *3*, e2722.

Locasale, J.W., Grassian, A.R., Melman, T., Lyssiotis, C.A., Mattaini, K.R., Bass, A.J., Heffron, G., Metallo, C.M., Muranen, T., Sharfi, H*., et al.* (2011). Phosphoglycerate dehydrogenase diverts glycolytic flux and contributes to oncogenesis. Nature genetics *43*, 869-874.

Lora, J., Alonso, F.J., Segura, J.A., Lobo, C., Marquez, J., and Mates, J.M. (2004). Antisense glutaminase inhibition decreases glutathione antioxidant capacity and increases apoptosis in Ehrlich ascitic tumour cells. European journal of biochemistry / FEBS *271*, 4298-4306.

Lu, C., Ward, P.S., Kapoor, G.S., Rohle, D., Turcan, S., Abdel-Wahab, O., Edwards, C.R., Khanin, R., Figueroa, M.E., Melnick, A*., et al.* (2012). IDH mutation impairs histone demethylation and results in a block to cell differentiation. Nature *483*, 474-478.

Lunt, S.Y., and Vander Heiden, M.G. (2011). Aerobic glycolysis: meeting the metabolic requirements of cell proliferation. Annual review of cell and developmental biology *27*, 441-464.

Majmundar, A.J., Wong, W.J., and Simon, M.C. (2010). Hypoxia-inducible factors and the response to hypoxic stress. Molecular cell *40*, 294-309.

Mannava, S., Grachtchouk, V., Wheeler, L.J., Im, M., Zhuang, D., Slavina, E.G., Mathews, C.K., Shewach, D.S., and Nikiforov, M.A. (2008). Direct role of nucleotide metabolism in C-MYC-dependent proliferation of melanoma cells. Cell Cycle *7*, 2392-2400.

Manning, B.D., and Cantley, L.C. (2007). AKT/PKB signaling: navigating downstream. Cell *129*, 1261-1274.

Mathupala, S.P., Heese, C., and Pedersen, P.L. (1997). Glucose catabolism in cancer cells. The type II hexokinase promoter contains functionally active response elements for the tumor suppressor p53. The Journal of biological chemistry *272*, 22776-22780.

Matoba, S., Kang, J.G., Patino, W.D., Wragg, A., Boehm, M., Gavrilova, O., Hurley, P.J., Bunz, F., and Hwang, P.M. (2006). p53 regulates mitochondrial respiration. Science *312*, 1650-1653.

Menendez, D., Inga, A., and Resnick, M.A. (2009). The expanding universe of p53 targets. Nature reviews Cancer *9*, 724-737.

Metallo, C.M., Gameiro, P.A., Bell, E.L., Mattaini, K.R., Yang, J., Hiller, K., Jewell, C.M., Johnson, Z.R., Irvine, D.J., Guarente, L*., et al.* (2012). Reductive glutamine metabolism by IDH1 mediates lipogenesis under hypoxia. Nature *481*, 380-384.

Morais, R., Zinkewich-Peotti, K., Parent, M., Wang, H., Babai, F., and Zollinger, M. (1994). Tumor-forming ability in athymic nude mice of human cell lines devoid of mitochondrial DNA. Cancer research *54*, 3889-3896.

Moreno-Sanchez, R., Rodriguez-Enriquez, S., Marin-Hernandez, A., and Saavedra, E. (2007). Energy metabolism in tumor cells. The FEBS journal *274*, 1393-1418.

Mullen, A.R., and DeBerardinis, R.J. (2012). Genetically-defined metabolic reprogramming in cancer. Trends in endocrinology and metabolism: TEM *23*, 552-559.

Mullen, A.R., Wheaton, W.W., Jin, E.S., Chen, P.H., Sullivan, L.B., Cheng, T., Yang, Y., Linehan, W.M., Chandel, N.S., and DeBerardinis, R.J. (2012). Reductive carboxylation supports growth in tumour cells with defective mitochondria. Nature *481*, 385-388.

Niemann, S., and Muller, U. (2000). Mutations in SDHC cause autosomal dominant paraganglioma, type 3. Nature genetics *26*, 268-270.

Nikiforov, M.A., Chandriani, S., O'Connell, B., Petrenko, O., Kotenko, I., Beavis, A., Sedivy, J.M., and Cole, M.D. (2002). A functional screen for Myc-responsive genes reveals serine hydroxymethyltransferase, a major source of the one-carbon unit for cell metabolism. Molecular and cellular biology *22*, 5793-5800.

O'Connell, B.C., Cheung, A.F., Simkevich, C.P., Tam, W., Ren, X., Mateyak, M.K., and Sedivy, J.M. (2003). A large scale genetic analysis of c-Myc-regulated gene expression patterns. The Journal of biological chemistry *278*, 12563-12573.

Owen, M.R., Doran, E., and Halestrap, A.P. (2000). Evidence that metformin exerts its anti-diabetic effects through inhibition of complex 1 of the mitochondrial respiratory chain. The Biochemical journal *348 Pt 3*, 607-614.

Papandreou, I., Cairns, R.A., Fontana, L., Lim, A.L., and Denko, N.C. (2006). HIF-1 mediates adaptation to hypoxia by actively downregulating mitochondrial oxygen consumption. Cell metabolism *3*, 187-197.

Parsons, D.W., Jones, S., Zhang, X., Lin, J.C., Leary, R.J., Angenendt, P., Mankoo, P., Carter, H., Siu, I.M., Gallia, G.L*., et al.* (2008). An integrated genomic analysis of human glioblastoma multiforme. Science *321*, 1807-1812.

Pfeiffer, T., Schuster, S., and Bonhoeffer, S. (2001). Cooperation and competition in the evolution of ATP-producing pathways. Science *292*, 504-507.

Phang, J.M., Liu, W., and Zabirnyk, O. (2010). Proline metabolism and microenvironmental stress. Annual review of nutrition *30*, 441-463.

Pollari, S., Kakonen, S.M., Edgren, H., Wolf, M., Kohonen, P., Sara, H., Guise, T., Nees, M., and Kallioniemi, O. (2011). Enhanced serine production by bone metastatic breast cancer cells stimulates osteoclastogenesis. Breast cancer research and treatment *125*, 421-430.

Possemato, R., Marks, K.M., Shaul, Y.D., Pacold, M.E., Kim, D., Birsoy, K., Sethumadhavan, S., Woo, H.K., Jang, H.G., Jha, A.K.*, et al.* (2011). Functional genomics reveal that the serine synthesis pathway is essential in breast cancer. Nature *476*, 346-350.

Raimundo, N., Baysal, B.E., and Shadel, G.S. (2011). Revisiting the TCA cycle: signaling to tumor formation. Trends in molecular medicine *17*, 641-649.

Rana, M., de Coo, I., Diaz, F., Smeets, H., and Moraes, C.T. (2000). An out-of-frame cytochrome b gene deletion from a patient with parkinsonism is associated with impaired complex III assembly and an increase in free radical production. Annals of neurology *48*, 774-781.

Ratcliffe, P.J., O'Rourke, J.F., Maxwell, P.H., and Pugh, C.W. (1998). Oxygen sensing, hypoxia-inducible factor-1 and the regulation of mammalian gene expression. The Journal of experimental biology *201*, 1153-1162.

Riley, T., Sontag, E., Chen, P., and Levine, A. (2008). Transcriptional control of human p53-regulated genes. Nature reviews Molecular cell biology *9*, 402-412.

Rohle, D., Popovici-Muller, J., Palaskas, N., Turcan, S., Grommes, C., Campos, C., Tsoi, J., Clark, O., Oldrini, B., Komisopoulou, E.*, et al.* (2013). An inhibitor of mutant IDH1 delays growth and promotes differentiation of glioma cells. Science *340*, 626-630.

Rossignol, R., Gilkerson, R., Aggeler, R., Yamagata, K., Remington, S.J., and Capaldi, R.A. (2004). Energy substrate modulates mitochondrial structure and oxidative capacity in cancer cells. Cancer research *64*, 985-993.

Rydstrom, J. (2006). Mitochondrial NADPH, transhydrogenase and disease. Biochimica et biophysica acta *1757*, 721-726.

Salway, J.G. (2004). Metabolism at a Glance, Third Edition edn (Blackwell Publishing).

Sazanov, L.A., and Jackson, J.B. (1994). Proton-translocating transhydrogenase and NAD- and NADP-linked isocitrate dehydrogenases operate in a substrate cycle which contributes to fine regulation of the tricarboxylic acid cycle activity in mitochondria. FEBS letters *344*, 109-116.

Schenk, G., Duggleby, R.G., and Nixon, P.F. (1998). Properties and functions of the thiamin diphosphate dependent enzyme transketolase. The international journal of biochemistry & cell biology *30*, 1297-1318.

Selak, M.A., Armour, S.M., MacKenzie, E.D., Boulahbel, H., Watson, D.G., Mansfield, K.D., Pan, Y., Simon, M.C., Thompson, C.B., and Gottlieb, E. (2005). Succinate links TCA cycle dysfunction to oncogenesis by inhibiting HIF-alpha prolyl hydroxylase. Cancer cell *7*, 77-85.

Semenza, G.L., Roth, P.H., Fang, H.M., and Wang, G.L. (1994). Transcriptional regulation of genes encoding glycolytic enzymes by hypoxia-inducible factor 1. The Journal of biological chemistry *269*, 23757-23763.

Sharma, L.K., Fang, H., Liu, J., Vartak, R., Deng, J., and Bai, Y. (2011). Mitochondrial respiratory complex I dysfunction promotes tumorigenesis through ROS alteration and AKT activation. Human molecular genetics *20*, 4605-4616.

Shechter, I., Dai, P., Huo, L., and Guan, G. (2003). IDH1 gene transcription is sterol regulated and activated by SREBP-1a and SREBP-2 in human hepatoma HepG2 cells: evidence that IDH1 may regulate lipogenesis in hepatic cells. Journal of lipid research *44*, 2169-2180.

Shen, C., Beroukhim, R., Schumacher, S.E., Zhou, J., Chang, M., Signoretti, S., and Kaelin, W.G., Jr. (2011). Genetic and functional studies implicate HIF1alpha as a 14q kidney cancer suppressor gene. Cancer discovery *1*, 222-235.

Snell, K., Natsumeda, Y., Eble, J.N., Glover, J.L., and Weber, G. (1988). Enzymic imbalance in serine metabolism in human colon carcinoma and rat sarcoma. British journal of cancer *57*, 87-90.

Sullivan, L.B., Martinez-Garcia, E., Nguyen, H., Mullen, A.R., Dufour, E., Sudarshan, S., Licht, J.D., Deberardinis, R.J., and Chandel, N.S. (2013). The Proto-oncometabolite Fumarate Binds Glutathione to Amplify ROS-Dependent Signaling. Molecular cell *51*, 236-248.

Suzuki, S., Tanaka, T., Poyurovsky, M.V., Nagano, H., Mayama, T., Ohkubo, S., Lokshin, M., Hosokawa, H., Nakayama, T., Suzuki, Y.*, et al.* (2010). Phosphate-activated glutaminase (GLS2), a p53-inducible regulator of glutamine metabolism and reactive oxygen species. Proceedings of the National Academy of Sciences of the United States of America *107*, 7461-7466.

Ternette, N., Yang, M., Laroyia, M., Kitagawa, M., O'Flaherty, L., Wolhulter, K., Igarashi, K., Saito, K., Kato, K., Fischer, R.*, et al.* (2013). Inhibition of mitochondrial aconitase by succination in fumarate hydratase deficiency. Cell reports *3*, 689-700.

Tomlinson, I.P., Alam, N.A., Rowan, A.J., Barclay, E., Jaeger, E.E., Kelsell, D., Leigh, I., Gorman, P., Lamlum, H., Rahman, S.*, et al.* (2002). Germline mutations in FH predispose to dominantly inherited uterine fibroids, skin leiomyomata and papillary renal cell cancer. Nature genetics *30*, 406-410.

Tong, L. (2013). Structure and function of biotin-dependent carboxylases. Cellular and molecular life sciences : CMLS *70*, 863-891.

Tong, W.H., Sourbier, C., Kovtunovych, G., Jeong, S.Y., Vira, M., Ghosh, M., Romero, V.V., Sougrat, R., Vaulont, S., Viollet, B.*, et al.* (2011). The glycolytic shift in fumarate-hydratase-deficient kidney cancer lowers AMPK levels, increases anabolic propensities and lowers cellular iron levels. Cancer cell *20*, 315-327.

Tong, X., Zhao, F., and Thompson, C.B. (2009). The molecular determinants of de novo nucleotide biosynthesis in cancer cells. Current opinion in genetics & development *19*, 32-37.

Turcan, S., Rohle, D., Goenka, A., Walsh, L.A., Fang, F., Yilmaz, E., Campos, C., Fabius, A.W., Lu, C., Ward, P.S.*, et al.* (2012). IDH1 mutation is sufficient to establish the glioma hypermethylator phenotype. Nature *483*, 479-483.

Vafai, S.B., and Mootha, V.K. (2012). Mitochondrial disorders as windows into an ancient organelle. Nature *491*, 374-383.

Vander Heiden, M.G., Cantley, L.C., and Thompson, C.B. (2009). Understanding the Warburg effect: the metabolic requirements of cell proliferation. Science *324*, 1029-1033.

Vousden, K.H., and Ryan, K.M. (2009). p53 and metabolism. Nature reviews Cancer *9*, 691-700.

Wakabayashi, N., Dinkova-Kostova, A.T., Holtzclaw, W.D., Kang, M.I., Kobayashi, A., Yamamoto, M., Kensler, T.W., and Talalay, P. (2004). Protection against electrophile and oxidant stress by induction of the phase 2 response: fate of cysteines of the Keap1 sensor modified by inducers. Proceedings of the National Academy of Sciences of the United States of America *101*, 2040-2045.

Wang, F., Travins, J., DeLaBarre, B., Penard-Lacronique, V., Schalm, S., Hansen, E., Straley, K., Kernytsky, A., Liu, W., Gliser, C.*, et al.* (2013). Targeted inhibition of mutant IDH2 in leukemia cells induces cellular differentiation. Science *340*, 622-626.

Warburg, O. (1956). On the origin of cancer cells. Science *123*, 309-314.

Warburg, O., Wind, F., and Negelein, E. (1927). The Metabolism of Tumors in the Body. The Journal of general physiology *8*, 519-530.

Ward, P.S., Cross, J.R., Lu, C., Weigert, O., Abel-Wahab, O., Levine, R.L., Weinstock, D.M., Sharp, K.A., and Thompson, C.B. (2011). Identification of additional IDH mutations associated with oncometabolite R(-)-2-hydroxyglutarate production. Oncogene.

Ward, P.S., Patel, J., Wise, D.R., Abdel-Wahab, O., Bennett, B.D., Coller, H.A., Cross, J.R., Fantin, V.R., Hedvat, C.V., Perl, A.E.*, et al.* (2010). The common feature of leukemia-associated IDH1 and IDH2 mutations is a neomorphic enzyme activity converting alpha-ketoglutarate to 2-hydroxyglutarate. Cancer cell *17*, 225-234.

Ward, P.S., and Thompson, C.B. (2012). Metabolic reprogramming: a cancer hallmark even warburg did not anticipate. Cancer cell *21*, 297-308.

Weinberg, F., Hamanaka, R., Wheaton, W.W., Weinberg, S., Joseph, J., Lopez, M., Kalyanaraman, B., Mutlu, G.M., Budinger, G.R., and Chandel, N.S. (2010). Mitochondrial metabolism and ROS generation are essential for Kras-mediated tumorigenicity. Proceedings of the National Academy of Sciences of the United States of America *107*, 8788-8793.

Wellen, K.E., Hatzivassiliou, G., Sachdeva, U.M., Bui, T.V., Cross, J.R., and Thompson, C.B. (2009). ATP-citrate lyase links cellular metabolism to histone acetylation. Science *324*, 1076-1080.

Wellen, K.E., and Thompson, C.B. (2010). Cellular metabolic stress: considering how cells respond to nutrient excess. Molecular cell *40*, 323-332.

Wise, D.R., DeBerardinis, R.J., Mancuso, A., Sayed, N., Zhang, X.Y., Pfeiffer, H.K., Nissim, I., Daikhin, E., Yudkoff, M., McMahon, S.B.*, et al.* (2008). Myc regulates a transcriptional program that stimulates mitochondrial glutaminolysis and leads to glutamine addiction. Proceedings of the National Academy of Sciences of the United States of America *105*, 18782-18787.

Wise, D.R., Ward, P.S., Shay, J.E., Cross, J.R., Gruber, J.J., Sachdeva, U.M., Platt, J.M., DeMatteo, R.G., Simon, M.C., and Thompson, C.B. (2011). Hypoxia promotes isocitrate dehydrogenase-dependent carboxylation of alpha-ketoglutarate to citrate to support cell growth and viability. Proceedings of the National Academy of Sciences of the United States of America *108*, 19611-19616.

Xiao, M., Yang, H., Xu, W., Ma, S., Lin, H., Zhu, H., Liu, L., Liu, Y., Yang, C., Xu, Y.*, et al.* (2012). Inhibition of alpha-KG-dependent histone and DNA demethylases by fumarate and succinate that are accumulated in mutations of FH and SDH tumor suppressors. Genes & development *26*, 1326-1338.

Xu, W., Yang, H., Liu, Y., Yang, Y., Wang, P., Kim, S.H., Ito, S., Yang, C., Xiao, M.T., Liu, L.X.*, et al.* (2011). Oncometabolite 2-hydroxyglutarate is a competitive inhibitor of alpha-ketoglutarate-dependent dioxygenases. Cancer cell *19*, 17-30.

Yan, H., Parsons, D.W., Jin, G., McLendon, R., Rasheed, B.A., Yuan, W., Kos, I., Batinic-Haberle, I., Jones, S., Riggins, G.J.*, et al.* (2009). IDH1 and IDH2 mutations in gliomas. The New England journal of medicine *360*, 765-773.

Yang, C., Sudderth, J., Dang, T., Bachoo, R.M., McDonald, J.G., and DeBerardinis, R.J. (2009). Glioblastoma cells require glutamate dehydrogenase to survive impairments of glucose metabolism or Akt signaling. Cancer research *69*, 7986-7993.

Yang, M., Soga, T., Pollard, P.J., and Adam, J. (2012). The emerging role of fumarate as an oncometabolite. Frontiers in oncology *2*, 85.

Yang, Y., Valera, V.A., Padilla-Nash, H.M., Sourbier, C., Vocke, C.D., Vira, M.A., Abu-Asab, M.S., Bratslavsky, G., Tsokos, M., Merino, M.J.*, et al.* (2010). UOK 262 cell line, fumarate hydratase deficient (FH-/FH-) hereditary leiomyomatosis renal cell carcinoma: in vitro and in vivo model of an aberrant energy metabolic pathway in human cancer. Cancer genetics and cytogenetics *196*, 45-55.

Yoo, H., Antoniewicz, M.R., Stephanopoulos, G., and Kelleher, J.K. (2008). Quantifying reductive carboxylation flux of glutamine to lipid in a brown adipocyte cell line. The Journal of biological chemistry *283*, 20621-20627.

Yuneva, M., Zamboni, N., Oefner, P., Sachidanandam, R., and Lazebnik, Y. (2007). Deficiency in glutamine but not glucose induces MYC-dependent apoptosis in human cells. The Journal of cell biology *178*, 93-105.

Zhang, D.D. (2010). The Nrf2-Keap1-ARE signaling pathway: The regulation and dual function of Nrf2 in cancer. Antioxidants & redox signaling *13*, 1623-1626.

Zu, X.L., and Guppy, M. (2004). Cancer metabolism: facts, fantasy, and fiction. Biochemical and biophysical research communications *313*, 459-465.